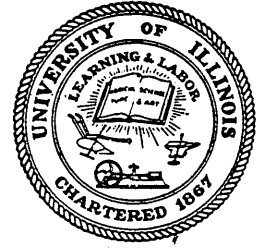# CIVIL ENGINEERING STUDIES

STRUCTURAL RESEARCH SERIES NO. 450

EXPERIMENTAL STUDY OF THE DYNAMIC RESPONSE OF A TEN-STORY REINFORCED CONCRETE FRAME WITH A TALL FIRST STORY

By

TIMOTHY J. HEALEY

and

METE A. SOZEN

Metz Reference Room
Civil Engineering Department
B106 C. E. Building
University of Illinois
Urbana, Illinois 61801

UNIVERSITY OF ILLINOIS
at URBANA-CHAMPAIGN
URBANA, ILLINOIS
AUGUST 1978

ii

BIBLIOGRAPHIC DATA SHEET	1. Report No. UILU-ENG-78-2012	2.	3. Recipient's Accession No.
4. Title and Subtitle EXPERIMENTAL STUDY OF THE DYNAMIC RESPONSE OF A TEN-STORY REINFORCED CONCRETE FRAME WITH A TALL FIRST STORY			5. Report Date August 1978
			6.
7. Author(s) T. J. Healey & Mete A. Sozen			8. Performing Organization Rept. No. SRS 450
9. Performing Organization Name and Address University of Illinois at Urbana-Champaign Urbana, Illinois 61801			10. Project/Task/Work Unit No.
			11. Contract/Grant No. NSF ENV-74-22962
12. Sponsoring Organization Name and Address National Science Foundation			13. Type of Report & Period Covered
			14.

15. Supplementary Notes

16. Abstracts

This report documents the experimental work and presents the response data obtained in three earthquake simulation tests of a ten-story reinforced concrete frame. Changes in the dynamic properties of the test structure, such as apparent frequencies and equivalent damping, are discussed. Observed maximum lateral displacements are compared with those obtained from modal spectral analysis.

17. Key Words and Document Analysis. 17a. Descriptors

Response spectrum, mode shape, modal spectral analysis, displacements, accelerations, story shear, overturning moment, Fourier amplitude spectrum, frequency, reinforcement, nonlinear

17b. Identifiers/Open-Ended Terms

17c. COSATI Field/Group

18. Availability Statement Release Unlimited	19. Security Class (This Report) UNCLASSIFIED	21. No. of Pages 122
	20. Security Class (This Page) UNCLASSIFIED	22. Price

FORM NTIS-35 (REV. 10-73) ENDORSED BY ANSI AND UNESCO. THIS FORM MAY BE REPRODUCED USCOMM-DC 8265-P74

TABLE OF CONTENTS

iv

LIST OF TABLES

v

LIST OF FIGURES

1

CHAPTER 1

INTRODUCTION

1.1 Object and Scope

The primary objective of this test was to study the nonlinear dynamic behavior of a small-scale ten-story three-bay reinforced concrete structure with a tall first story. Actually both the first story and the tenth story were 20% longer than each of the other stories of the structure.

The test procedure included a series of strong base motions simulating a scaled version of the north-south component of the El Centro earthquake of 1940. Reinforcement was selected with guidance from a linear dynamic analysis using a specific design spectrum.

This report documents the experimental work and presents the acceleration and displacement data obtained in three earthquake-simulation tests. Changes in the dynamic properties of the test structure, such as apparent frequencies and equivalent damping, are discussed. Observed maximum lateral displacements are compared with those obtained from modal spectral analysis.

1.2 Acknowledgment

This investigation is part of a continuing study of the effects of earthquake motions on reinforced concrete systems being carried out at the Structural Research Laboratory of the Department of Civil Engineering of the University of Illinois. The work was sponsored by the National Science Foundation under Grant NSF-ENV-74-22962

The writers wish to thank D. Abrams, B. Algan, H. Cecen, J. Moehle, D. Schipper, and B. Volkert, research assistants in the Department of Civil Engineering for their generous advice and assistance. Acknowledgment

CHAPTER 2

TEST STRUCTURE

2.1 Description of Test Structure and Test Setup

The test structure was a small scale ten-story building comprising two frames working in parallel to carry a total mass of 4540 kg distributed equally to each level (Fig. 2.1). The frames were cast horizontally out of the same batch of concrete. The compressive strength of the concrete was 40 MPa at time of test. The yield stress for the longitudinal reinforcement was 350 MPa.

(a) Dimensions

The overall nominal dimensions of the frames are shown in Fig. 2.2. The measured dimensions are summarized in Table A.3.

The story heights from center line to center line of the beams were 229 mm for the second level through the ninth level, and 279 mm for the tenth level. The first level height from the top of the base girder to the centerline of the first level beam was 279 mm. The columns were 58 mm deep by 38 mm wide.

Each of the three spans from center line of column to center line of column was 305 mm. The cross section of the beams was 38 by 38 mm.

(b) Test Setup

The test structure was tested using the University of Illinois Earthquake Simulator (Figures 2.3 and 2.4. A detailed discussion of the simulator is given by Sozen and Otani (1970).

Before the frames were placed on the test platform, the masses were stacked on the platform with adjustable wooden blocks in between each mass. In this way, as the masses were stacked, their positions could be adjusted so that the center of gravity of a mass was at each of the story levels.

The frames were then placed on the test platform parallel to each other on opposite sides of the masses. They were positioned so that the major axis of the test structure was parallel to the direction of the input motion (Figures 2.3 and 2.4). The frames were bolted to the platform through vertical holes in the base girder.

The masses were then connected to the frame. The process began at the tenth level and continued in descending order, one level at a time, to the first level. The wooden blocks were not removed during this procedure and were kept in place until the day of the test. The structure did not carry dead load until then. The connection of the masses to the frame was designed so that the reactions at the joints were determinate. Each story mass was supported by two steel channel cross beams. The cross beams were positioned so that the weight of the mass would be carried to the centerline of the exterior bay of each frame. Pinned to each end of the cross beams were a pair of channels which distributed the reaction equally to an exterior and an interior column (Figures 2.1 and 2.3). Thus, each joint in the frame was designed to carry one eighth of the weight of the story mass transferred to the joint through a pin connection.

To provide stability of the test structure about its weak axis and to provide torsional stiffness about its vertical axis, steel plate hinges were provided between masses at each level (Fig. 2.1). The light hinges were well lubricated to minimize restraint in the direction parallel to the input motion.

2.2 Reinforcing Arrangement

(a) Design Process

The test structure was designed using the substitute-structure method (Shibata, 1976). The objective of this design method is to establish the minimum strengths which the members of the structure must have so that a tolerable response is not likely to be exceeded.

The test structure was reinforced to resist lateral loads based on a design response spectrum. The design concrete strength was 30 MPa at a strain of .003 with a Young's Modulus (E_c) of 21,000 MPa. The yield stress of the reinforcing steel, based on the average value obtained from coupon tests, was taken as 350 MPa (Table A.2).

Response spectrum A (Figure 2.5) (Shibata, 1976) modified to a time scale 1/2.5 was used for the dynamic analysis of the substitute structure. The maximum base acceleration for the design earthquake was 0.4g. A comparison of the assumed and obtained spectra is given in Chapter 5.

The flexural stiffnesses of the substitute frame elements are related to the stiffnesses of the actual frame elements by the relation

$$(EI)_{si} = (EI)_{ai/\mu} \qquad (2-1)$$

where $(EI)_{si}$ and $(EI)_{ai}$ are flexural stiffnesses of member i for the substitute and actual structure, respectively, and μ is the selected tolerable "damage ratio" for element i.

The cracked section stiffnesses of each member in the frame, modified by the appropriate damage ratio, μ, was used in the analysis of the substitute structure. Since the amount of reinforcement was not known at

the initial stage of design, it was assumed that the ratio of cracked-to-gross-section moment-of-inertia was 1/3 for beams and columns.

The damage ratio was taken as four for beams (μ = 4) and one for columns (μ = 1) in the substitute-structure. These damage ratios were chosen with the intent that energy be dissipated primarily in the beams during the design earthquake.

A linear dynamic response analysis was made to obtain modal periods, shapes, and forces for the first three modes of the substitute structure. For this preliminary analysis, the modal damping was taken as 10% for all three modes. Motion was considered only in one horizontal direction.

Trial design moments at critical sections were obtained as the square root of the sum of the squares RSS moments for the beams and 1.2 * RSS moments for the columns. The column RSS moments were amplified by 1.2 to reduce the risk of inelastic action in the columns.

A steel reinforcement arrangement was selected, and another linear dynamic response analysis was made. Shapes of the first three modes of the substitute structure for this final trial are shown in Fig. 2.6.

The substitute modal damping factors were obtained from the following expressions (Shibata) 1976

$$\beta_m = \frac{\Sigma P_i {}^* \beta_{si}}{\Sigma P_i} \tag{2.2}$$

where

$$P_i = \frac{L}{6(EI)_{si}} (M_{ai}^2 + M_{bi}^2 - M_{ai} M_{bi}) \tag{2.3}$$

$$\beta_{si} = 0.2 (1 - (1/\mu_i)^{1/2}) + 0.02 \tag{2.4}$$

where

β_m = "smeared" damping factor for mode m

P_i = strain energy of member i

β_{si} = substitute viscous damping factor for member i

μ_i = damage ratio for member i

L = length of structural member

M_{ai} & M_{bi} = end moments of substitute-structure element i for

mode m

It was assumed that the design response acceleration for any damping factor, β, was related to the response for $\beta = 0.02$ by the equation (Shibata, 1976)

$$\frac{\text{Response Acceleration for } \beta}{\text{Response Acceleration for } \beta = .02} = \frac{8}{6+100\beta} \qquad (2.5)$$

The modal forces for the first three modes were then modified using equation (2.5) according to their respective "smeared" damping ratio from equation (2.2).

The RSS of the modal beam moments were used for design. The design beam moment per level along with the yield strength provided is shown in Fig. 2.7.

The RSS of the column shear forces were used for design of the spiral shear reinforcement. The distribution of those forces are shown in Figure 2.8. All beams and columns had more transverse shear reinforcement than required by the design forces to minimize the risk of primary failure in shear.

The design axial forces on columns were taken as the dead weight of the masses ± RSS axial forces. The design column moments were taken as

the RSS moments amplified by 1.2, except at the base where the RSS moments were used. The first story RSS moments were not amplified by 1.2 with the notion that inelastic action is difficult to avoid at the base. The distribution of the design axial forces and design moments are shown in Figures 2.9 and 2.10.

An interaction diagram for the columns is shown in Fig. 2.11. The position of the columns are also plotted on the interaction diagram. All columns fall within the diagram except the exterior column at the base on the tension side of the frame.

To investigate the effects of an exterior column yielding, a second linear dynamic response analysis was made with the same assumed section stiffnesses as before, with the exception that a damage ratio of two (μ = 2) was assumed for one exterior column at the first level. For the most part, the results of this analysis were not different from those of the original analysis. As would be expected, the moments at the base shifted from the soft column to the other three columns which had reserve capacity. The new positions for the base moments for this analysis are shown by arrows in Fig. 2.11. The distribution of moments from this analysis is shown in Fig. 2.12.

(b) <u>Reinforcing Steel Distribution</u>

The arrangement of the longitudinal reinforcement is schematically shown in Figures 2.2 and 2.13 and is given by the schedule in Table 2.1.

The columns at the base and the second level interior columns were reinforced with three No. 13 gage wires per face for a reinforcement ratio of 1.32%. All other columns in the frame contained two No. 13 gage wires per face for a reinforcement ratio of 0.88%.

The beams at the first through the seventh levels were reinforced with three No. 13 gage wires per face for a flexural reinforcement ratio of 1.10%. The beams at the eighth trhough the tenth levels had two No. 13 gage wires per face for a flexural reinforcement ratio of 0.74%.

All beams and columns were reinforced to resist shear forces with No. 16 gage wire "spirals" (Fig. 2.2 and 2.13). The spirals were continuous and had a pitch of 3 mm. The joint details are described in Appendix A.

CHAPTER 3

TEST PROCEDURE

On the day of the test, the adjustable wooden blocks were removed from between the masses. At this time all cracks observed on the specimen were recorded. To locate the cracks, the specimen was coated with "Partek" P1-A Fluorescent and black light was applied.

The tightness of all bolts on the test setup was then checked. This included the connections of the masses to the frames, the specimen base to the test platform, the instrumentation fixtures, and the A-frame to the test platform (Fig. 2.3).

Hydrocal was then placed at various locations along the connection of the base of the frame to the test platform. The hydrocal was used as a check for slip between the test specimen and the platform during the testing.

The following sequence of operations was performed for each test run:

(1) The tightness of bolts fixing the specimen to the platform was checked.

(2) The tenth level of the structure was given a small initial displacement to induce a low-amplitude free vibration. This displacement was obtained by hanging a small weight from the tenth level over a pulley (Fig. 3.1). Free vibration was initiated by cutting the wire supporting the weight.

(3) The specimen was subjected to the desired earthquake base motion at the specified acceleration level.

(4) The specimen was coated with "Partek" P-1A Fluorescent and the new cracks were marked and recorded.

(5) A low-amplitude free-vibration test was made as described in (2).

(6) The structure was subjected to a sinusoidal base motion "sweep" of the form

$$X_b = X_o \sin\omega t \qquad (3\text{-}1)$$

where X_b is the input base motion, X_o is a constant amplitude of the input base motion, and ω is the "sweeping" driving frequency. These tests will be referred to as "steady-state tests" throughout this report.

This sequence was followed three times throughout the entire testing procedure. Table 3.1 summarizes the events of the experiment in chronological order.

The input motion for the three earthquake simulation tests was the recorded north-south component of the earthquake motion measured at El Centro, California (1940). The acceleration level was magnified for each test run. The maximum recorded base acceleration for the first through the third test was 0.4 g, 0.95 g and 1.42 g, respectively.

The displacement amplitude, X_o (Eq. 3.1) was chosen so that ideally no damage would occur during the steady state tests. The driving frequency was varied throughout each individual run. The value of the driving frequency was taken as .8 Hz below the estimated first natural frequency initially, and gradually increased in increments of .2 Hz up to .8 Hz above the frequency at which maximum response amplitude was observed.

CHAPTER 4

OBSERVED RESPONSE

4.1 Introductory Remarks

(a) General Comments

The results of the earthquake simulation tests previously described
in Chapter 3 are presented in this chapter. The presentation is based
on instrument signals which were recorded during each earthquake test,
and on observed crack patterns of the structure. For a complete descrip-
tion of the data recording procedure, see Appendix A. The process for
marking and recording the crack pattern of the structure is described in
Chapter 3.

(b) Terminology

Certain terms are used throughout this chapter and are defined here
for clarity. Throughout this chapter "test run" will refer to one of
the earthquake simulation tests.

A response spectrum refers to the response of a linear single-degree-
of-freedom system subjected to a given base motion for a given level of
damping. In this chapter the base motion is the base acceleration recorded
during a test run. For each test run a response spectrum is presented for
various damping levels.

In describing the base motion, it is sometimes advantageous to use
the spectrum intensity as well as the maximum base acceleration. The
spectrum intensity, as defined by Housner, is the area under the velocity
response spectrum from periods of 0.1 to 2.5. The maximum base accelera-
tion and the spectrum intensity for various damping levels are given for

each test run. To fit the time scale (2.5) of the earthquake motions used in the tests, Housner's Intensity is redefined to include the area under the velocity-response curve over the period range 0.04 to 1.0 sec.

Reference is made to response in a given mode. The mode of vibration refers to the phase relationship of the responses of the ten floor levels. For instance, by "first mode" it is meant that the responses of all ten levels are oscillating in the same phase. By "second mode" it is meant that some of the levels are oscillating in one phase while the remaining levels are oscillating in another phase.

The histories of the displacements and accelerations at each story level for each test run are presented. From these records the story level shear and base overturning moment waveforms were obtained. The story level shears and base overturning moments are also presented.

It should be mentioned that a frequency-filtered portion of each waveform is superimposed on the true waveform of all time histories presented in this chapter. The filtered waveform is shown as a solid line, while the total record is shown as a broken line. The filtered waveforms will be discussed in Chapter 5 and are of no consequence in this chapter.

In all three test runs, the responses of the north frame and the south frame at each level were almost identical. Therefore in this chapter, only the responses associated with the north frame are reported. The north side was chosen arbitrarily.

4.2 Earthquake Simulation Tests

(a) Condition of the Specimen Prior to Testing

Small cracks in the structure due to shrinkage and handling were observed prior to test run one. The crack pattern is depicted in Fig. 4.26.

As shown in the figure, cracking was negligible with all crack widths being much less than 0.05 mm.

(b) Base Motion

The maximum observed base acceleration for runs one, two and three was 0.40 g, 0.98 g and 1.42 g, respectively. The measured base accelerations are shown in Fig. 4.8 for run one, Fig. 4.10 for run two, and Fig. 4.12 for run 3. Response spectra for the base motions for each run are shown in Fig . 4.1 through 4.6. Spectrum intensities are given in Table 4.1. Fig. 4.25 shows maximum observed base acceleration versus spectrum intensity (SI_{20}). As seen in the figure, the relationship is linear. Thus, the base motion can be described equally well using either parameter.

(c) Accelerations

The response histories for horizontal accelerations at each level are shown in Fig . 4.7 through 4.12 for each of the three test runs. The maximum observed horizontal accelerations at each level are summarized in Table 4.2.

As shown in the figures, the horizontal accelerations seem to have very little high-frequency components. The acceleration histories were almost completely in phase consistent with the first mode, for each of the three test runs.

(d) Displacements

The horizontal displacement records for the three test runs are presented in Fig. 4.13 through 4.18. The single-amplitude displacement maxima are listed in Table 4.3.

As would be expected, the horizontal displacement records exhibited little or no high-frequency components. For each test run, all ten levels were in phase consistent with the first-mode.

(e) <u>Story Shears and Base Overturning Moments</u>

Histories of story shears for each test run are given in Fig. 4.19 through 4.24. The single-amplitude maximum observed story shears are summarized in Table 4.4.

Not unlike the acceleration records, the story shear records are first-mode dominated for each of the three test runs.

The base overturning moment records are shown in Fig. 4.13 for run one, Fig. 4.15 for run two and Fig. 4.17 for run three. The maximum base moments are summarized in Table 4.4.

The base overturning moment records are shown along with the horizontal displacement records. As seen in the figures, the base overturning moment time histories are in phase with the displacement records for each of the test runs.

(f) <u>Crack Patterns</u>

Figure 4.27 depicts the crack pattern after test run one. The structure incurred little additional cracking during run one with all observed crack widths being less than or equal to 0.10 mm.

Figure 4.28 shows the crack pattern after test run two. Cracking observed after run two was extensive. Crack widths at the first level were measured to be as high as 0.25 mm. Spalling occurred at the base on the outside of one of the exterior columns. Figure 4.30 shows a photograph taken of the spalling after run two.

Figure 4.29 depicts the crack pattern of the structure after test run three. The structure suffered additional cracking with crack widths at the second level measuring 0.38 mm. Spalling occurred at the base of

the outside of both exterior columns. A photograph of the spalling is
shown in Fig. 4.31.

CHAPTER 5

DISCUSSION OF OBSERVED RESPONSE

5.1 Introductory Remarks

· The presentation in this chapter is based on the observed response
of the structure during the earthquake simulation tests and on the results
of the free-vibration and steady-state tests. The testing procedure is
described in Chapter 3. The response histories, response maxima, and
response spectra for the earthquake simulation tests are presented in
Chapter 4. In this chapter an earthquake simulation test will be referred
to as a "run".

5.2 Apparent Frequencies of the Test Structure

(a) Frequency-Domain Response

To investigate the apparent frequency of the response of the test
structure, the response histories were transformed into the frequency
domain. The transformation into the frequency domain was accomplished
by means of the Fourier transform. Fourier amplitude spectra for the
horizontal displacement and acceleration histories for each test run are
given in Fig. 5.1 through 5.6. From these spectra it is seen that the
displacement and, to some extent, acceleration records are dominated by
components in the 0.0 to 3.0 Hz range. The apparent first-mode frequency
co responds to the spike in the Fourier amplitude within this range. The
measured first-mode frequencies were 2.0 Hz, 1.4 Hz and 1.0 Hz for run
one, two and three, respectively.

To investigate the contribution of the apparent first mode to the response of the test structure during the earthquake simulation tests, the response histories were filtered of components with frequencies greater than 3.0 Hz. The filtered response histories are presented in Chapter 4 in Fig. 4.7 through 4.24. As previously described in Chapter 4, the filtered record is shown as a solid line superimposed over the total record which is shown as a broken line. As might be expected, the filtered records match the total records well. However, as seen in Fig. 4.9 through 4.12, the contribution of higher modes is detected in the acceleration histories for both the second and third runs.

The contribution of higher modes on the response of the structure can be seen in the Fourier amplitude spectra for the acceleration records only. As shown in Fig. 5.2, the second through fourth level acceleration records for run one have perceptible contributions at frequencies 7.7 Hz and 15.0 Hz, which are the apparent second and third-mode frequencies, respectively. The motion at the first level is strongly influenced by the base motion.

In run two the second through fourth level acceleration histories have a high second mode contribution with an apparent frequency of 6.2 Hz (Fig. 5.4). The acceleration records at levels two, six and seven show a moderate third-mode contribution at 12.3 Hz.

In run three (Fig. 5.6) levels two through six and ten had an apparent second-mode component at 5.4 Hz. A third-mode contribution at 9.6 Hz can be seen at levels two, three, six and ten. Table 5.1 summarizes the apparent frequencies of the test structure obtained from the Fourier amplitude spectra.

(b) <u>Free-Vibration Tests</u>

As previously described in Chapter 3, before and after each test run, the structure was given an initial-displacement free vibration. The tenth level acceleration response and the Fourier amplitude spectrum for each free-vibration test are provided in Fig. 5.7 and 5.8. The response histories were filtered of components with frequencies greater than 4 Hz so that the first-mode frequency of the structure could be measured.

As shown in Fig. 5.7, prior to run one, the response of the structure in the free-vibration test exhibits contributions from several modes. From the Fourier spectrum, the apparent first-mode frequency is 3.2 Hz. However, another strong modal contribution is seen at 6.7 Hz, which is much too low to represent a second-mode frequency. This frequency is attributable to a "torsional" mode in which the two parallel frames were vibrating out of phase. Torsional vibration could have arisen as a result of either a difference in the initial stiffness of the two frames comprising the test structure, or a difference in the initial displacements of the two frames at the start of the test. However, since the apparent torsional mode was not present in the other free vibration tests as evidenced by the Fourier amplitude spectra, it may be assumed that the two frames had initial stiffnesses sufficiently different to cause torsional vibrations.

From Fig. 5.7 and 5.8 the measured first-mode frequencies are 3.2 Hz, 2.9 Hz, 2.3 Hz and 1.9 Hz for tests prior to run one, after run one, after run two and after run three, respectively. In the same order, the apparent second-mode frequencies are 15.6 Hz, 10.6 Hz, 8.7 Hz and 7.5 Hz. The apparent third-mode frequencies are 26.5 Hz, 19.0 Hz, 15.4 Hz and 12.9 Hz. The measured frequencies obtained from the free vibration tests are summarized in Table 5.1.

(c) Steady State Tests

After each test run, the structure was given a steady-state test as described in Chapter 3. The structure was subjected to low-amplitude sinusoidal base excitation. The base excitation was swept through various frequencies near the expected apparent frequency of the structure. The results of the tests in the form of amplication ratio versus input frequency of the base motion, are shown in Fig. 5.9.

The amplification ratio was calculated by normalizing the observed tenth level amplitude with respect to the input base amplitude and the first-mode participation. The participation of the first mode was calculated from the observed displaced shape of the structure at apparent resonance. Thus it was assumed that the contribution of higher modes on the response of the structure within this low frequency range was negligible. From Fig. 5.9, apparent resonance occurred at 2.1 Hz, 1.7 Hz and 1.4 Hz during the steady state tests after run one, two and three, respectively. The results of the steady-state test are summarized in Table 5.2.

Figure 5.10 is a plot of the measured first-mode frequency of the test structure versus one-half the maximum double amplitude displacement of the test structure during the earthquake simulation tests. That is, the frequencies measured after the run are correlated with the maximum displacement of that particular run. As shown in the figure, the measured frequencies associated with the free vibration tests were consistently higher while the measurements from the earthquake simulation tests were consistently lower.

It should be pointed out that the free-vibration and steady state tests were conducted at low amplitudes. The maximum tenth-level displacements during the free-vibration and steady-state tests were approximately 1mm and 7 mm, respectively. Given that the effective stiffness of

a nonlinear structural system is higher at low amplitudes of vibration, the observed difference in the apparent frequencies for the different types of tests would be expected. From Table 5.1, a similar trend may be seen to have occurred for the measured second and third-mode frequencies.

5.3 Measured Energy Dissipation Indices

The response histories for the free-vibration tests were used as an indication of the capacity of the test structure to dissipate energy under dynamic loading. Log-decrement measurements were taken of the filtered portion of each record to obtain equivalent viscous damping ratios. Following in the chronological order at which the free-vibration tests were administered (Table 3.1), the measured damping factors expressed as a percentage of critical damping, are summarized in Table 5.3.

The equivalent damping ratio increased as the test procedure progressed. As the test structure was subjected to more severe base motions and thus pushed farther into the inelastic range, apparently the capacity of the structure to absorb energy at low amplitude was also enhanced. Assuming that the measurements are not reliabile for differentiating between fractions of a percent, it would appear that the change in damping from before and after the steady-state tests was negligible. However, an appreciable increase in equivalent damping for low amplitude displacements occurred after each earthquake simulation test.

The trend of an increase in the apparent equivalent damping of the test structure after each run is also seen in the results from the steady-state tests. As shown in Fig. 5.9, the maximum amplification ratios for the steady-state tests are 5.7 after run one, 4.1 after run two and 3.8

after run three. As described in Chapter 3, the base motion in each

steady-state test was the same within the limitations of the earthquake

simulation system. From these results, there appears to have been a

large increase in the energy dissipation capacity of the structure at

moderate amplitudes from one to run two. Results of the steady-state tests

are not interpreted in terms of damping factors because, especially in runs

two and three, the response of the system was perceptibly nonlinear.

5.4 Response During the Design Earthquake

As previously described in Chapter 2, the test structure was designed

for an idealized response spectrum at an effective peak acceleration of

0.4 g. Fig. 5.11 compares the obtained response spectra from the measured

base acceleration of run one with the assumed response spectra used for the

design. The assumed acceleration response was less than the obtained

response in the low frequency region. For comparison, a linear dynamic

response analysis was made of the substitute-structure (Chapter 2) using

the obtained response spectrum. Another analysis was made of the test

structure assuming gross-section stiffnesses for the components of the

structure and using the obtained response spectrum.

(a) Displacements

The maximum single-amplitude displacements and one-half the maximum

double-amplitude displacements observed in run one are provided in Fig.

5.12. These maximum displacements occurred simultaneously during run one.

The calculated displacements given by the various linear dynamic response

analyses described above, are also shown in Fig. 5.12.

The calculated displacements given by the gross-section analysis

result in a low estimate of both the single-amplitude and one-half

double amplitude maximum observed displacements. The substitute-structure analysis based on the assumed design spectrum leads to displacements that were exceeded at all levels by the observed single-amplitude displacements and at the first six levels by one-half the observed double-amplitude displacements. The substitute-structure analysis based on the response spectrum from run one indicates displacements which were not exceeded in the top five levels by either single-amplitude or one-half double-amplitude observed displacements. However, the single-amplitude displacements observed at levels one through four and one-half the double-amplitude displacements observed at levels one and two were greater than those indicated by this analysis.

The gross-section analysis would be expected to five a poor estimate of the observed maximum displacements. Although the substitute-structure analysis indicates displacements that are comparable to those observed, the displacements indicated were exceeded at the lower stories. Since the primary objective of the substitute-structure method was to produce a structure to stay within tolerable displacement limits, these results suggest that some modifications need to be made to the procedure used for the selection of reinforcement in the lower-story columns and beams. It is quite likely that another base motion having the same intensity might excite the structure into larger displacements.

(b) Forces

As mentioned earlier in this chapter, the response of the structure seems to have been dominated by the first-mode, especially during the design earthquake. This is demonstrated in Fig. 5.13 which shows the displacements, lateral forces, shears and overturning moments at each level at time 1.42 seconds into run one. The maximum displacements, base shear and overturning moment occurred simultaneously.

Fig. 5.14 shows the observed and the calculated maximum story shears and overturning moments. Both the substitute-structure analyses resulted in forces less than the maximum observed. On the other hand, the gross-section analysis indicates forces that are much larger than those observed. It should be noted that the forces developed in the structure are a function of the actual strength of the structure. Because of the general trend of the decisions made in going from design requirements to reinforcement, the design forces are likely to be exceeded.

(c) Frequencies

A comparison of the calculated frequencies of the structure with the observed frequencies, previously discussed in section 5.2, provides insight into the apparent discrepancy between the observed and calculated forces in the structure. Table 5.4 summarizes the calculated first-mode frequencies. The apparent first-mode frequency was 2.0 Hz in run 1. The calculated first mode frequencies are 1.8 Hz and 3.6 Hz for the substitute-structure and gross-section analyses, respectively. The substitute-structure model was evidently more flexible than the actual test structure was observed to be. However, the gross-section model is far too stiff, thus leading to low deflections and very high forces.

5.5 General Features of Response

(a) Displacements

The maximum observed single-amplitude tenth level displacement versus spectrum intensity (SI_{20}) is shown in Fig. 5.15. As seen in the figure there is a linear relation between the two.

In run one the maximum tenth-level displacement was 23.6 mm or 1% of the total height of the structure. The maximum inter-story displacement occurred between the base and the first level, measuring 4.8 mm, or 1.7% of the story height. During run two the maximum tenth level displacement was 51.2 mm, or 2.2% of the height of the structure. The maximum inter-story displacement was 9 mm, or 3.9% of the story height, occurring between the second and third level. The maximum tenth level displacement in run three was 68.1, or 2.9% of the height of the structure. The maximum inter-story displacement occurred between levels two and three and measured 9.9 mm, or 4.3% of the story height.

(b) Forces

Unlike the response of the test structure during run one, for runs two and three the maximum base shear and overturning moment occurred at slightly different times. This is attributed to the contribution of higher modes to the response of the structure. Figures 5.16 and 5.17 show the displacements, lateral force distribution, story shears and overturning moments for run two at the instances of maximum base shear and overturning moment, respectively. Similarly, Fig. 5.18 and 5.19 shows the same sequences of distribution for run three. Notice that although the maximum base shear and overturning moment occur at different time instances, in both run two and three they are less than 0.1 second apart.

As presented in Chapter 4, the maximum base shear and overturning moment during run two was measured at 31.4 kN-m and 16.5 kN, respectively. During run three the observed maximums were 30.0 kN-m and 16.2 kN. The test structure apparently developed slightly less force in the third run than in the second, even though the maximum base acceleration and spectrum intensity of run three were approximately 1.5 times as great as those of run two.

(c) Force-Displacement Relation

The maximum base shear versus the maximum tenth-level displacement observed during the earthquake simulation tests is provided in Fig. 5.20. The points along the initial slope were obtained from the observed tenth-level displacement and base-shear "peak" at the beginning of run one. As seen in the figure, the maximum base shear starts to level off at 15 kN with a displacement of 23.6 mm which occurred early in run one. The data in the figure suggest that general yielding of the structure was reached in run one, the "design earthquake."

(d) Limit Strengths of the Test Structure

For the purpose of comparison with the observed maximum base shear, a limit analysis was made of the test structure. In this analysis it was assumed that the structure was subjected to a first-mode (triangular) loading. The beam ultimate moments used in the analysis were obtained from static tests performed on models of beam-column joints (Kreger, 1978[†]). The column ultimate moments were calculated assuming an ultimate stress in the steel of 410 MPa. Assuming various collapse mechanisms, the ultimate base shear was calculated. Figure 5.21 shows a plot of ultimate base shear versus collapse mechanism.

From the figure, the observed maximum base shear is 16.5 kN, and the maximum ultimate base shear corresponding to a first-story mechanism is 18.5 kN. The minimum base shear, corresponding to a mechanism with yielded fifth level columns and first through fourth level beams, is 12.3 kN. However, observing the crack pattern of the structure after run two and three (Fig. 4.28 and 4.29) suggests that all or most of the beams had yielded in the structure. Thus, the last mechanism shown in Fig. 5.21 with all beams yielding is probably the most reasonable one for the test structure. The base shear corresponding to this mechanism is 14.4 kN.

[†]Not published

It should be remembered that several simplifying assumptions were made in the limit analysis. For example, in the analysis it was assumed that the loading was triangular and constant with time. In fact, during the earthquake simulation tests the magnitude and distribution of the lateral loading is constantly changing with time. Also no account was made for strain rate or strain hardening in the components of the structure.

CHAPTER 6

SUMMARY

6.1 Object and Scope

The purpose of this study was to investigate the dynamic behavior of a ten-story reinforced concrete structure with a tall first story. As part of the testing procedure, the structure was subjected to strong base motions simulating the north-south component of the earthquake recorded at El Centro, California (1940).

The structure was designed on the basis of a linear dynamic analysis using a smooth design spectrum for the input motion (Shibata, 1976). A "substitute-structure" model for the analysis incorporated the expected change in strength of the structure.

6.2 Test Structure

The test structure comprised two small scale ten-story three-bay frames working in parallel to carry a 454 kg mass at each level (Fig. 2.1). The frames were cast horizontally out of the same batch of concrete. The compressive strength of the concrete on the day of the test was 40 MPa. The yield stress for the longitudinal reinforcement was 350 MPa.

The story heights from beam centerline-to-centerline were 279 mm for levels one and ten and 229 mm for levels two through eight. Each of the three bay widths were 305 mm from column centerline-to-centerline (Fig. 2.2).

The reinforcement was proportioned in relation to an effective peak acceleration of 0.4 g. The first-level columns and the interior second-level columns had a reinforcement ratio of 1.32%. All other columns in the structure had a reinforcement ratio of 0.88%. The flexural reinforcement ratios for the beams were 1.10% at levels one through seven and .74% at levels eight through ten (Fig. 2.2 and 2.13). The design base shear coefficient was 0.24.

6.3 Test Procedure

The test structure was subjected to three earthquake simulation tests. The input motion for the three tests was a scaled version of the north-south component of the earthquake recorded at El Centro, California (1940). The acceleration level was magnified for each test run. The maximum recorded base acceleration for runs one, two and three were 0.4 g, 0.95 g, and 1.42 g, respectively.

Before and after each earthquake simulation test, the structure was given a low-amplitude free vibration. Also after each earthquake simulation test, the structure was subjected to a steady-state test by means of a sweeping sinusoidal base motion. Table 3.1 summarizes the testing sequence.

6.4 Behavior of the Test Structure

One of the striking features of the observed response of the test structure was the apparent domination of the first mode. As seen in Fig. 4.7 through 4.24 the response histories for each particular test run were in phase, especially in run one. However, the influence of higher modes can be seen in the acceleration histories of both runs two and three.

In general, the apparent natural frequency decreased with the maximum amplitude of motion previously experienced by the test structure as shown in Fig. 5.10. However, frequency measurements differ as a function of the amplitude of motion of the particular test to measure the frequency. The measured frequencies from the free-vibration tests were consistently higher while those from the earthquake simulation tests were consistently lower. A similar trend may be seen to have occurred for the measured second and third-mode frequencies. Table 5.1 summarizes the measured frequencies of the structure.

Damping factors obtained from the free-vibration tests using the logarithmic decrement method, were found to have increased after each earthquake simulation test. The measured equivalent damping factors are given in Table 5.3. A similar trend can be seen in the results of the steady state tests (Fig. 5.9). The amplification ratio at apparent resonance decreased from test to test, especially from the first to the second test.

The response maxima of the earthquake simulation tests are summarized in Tables 4.2, 4.3 and 4.4. The maximum tenth-story displacement in the design earthquake test was 23.6 mm, or 1% of the height of the structure. The maximum inter-story displacement was 4.8 mm, or 1.7% of the story height, occurring between the base and the first level.

The maximum observed displacements in the design earthquake test along with maximum displacements indicated by various linear dynamic response analyses are shown in Fig. 5.12. The linear analyses included a substitute-structure model based on both the assumed and obtained response spectra. An "elastic" analysis was made of the structure using the gross-section stiffness for the components of the structure. The displacements

indicated by the elastic analysis are appreciably lower than those observed. Although the substitute-structure analysis indicates displacements comparable to those observed, the calculated displacements at the lower four stories were exceeded during the design earthquake.

The maximum observed base shear during the first run was 15.6 kN, or 0.35 W, where W is the weight of the test structure. The elastic analysis (based on response to measured base motion at a damping factor of 0.1) described above indicates a maximum base shear of 24 kN, or 0.54 W. As might be expected, the elastic analysis indicated displacements much lower and forces much higher than those observed.

The maximum observed base shear versus the maximum tenth-level displacement in the earthquake simulation test is presented in Fig. 5.20. The plot suggests that general yielding of the structure was reached during the "design earthquake." However, the crack pattern in the structure after run one (Fig. 4.27) showed little visible damage to the structure. In fact, most residual crack widths were too small to measure (less than 0.05 mm). The crack pattern in the structure after runs two and three (Fig. 4.28 and 4.29) showed spalling at the exterior base columns and substantial cracking throughout the structure.

Based on the little apparent damage incurred to the structure and the maximum observed displacements of the structure during run one, the structure was well behaved during the "design earthquake". However, the fact that observed displacements at the lower levels of the structure exceeded the displacements indicated by the substitute-structure analysis suggests that modifications need to be incorporated into the design process at the lower levels of the structure.

LIST OF REFERENCES

1. Aristizabal-Ochao, J. D., and M. A. Sozen, "Behavior of Ten-Story Reinforced Concrete Walls Subjected to Earthquake Motions," Civil Engineering Studies, Structural Research Series No. 431, University of Illinois, Urbana, October 1976.

2. Clough, R. W., and J. Penzien, Dynamics of Structures, McGraw-Hill, 1975.

3. Gulkan, P., and M. A. Sozen, "Response and Energy-Dissipation of Reinforced Concrete Frames Subjected to Strong Base Motions," Civil Engineering Studies, Structural Research Series No. 377, University of Illinois, Urbana, May 1971.

4. Jacobsen, L. S., "Steady Forced Vibration as Influenced by Damping," Transactions, ASME, Vol. 52, Part 1, 1930.

5. Lybas, J. M., and M. A. Sozen, "Effect of Beam Strength and Stiffness on Dynamic Behavior of Reinforced Concrete Coupled Walls," Civil Engineering Studies, Structural Research Series No. 444, University of Illinois, Urbana, July 1977.

6. Otani, S., and M. A. Sozen, "Behavior of Multistory Reinforced Concrete Frames During Earthquakes," Civil Engineering Studies, Structural Research Series No. 392, University of Illinois, Urbana, November 1972.

7. Shibata, A., and M. A. Sozen, "The Substitute-Structure Method for Earthquake-Resistant Design of Reinforced Concrete Frames," Civil Engineering Studies, Structural Research Series No. 412, University of Illinois, Urbana, October 1974.

Table 2.1 Flexural Reinforcing Schedule

Level	Number of No. 13g Wires Per Face		
	Beams	Interior Columns	Exterior Columns
10	2	2	2
9	2	"	"
8	2	"	"
7	3	"	"
6	"	"	"
5	"	"	"
4	"	"	"
3	"	2	"
2	"	3	2
1	3	3	3

Table 3.1

Sequence of Test Procedure

1. Free Vibration

2. Earthquake Motion Run 1

3. Free Vibration

4. Steady State Run 1

5. Free Vibration

6. Earthquake Motion Run 2

7. Free Vibration

8. Steady State Run 2

9. Free Vibration

10. Earthquake Motion Run 3

11. Free Vibration

12. Steady State Run 3

13. Free Vibration

Table 4.1 Spectrum Intensities for Observed Base Motions

Test Run	Spectrum Intensity, mm $* 10^{-3}$				
	Damping Factor B				
	0.0	0.02	0.05	0.10	0.20
1	0.598	0.378	0.299	0.241	0.199
2	1.061	0.671	0.534	0.433	0.362
3	1.274	0.799	0.634	0.517	0.435

Note: Housner's Intensity over a period range of 0.04 to 1.0 sec.

Table 4.2 Observed Maximum Single-Amplitude Horizontal Accelerations

Story Level	Acceleration, g		
	Run 1	Run 2	Run 3
10	0.76	1.24	1.64
9	0.60	0.87	1.06
8	0.51	0.67	0.73
7	0.49	0.59	0.72
6	0.41	0.54	0.78
5	0.40	0.68	0.74
4	0.43	0.81	0.78
3	0.46	0.77	0.77
2	0.50	0.66	1.09
1	0.40	0.59	1.21
Base	0.40	0.93	1.42

Table 4.3 Observed Maximum Single-Amplitude Horizontal Displacements

Story Level	Displacement, mm		
	Run 1	Run 2	Run 3
10	23.6	51.2	68.1
9	22.8	48.6	66.3
8	21.3	46.3	60.9
7	20.7	44.5	57.4
6	18.6	40.6	52.2
5	16.7	33.0	40.0
4	14.4	31.0	38.3
3	12.3	25.7	30.0
2	8.3	16.7	20.1
1	4.8	9.9	11.9

Table 4.4 Observed Maximum Single-Amplitude Story Shears and Base Overturning Moment

Story Level	Shear, kN		
	Run 1	Run 2	Run 3
10	4.0	5.6	7.4
9	5.9	9.4	11.0
8	8.1	11.8	13.2
7	9.6	13.0	14.1
6	10.9	13.7	14.3
5	12.3	14.0	14.8
4	13.3	14.9	14.9
3	14.2	15.8	15.4
2	15.1	15.6	15.2
1	15.6	16.5	16.2
	Overturning Moment, kN-M		
Base	25.3	31.4	30.0

Table 5.1

Measured Frequencies of the Test Structure

Test	Run	Frequency (Hz)		
		Mode 1	Mode 2	Mode 3
Earthquake	1	2.0	7.7	15.0
simulation	2	1.4	6.2	12.3
	3	1.1	5.4	9.6
Free Vibration	before run 1	3.2	15.6	26.5
	after run 1	2.9	10.6	19.0
	after run 2	2.3	8.7	15.4
	after run 3	1.9	7.5	12.9
Steady State	after run 1	2.1		
	after run 2	1.7		
	after run 3	1.4		

Table 5.2

Maximum Amplification Ratio and Apparent
Resonance from the Steady-State Tests

Test Sequence	Maximum Amplification Ratio	Apparent Resonance (Hz)
After run 1	5.7	2.1
After run 2	4.1	1.7
After run 3	3.8	1.4

Table 5.3

Measured Equivalent Damping Factor
from the Free-Vibration Tests

Test Sequence	Damping Factor
Before run 1	1.9
After run 1	5.6
Before run 2	5.8
After run 2	7.8
Before run 3	8.4
After run 3	10.2

Table 5.4

Calculated First-Mode Frequencies
of the Test Structure

Analysis Type	First Mode Frequency (Hz)
Substitute-structure	1.8
Gross-section	3.6

914 mm

Masses

Bellows

Reinforced
Concrete
Frames

Pin Connection
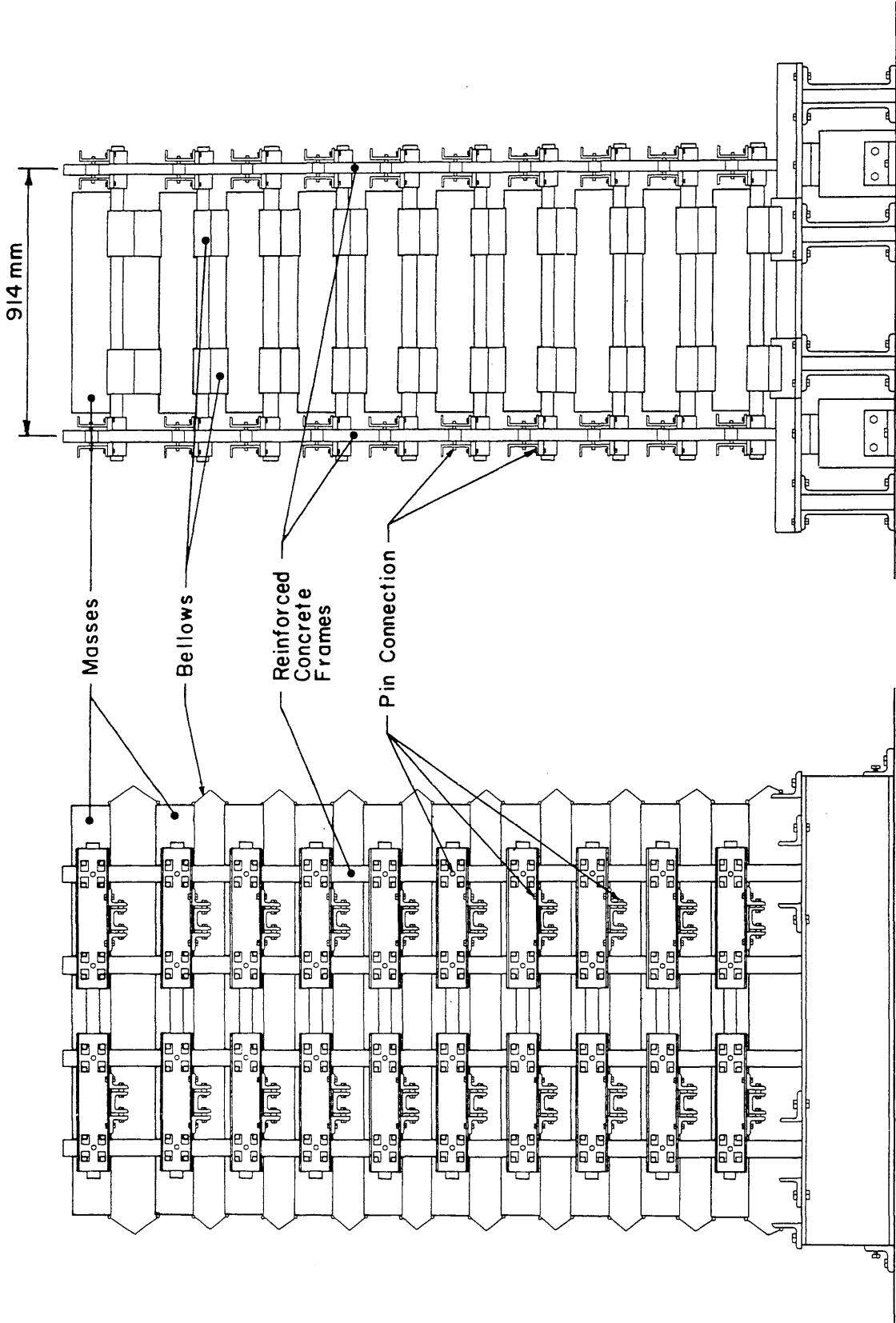
b) Front View

a) Side View

Fig. 2.1 Test Structure
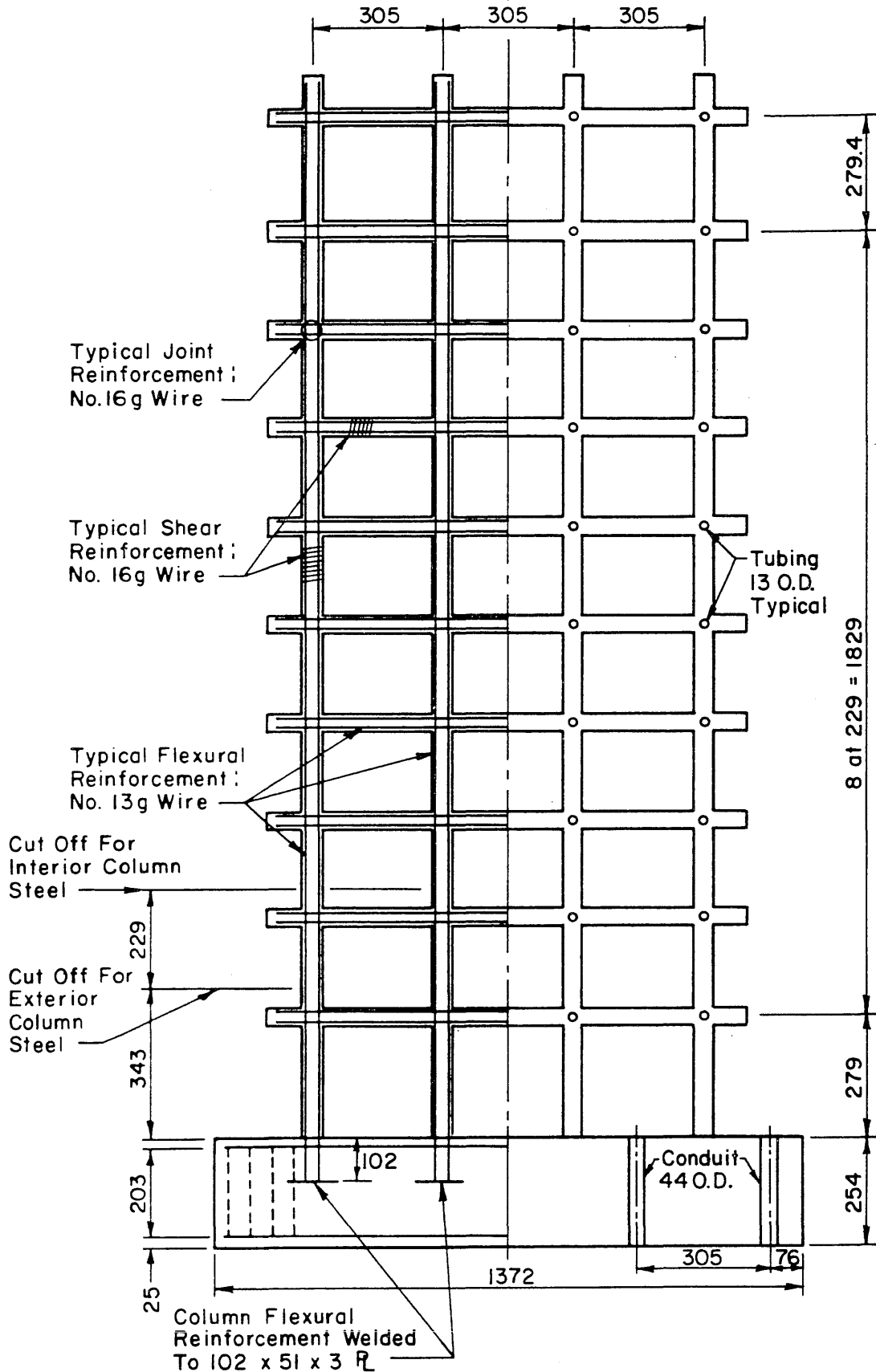
Fig. 2.2 Reinforcement Detail and Dimensions of the Test Structure

(All Dimensions In Meters)

Test Structure

Steel Reference
Frame

Test Platform

Hydraulic Servoram

Steel Pedestal

Laboratory
Test Floor

Pin-Ended
Supports

2.7

0.14

0.8

0.91

2.29

0.91

0.91

0.91

41
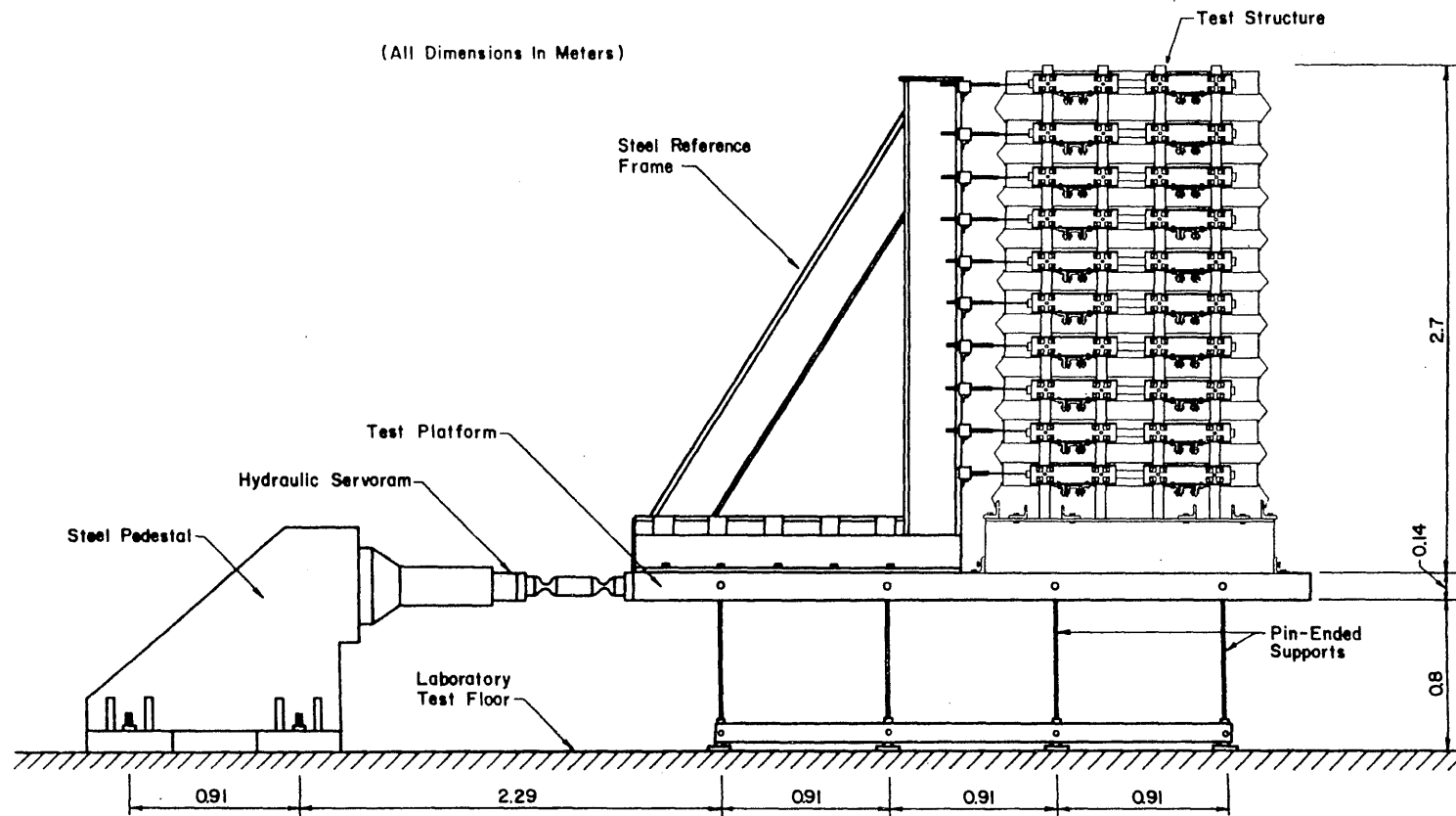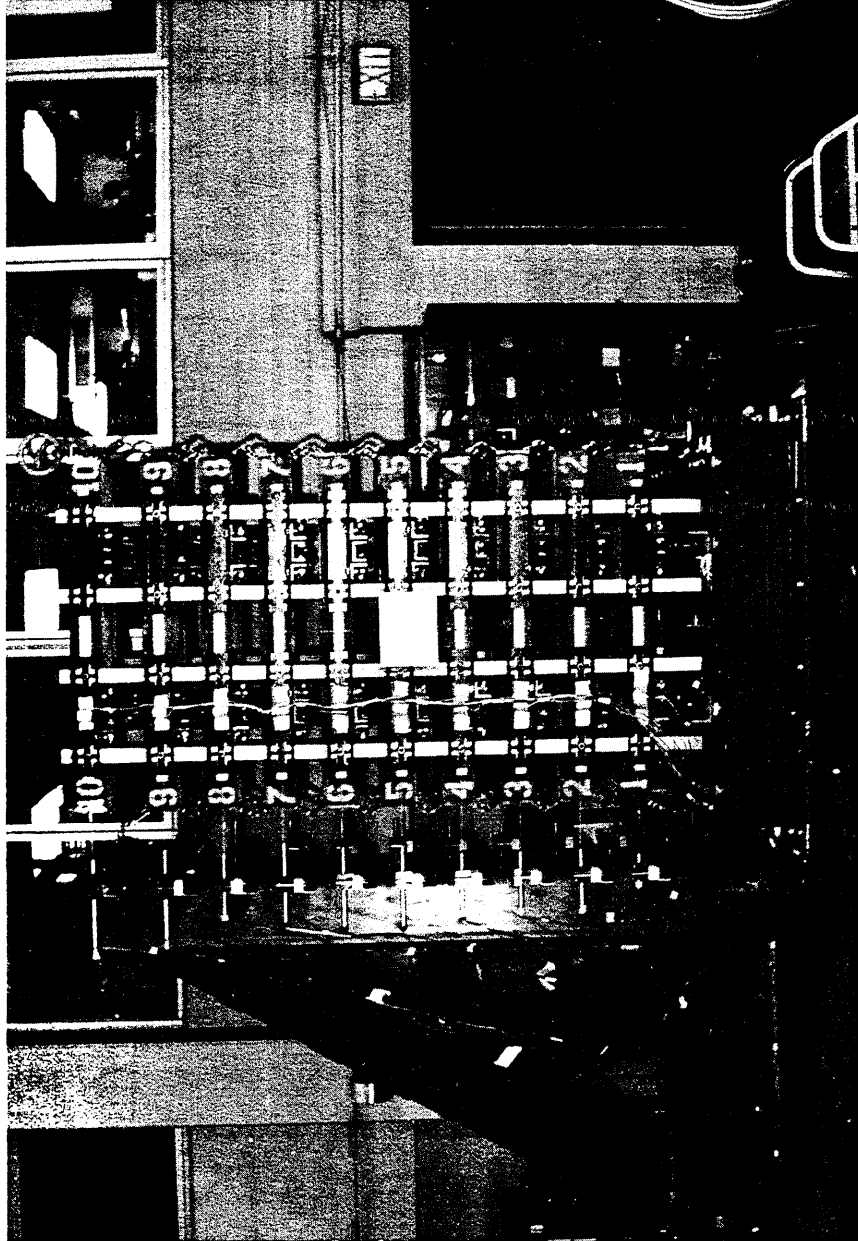
Fig. 2.3 Test Setup

Fig. 2.4 Photograph of Test Setup
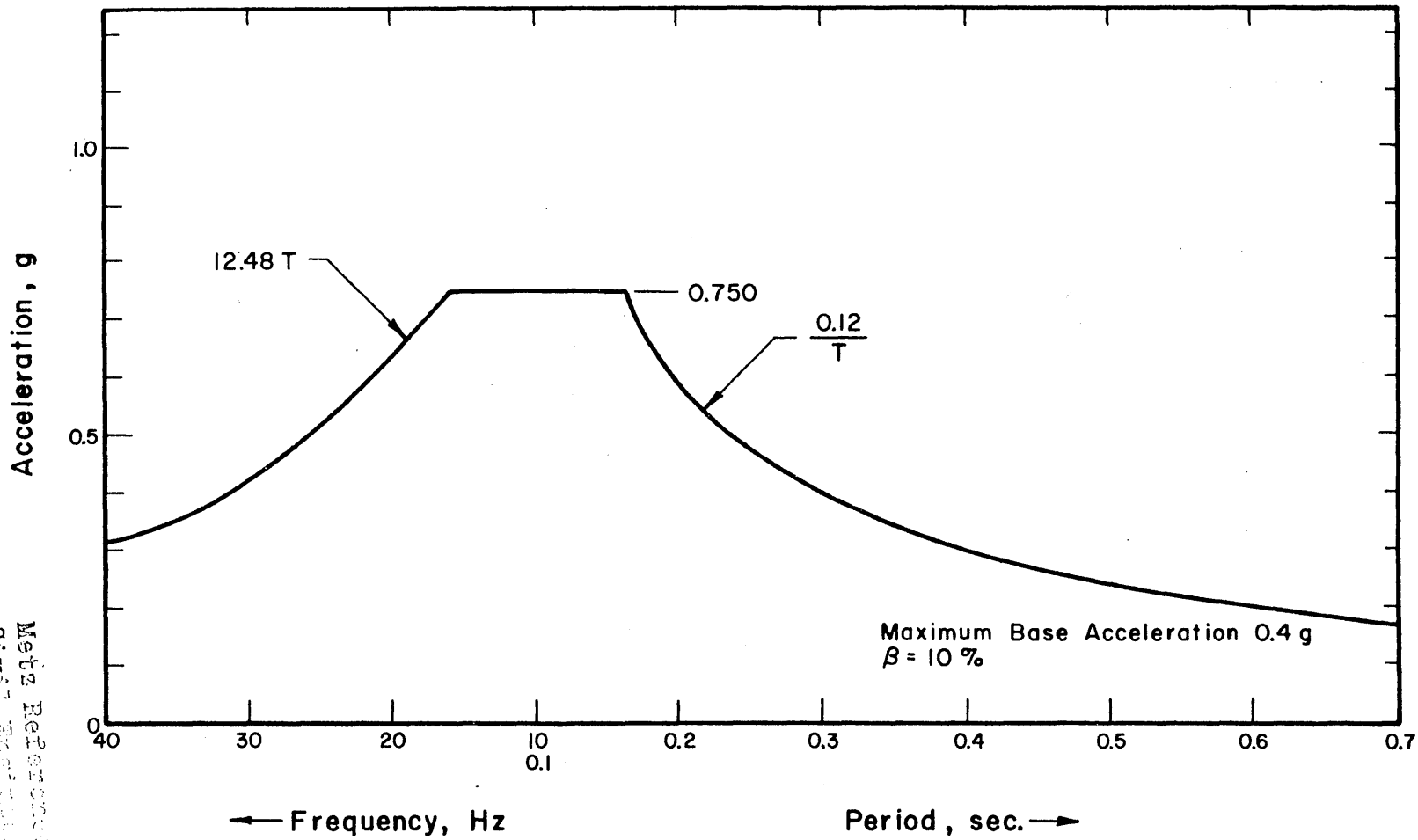
Fig. 2.5 Design Spectrum

43
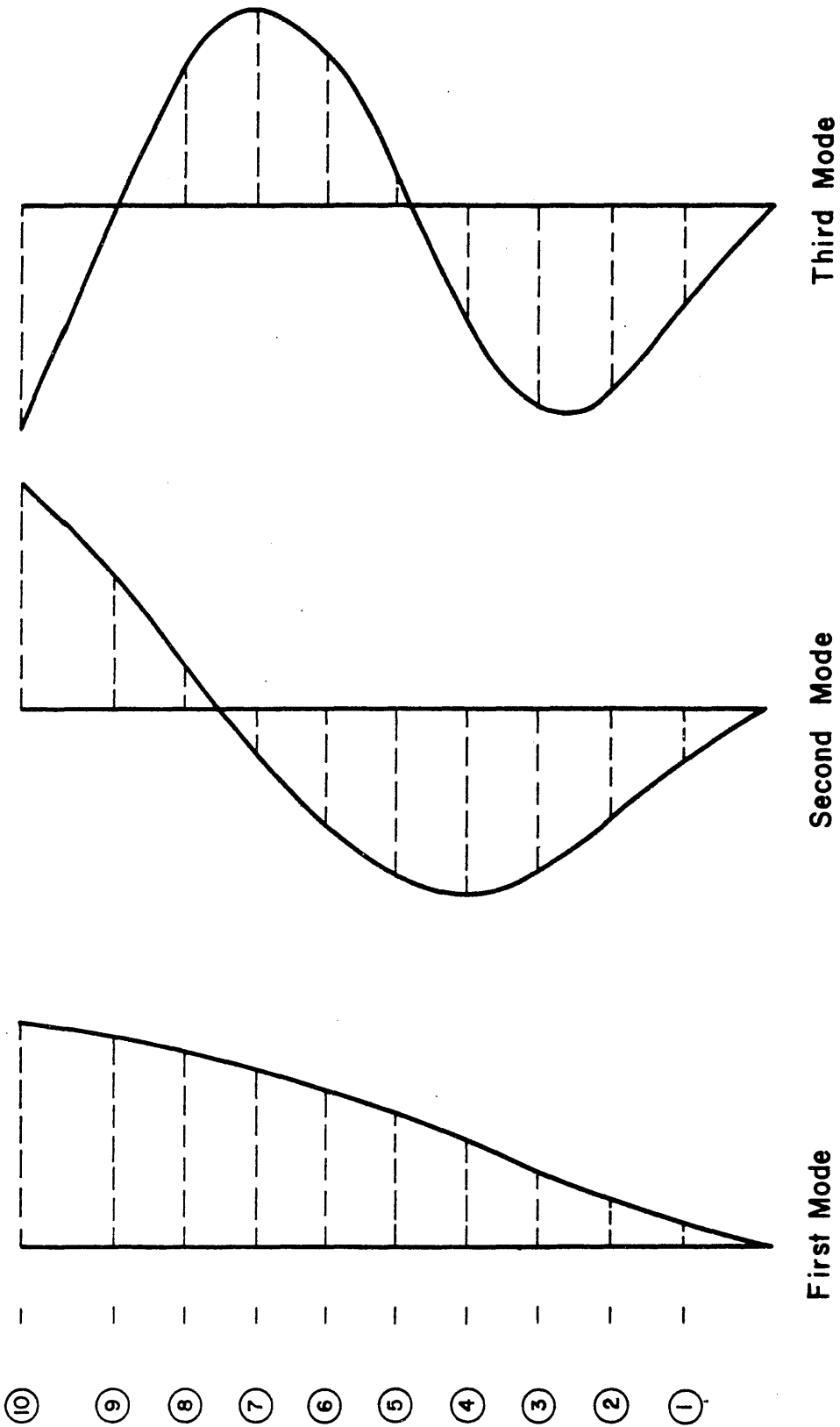
Fig. 2.6 Mode Shapes Used for Force Calculations
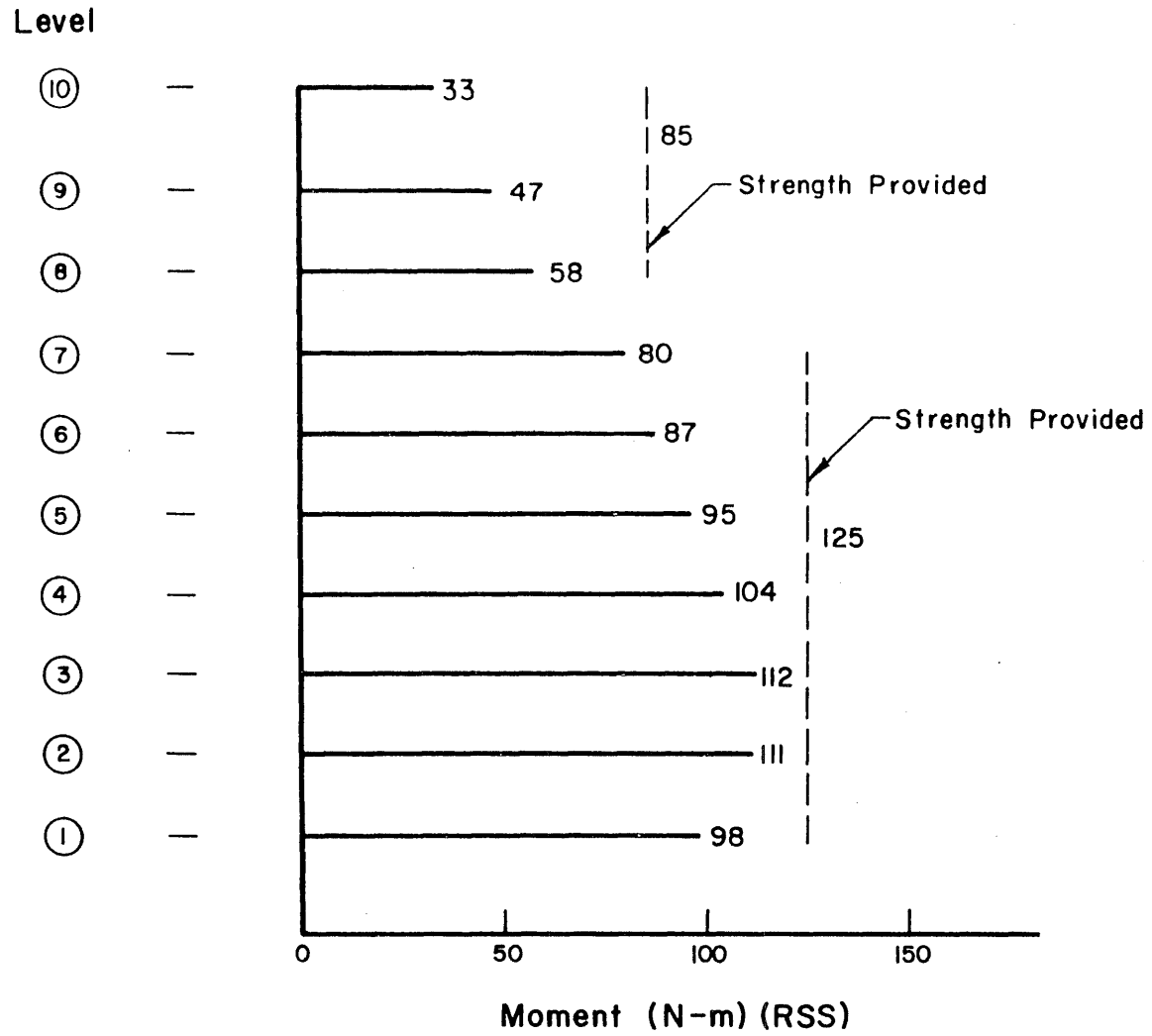
Fig. 2.7 Design Beam Moments and Strength Provided in the Beams

Level

⑩

⑨

⑧

⑦

⑥

⑤

④

③

②

①

170

340

400

440

500

560

600

700

650

930

0　　　　500　　　1000
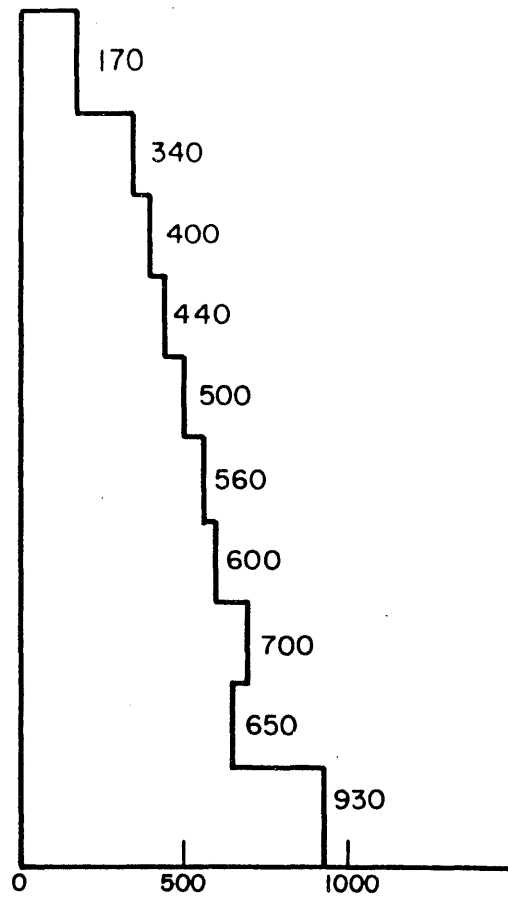
**Story Shear Force
Exterior Columns (N)(RSS)**

410

590

760

890

980

1060

1170

1200

1390

1130

0　　　　500　　　1000
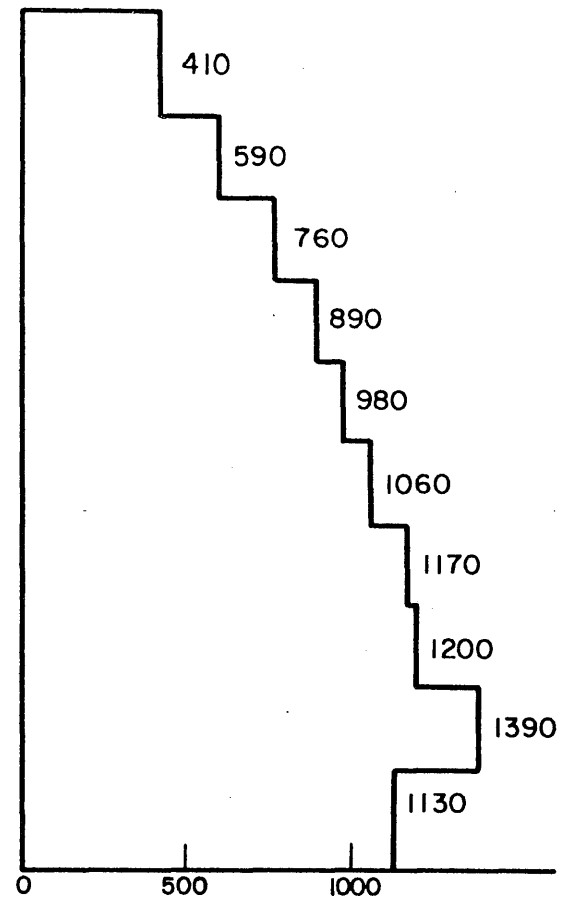
**Story Shear Force
Interior Columns (N)(RSS)**

46

Fig. 2.8 Distribution of Column Design Shear Forces
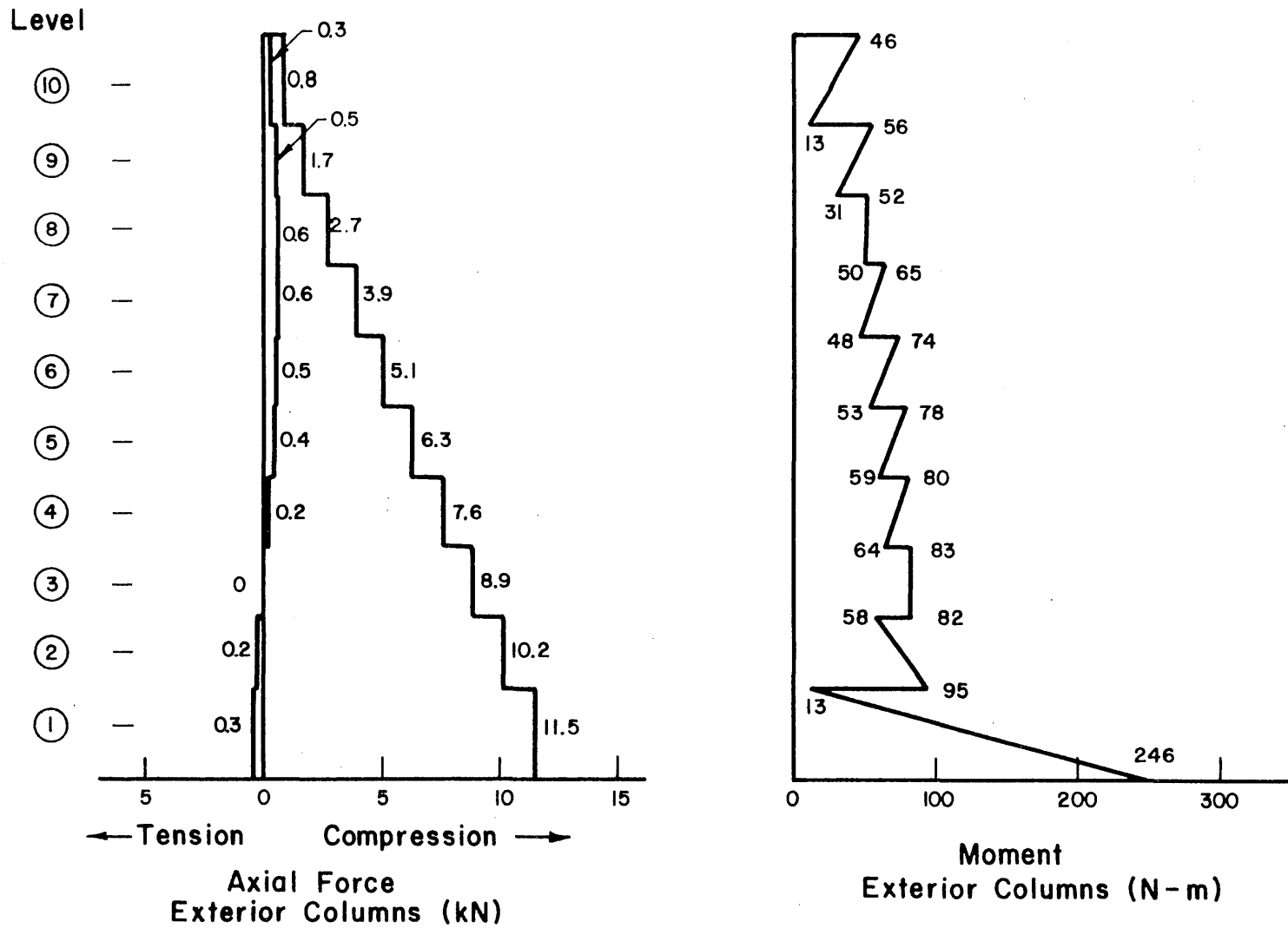
Fig. 2.9 Design Axial Forces and Moments for Exterior Columns

Level

10	—	0.6
9	—	1.1
8	—	1.7
7	—	2.2
6	—	2.8
5	—	3.3
4	—	3.9
3	—	4.4
2	—	5.0
1	—	5.6

Compression ⟶

**Axial Force
Interior Columns**

84
37   84
55   89
90   113
94   124
103   134
114   143
126   143
132   134
          186
35   259

**Moment
Interior Columns (N-m)**
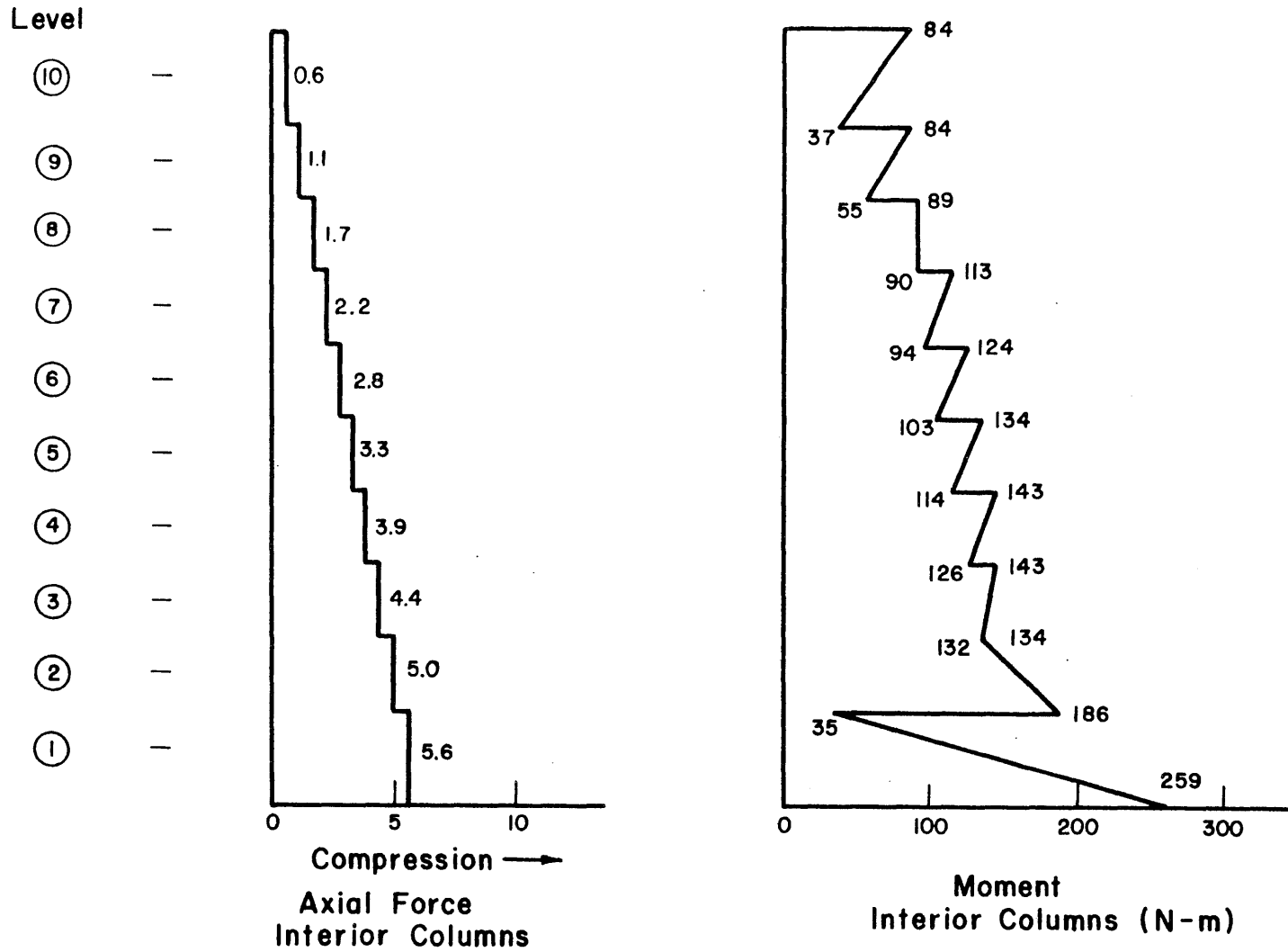
Fig. 2.10 Design Axial Forces and Moments for Interior Columns
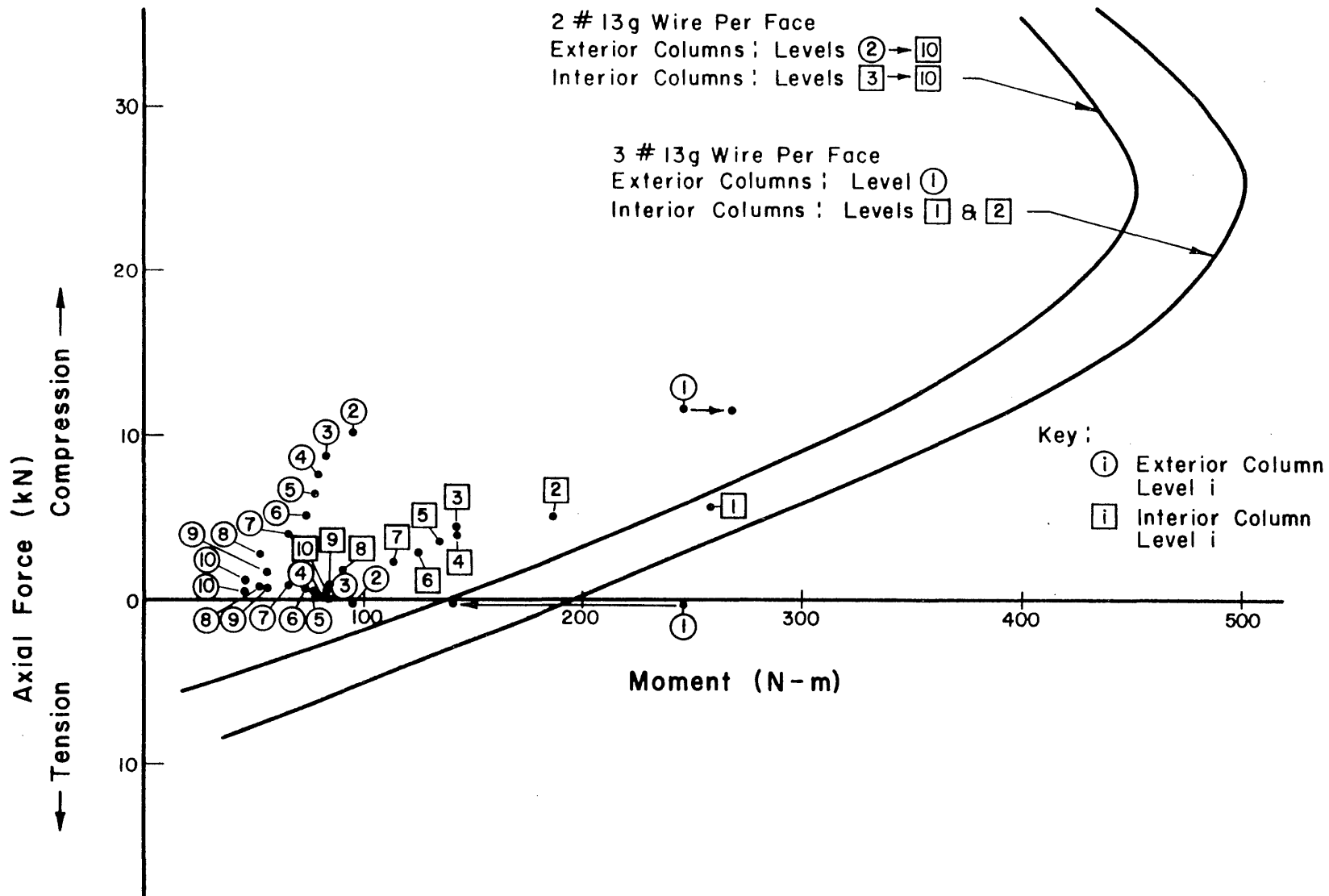
Fig. 2.11   Interaction Diagram for Columns
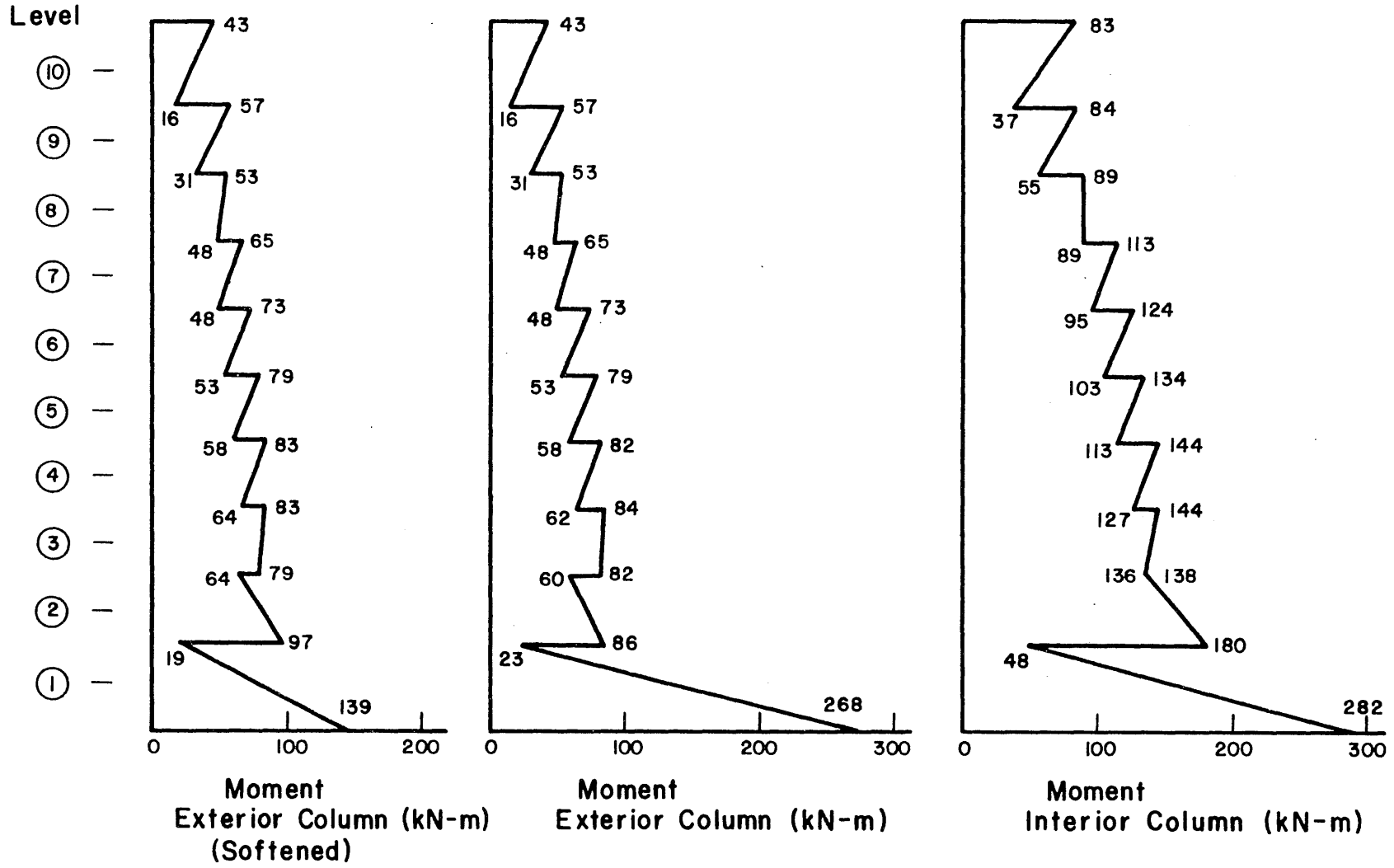
Fig. 2.12 Distribution of Moments in the Columns from a Softened-Exterior-Column Analysis

Typical Top/Column Detail

Cutoff Point For Additional Reinforcement

No. 16g Wire Spirals 31.8 O.D.- Pitch = 10

Typical End/Beam Detail

No. 16g Spirals (Typ.)

12.7 O.D. x .56 Thick Tubing

No. 13g Wire – See Frame Reinforcing Schedule For Number of Bars Per Face

Section "A"-"A"

Section "B"-"B"
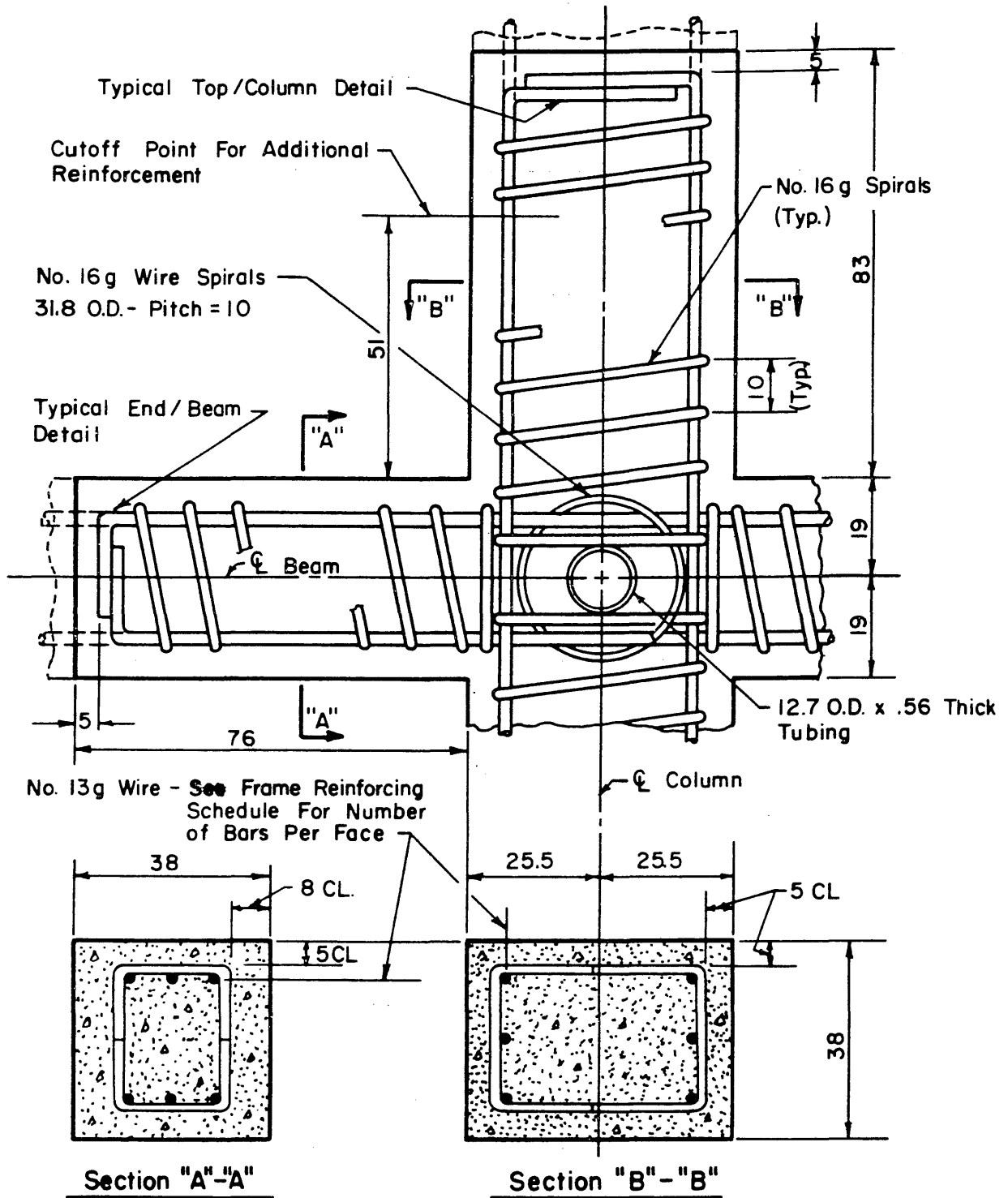
(All Dimensions Are In Millimeters)

Fig. 2.13 Typical Joint Detail in the Test Structure

Free Vibration

1. Weight Hung from Wire to Displace Structure
2. Wire Cut to Release Structure

Pulley

Wire

45 kg
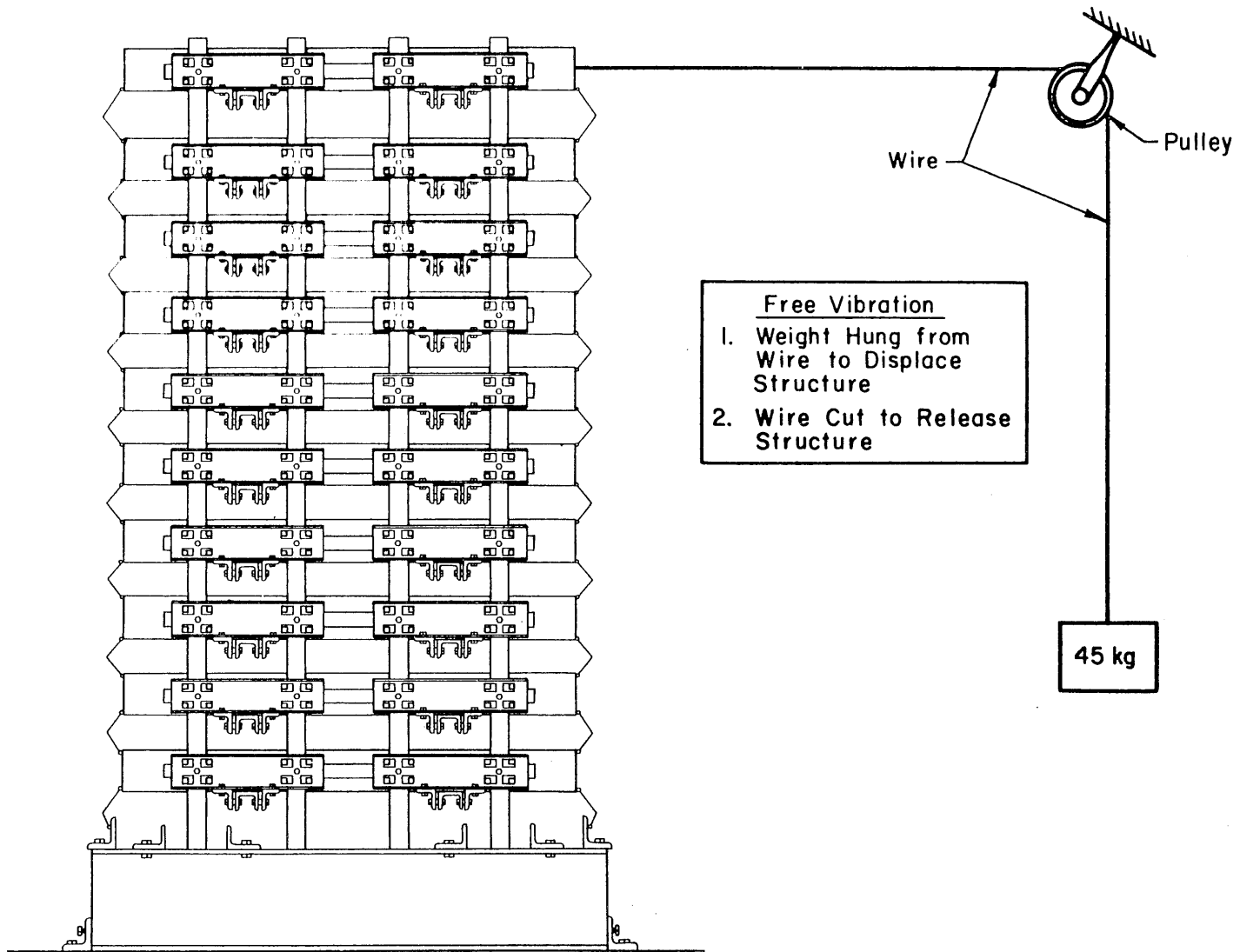
Fig. 3.1 Free Vibration Test Setup
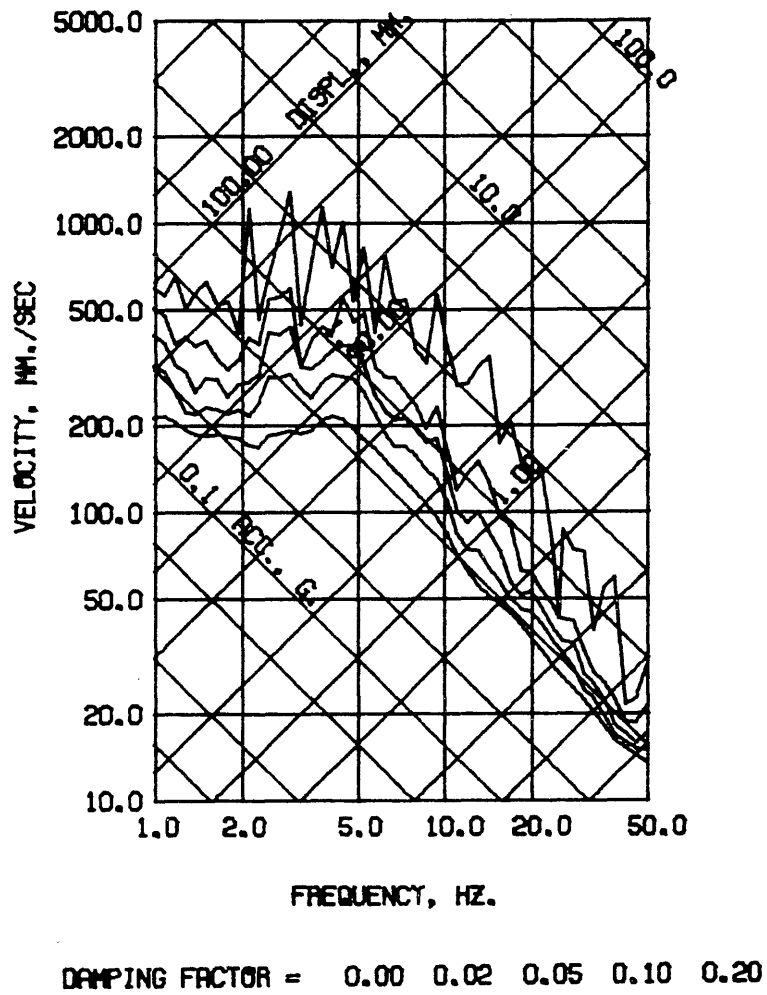
Fig. 4.1 Linear Response Spectrum, Run One
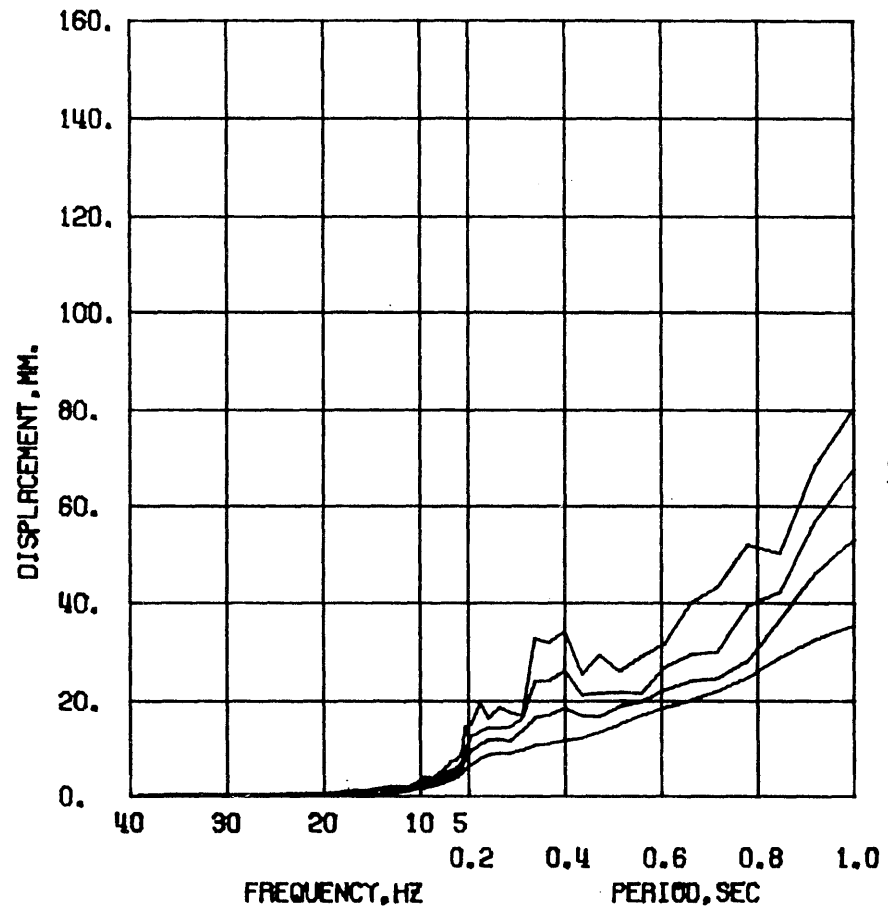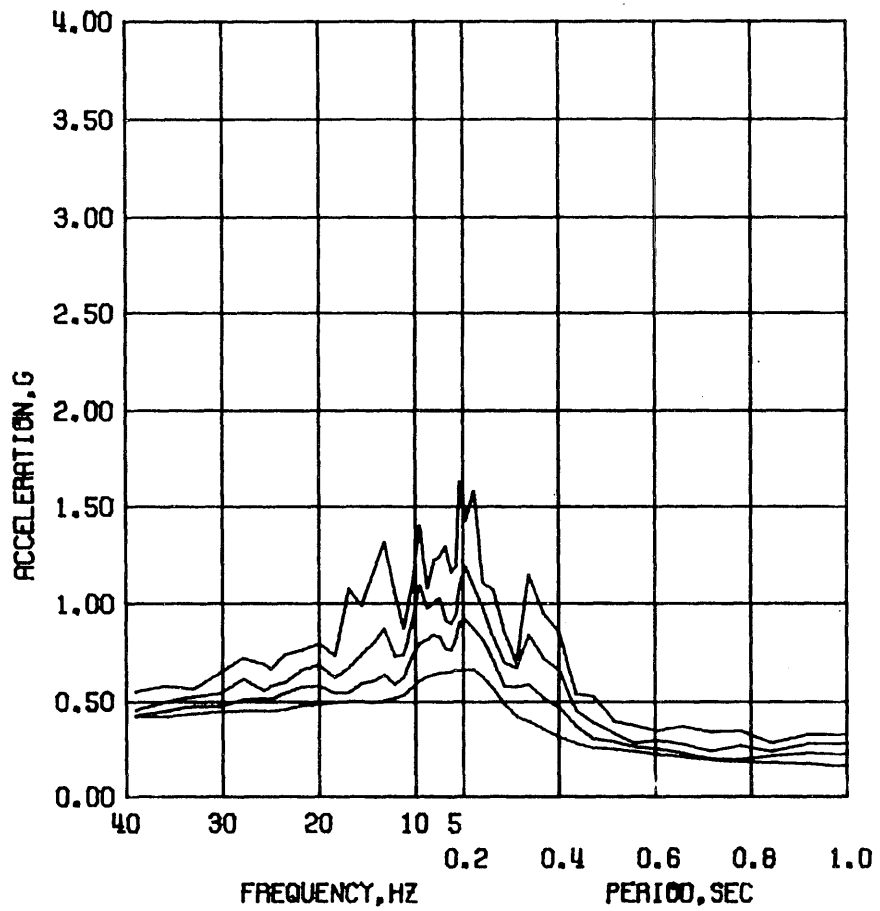
Fig. 4.2 Linear Response Spectrum, Run One
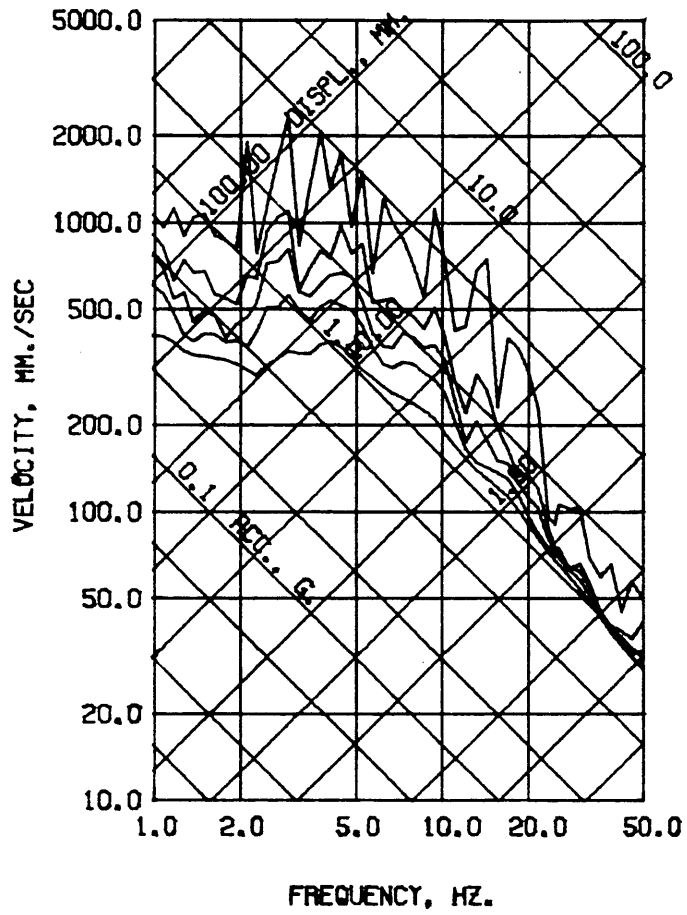
Fig. 4.3 Linear Response Spectrum, Run Two
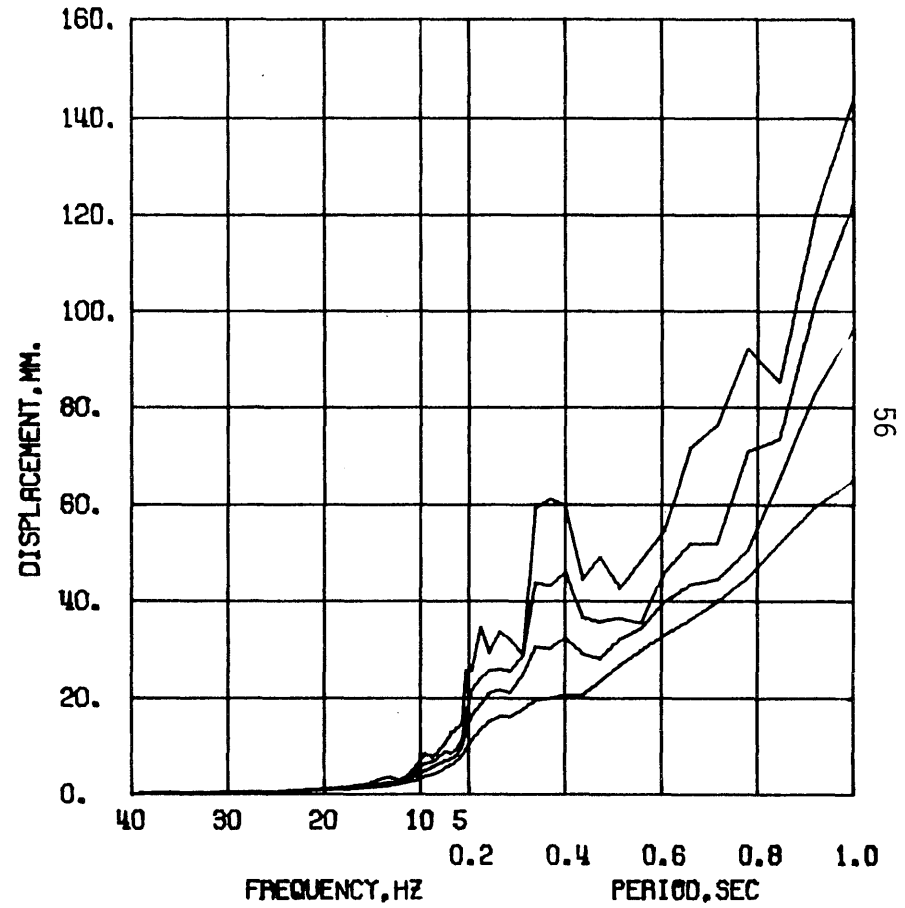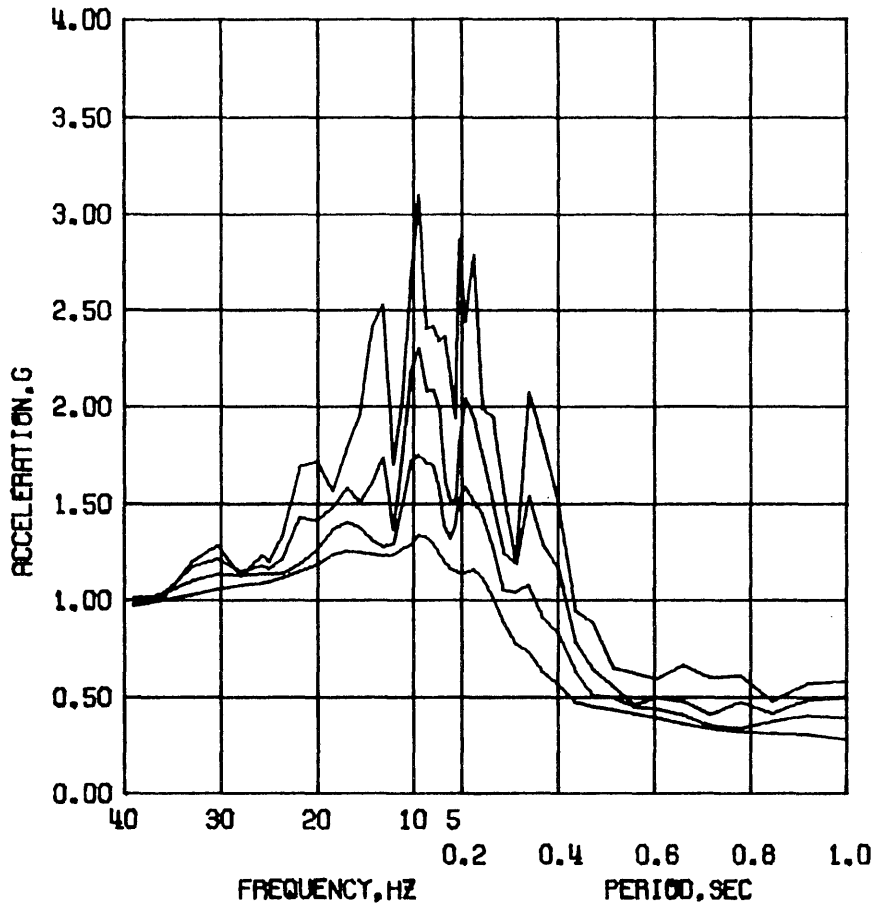
Fig. 4.4 Linear Response Spectrum, Run Two

Fig. 4.5 Linear Response Spectrum, Run Three

Fig. 4.6 Linear Response Spectrum, Run Three

TENTH LEVEL ACCELERATION. UNIT = G

NINTH LEVEL ACCELERATION. UNIT = G

EIGHTH LEVEL ACCELERATION. UNIT = G

SEVENTH LEVEL ACCELERATION. UNIT = G

SIXTH LEVEL ACCELERATION. UNIT = G

T.SEC.
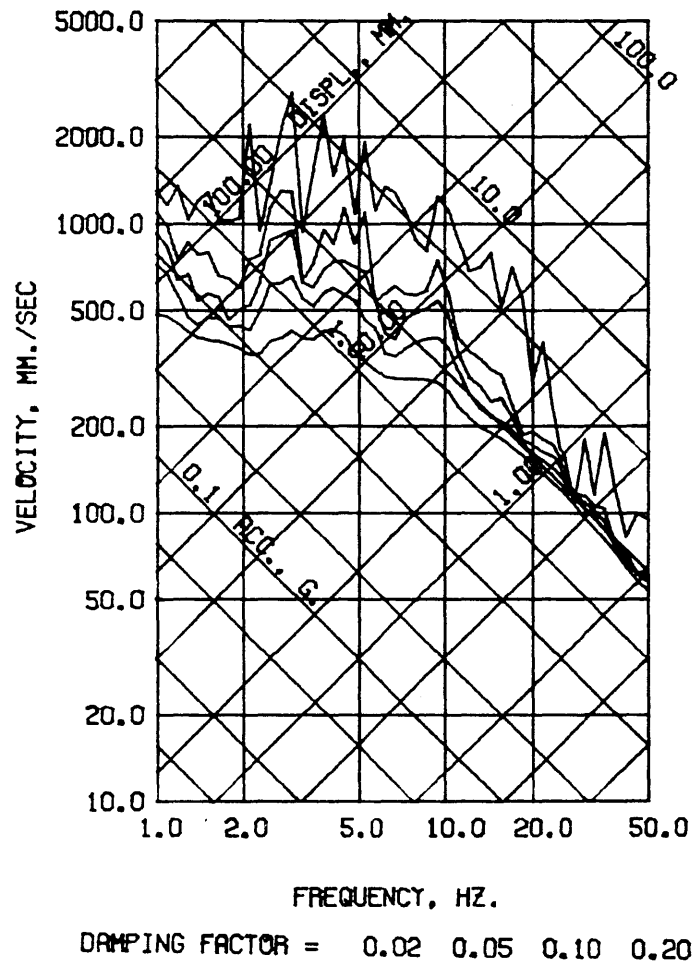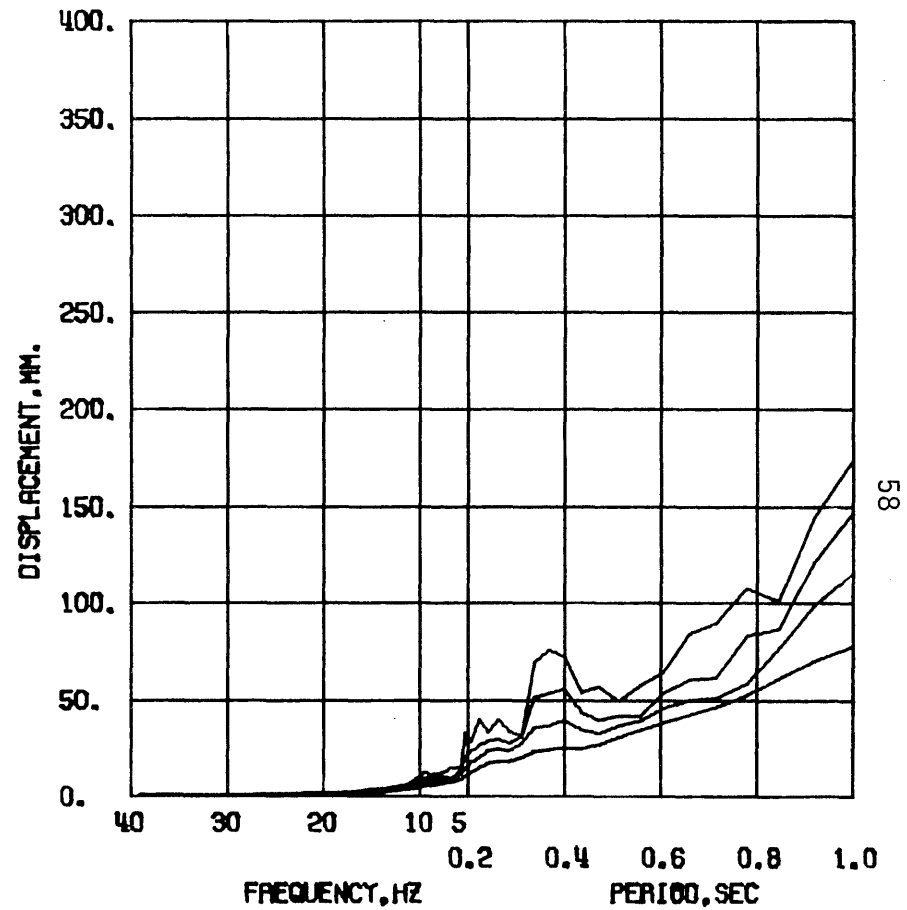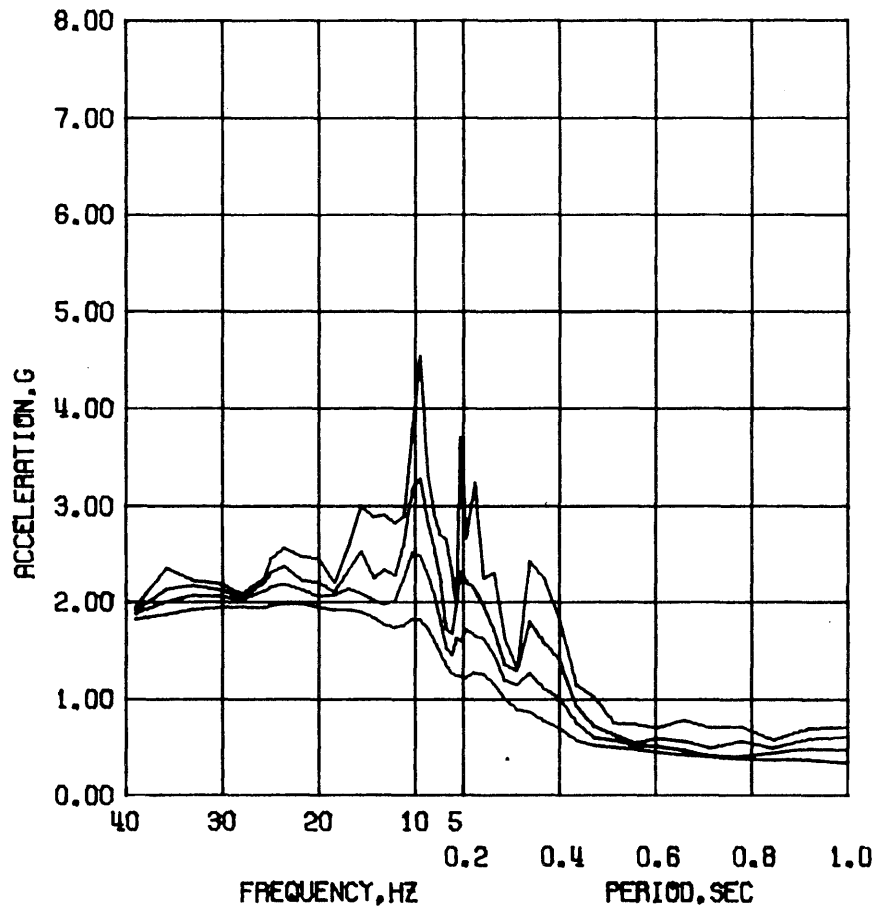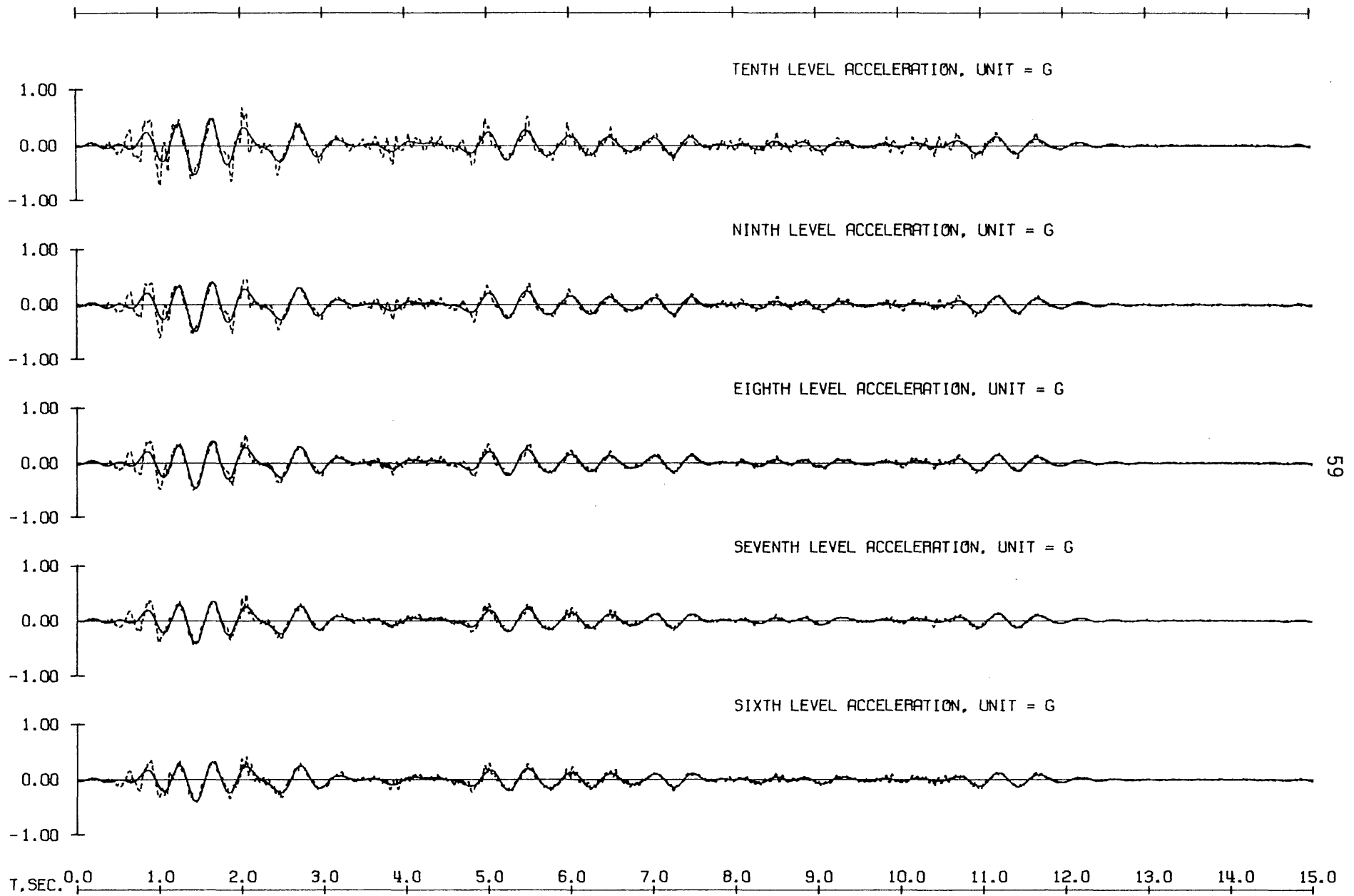
Fig. 4.7 Observed Horizontal Accelerations, Run One

Fig. 4.8 Observed Horizontal Accelerations, Run One

Fig. 4.9 Observed Horizontal Accelerations, Run Two
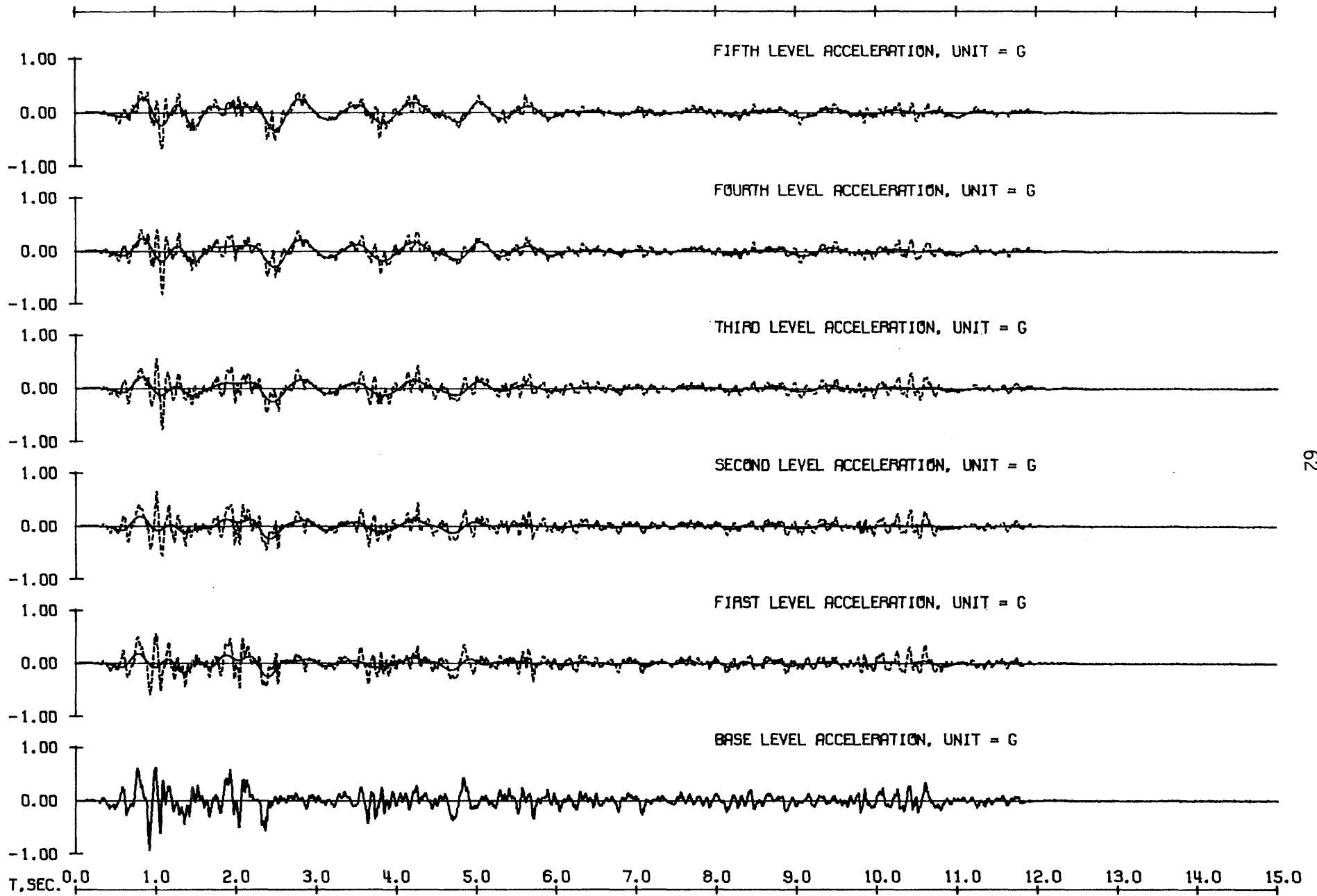
Fig. 4.10 Observed Horizontal Accelerations, Run Two
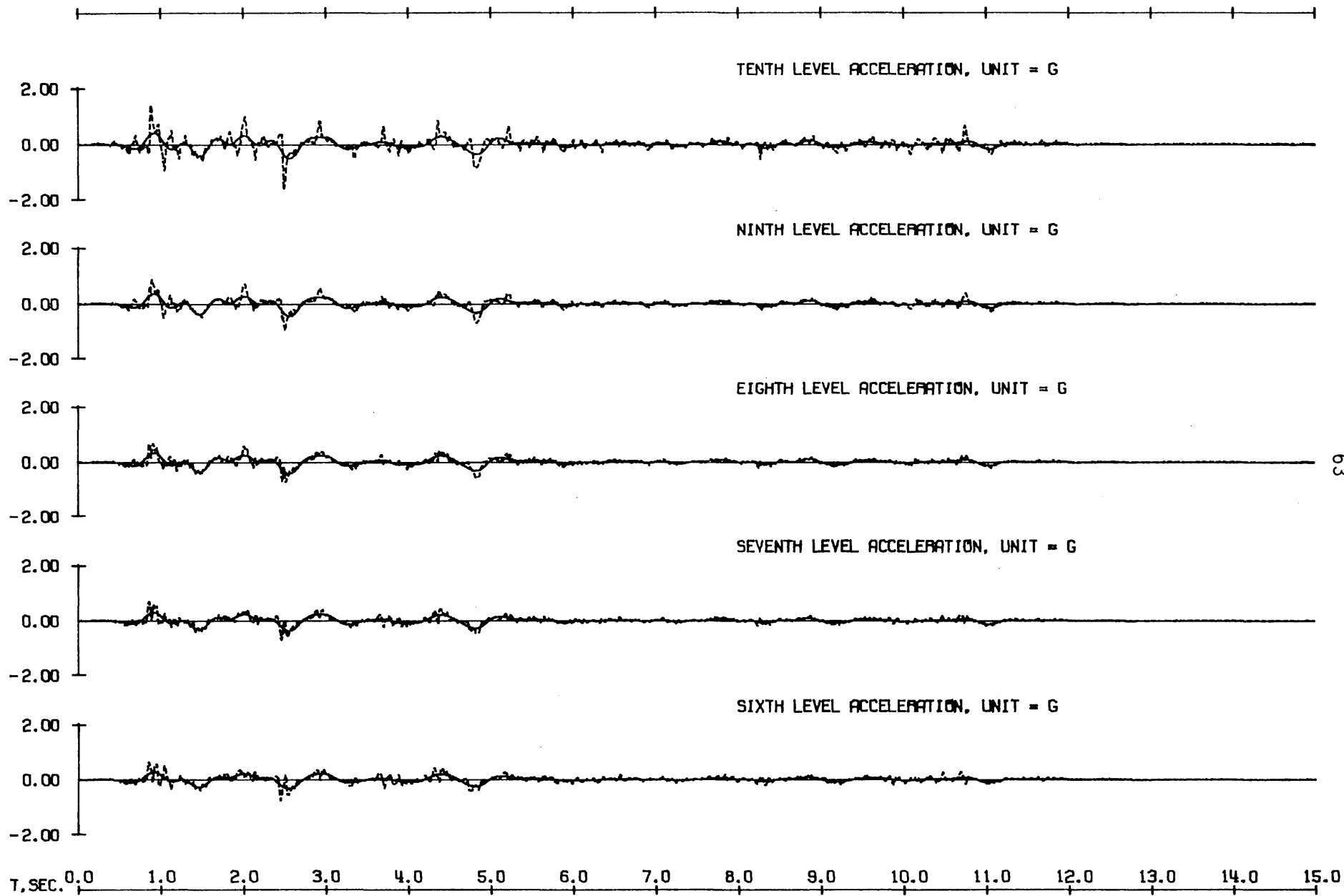
Fig. 4.11 Observed Horizontal Accelerations, Run Three
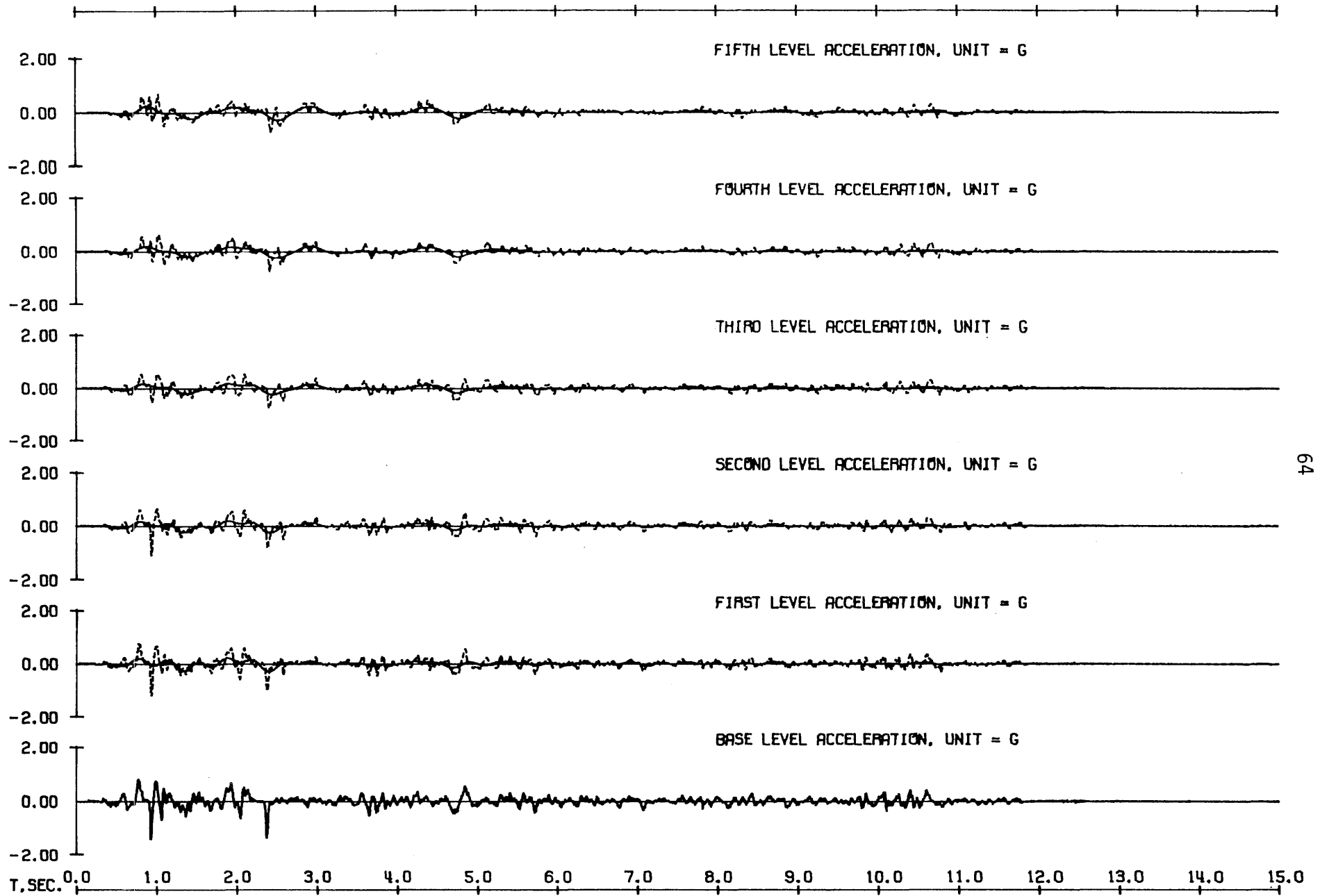
Fig. 4.12 Observed Horizontal Accelerations, Run Three
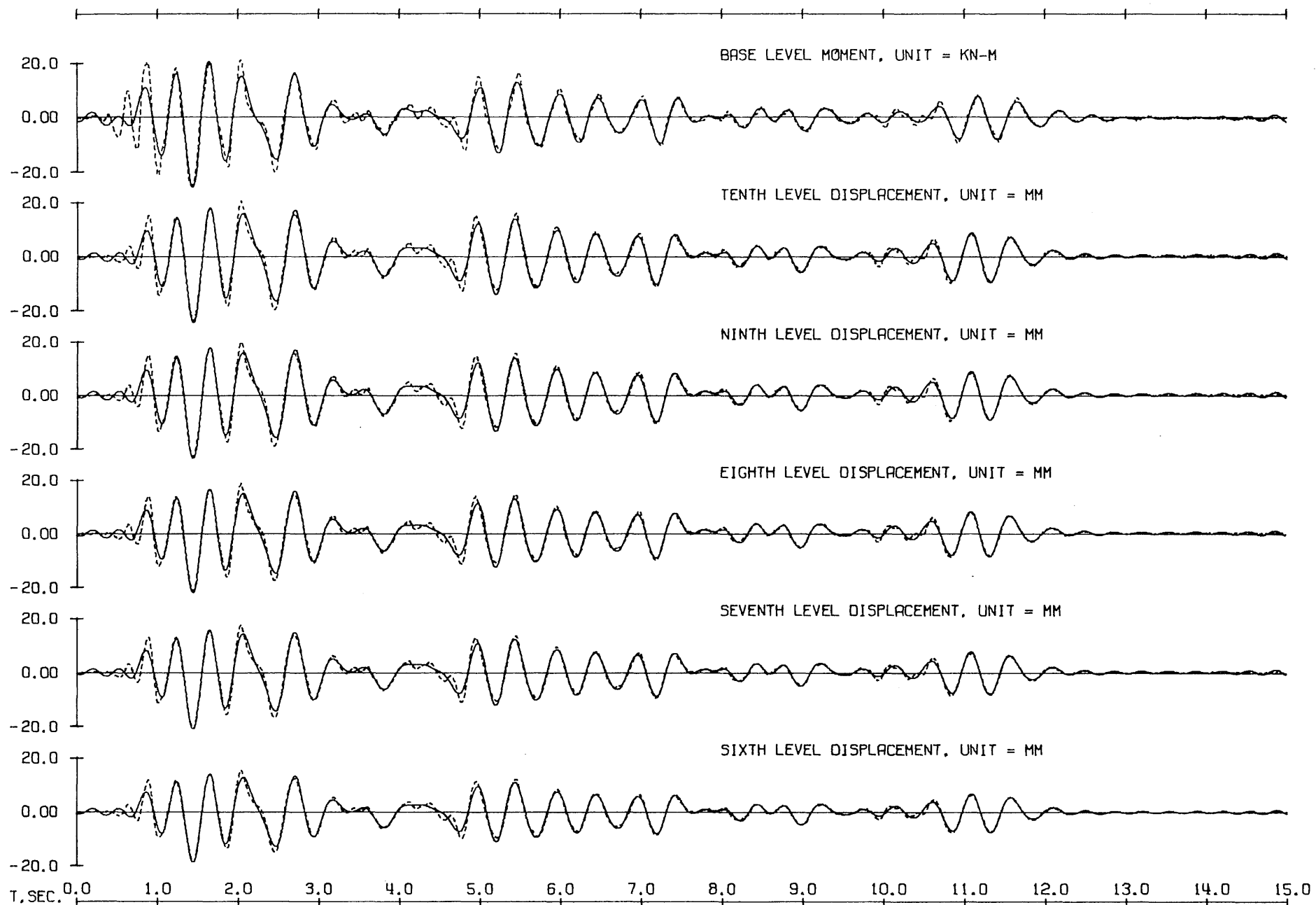
Fig. 4.13 Observed Base Overturning Moment and Horizontal Displacements, Run One

65
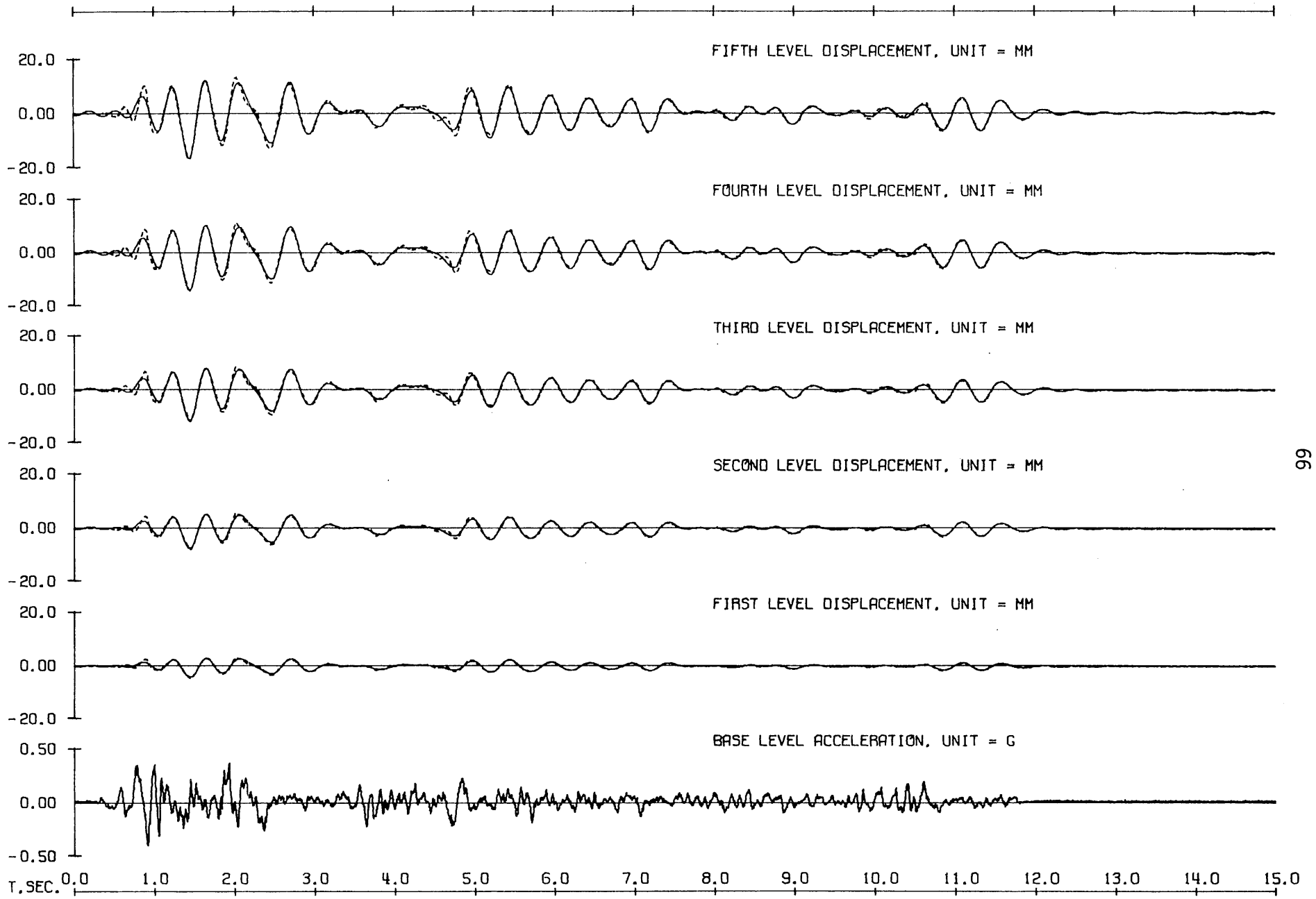
Fig. 4.14 Observed Horizontal Displacements, Run One
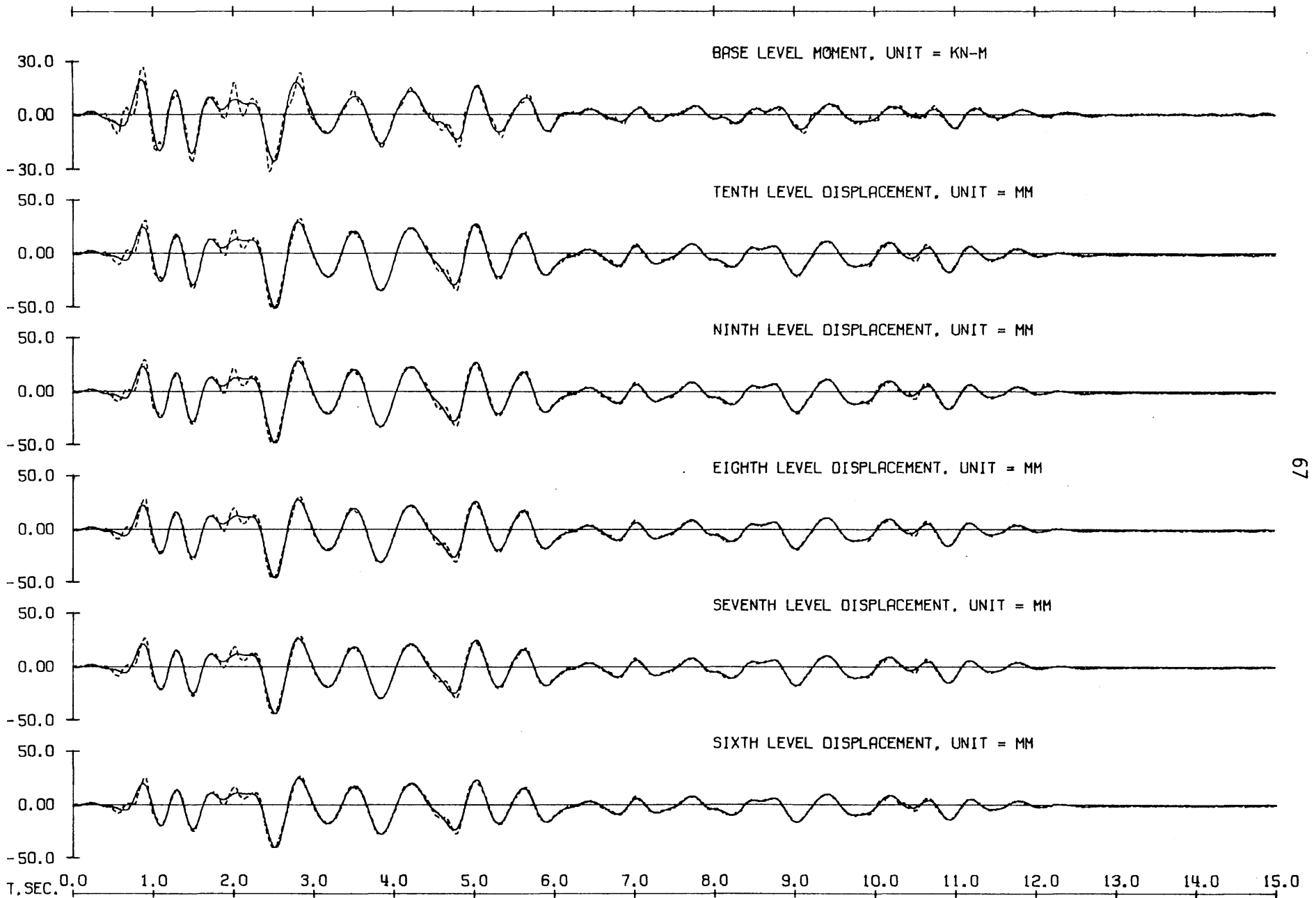
Fig. 4.15 Observed Base Overturning Moment and Horizontal Displacements, Run Two

FIFTH LEVEL DISPLACEMENT. UNIT = MM

FOURTH LEVEL DISPLACEMENT. UNIT = MM

THIRD LEVEL DISPLACEMENT. UNIT = MM

SECOND LEVEL DISPLACEMENT. UNIT = MM

FIRST LEVEL DISPLACEMENT. UNIT = MM

BASE LEVEL ACCELERATION. UNIT = G
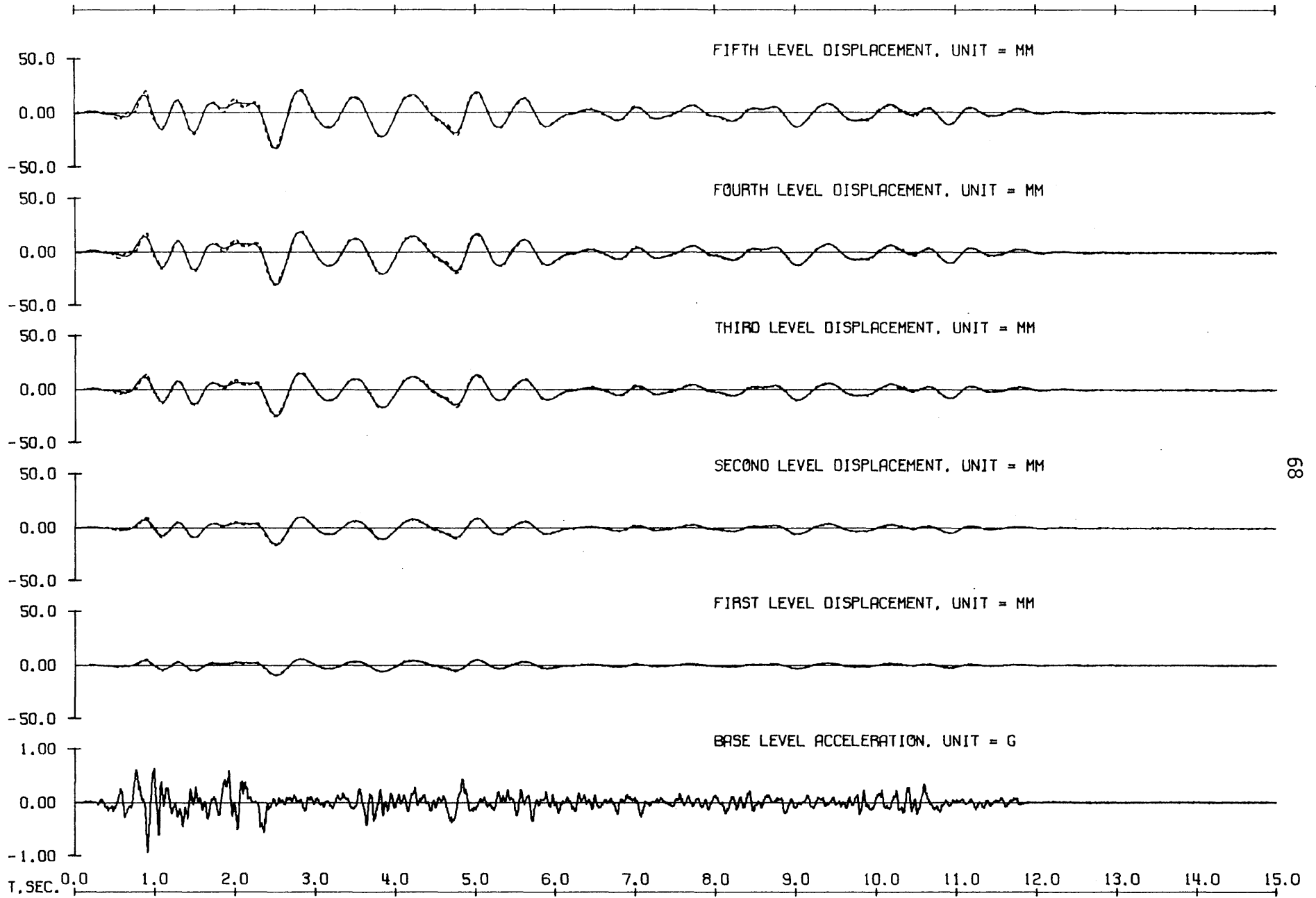
Fig. 4.16 Observed Horizontal Displacements, Run Two

BASE LEVEL MOMENT, UNIT = KN-M

TENTH LEVEL DISPLACEMENT, UNIT = MM

NINTH LEVEL DISPLACEMENT, UNIT = MM

EIGHTH LEVEL DISPLACEMENT, UNIT = MM

SEVENTH LEVEL DISPLACEMENT, UNIT = MM

SIXTH LEVEL DISPLACEMENT, UNIT = MM
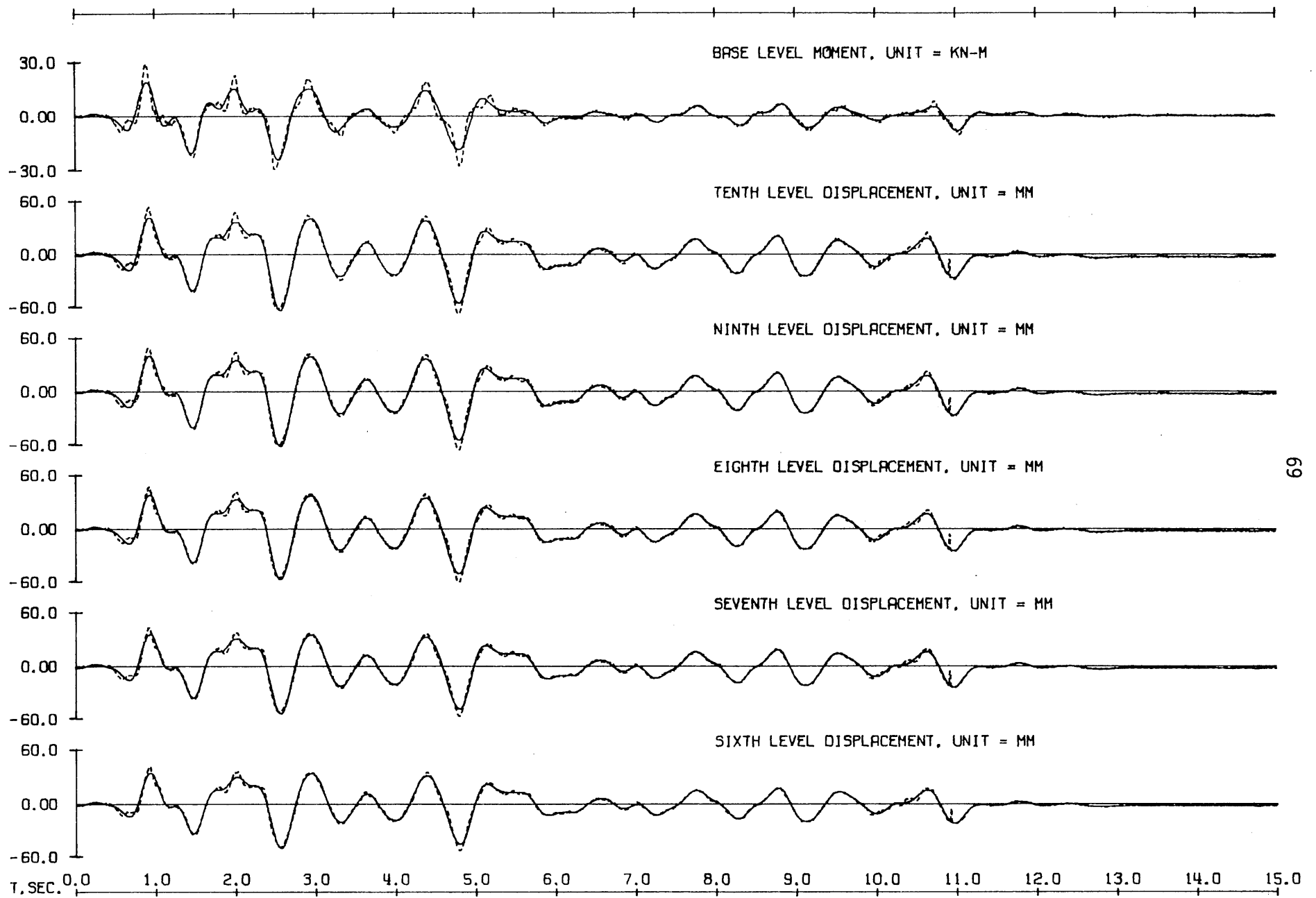
Fig. 4.17 Observed Base Overturning Moment and Horizontal Displacements, Run Three

69
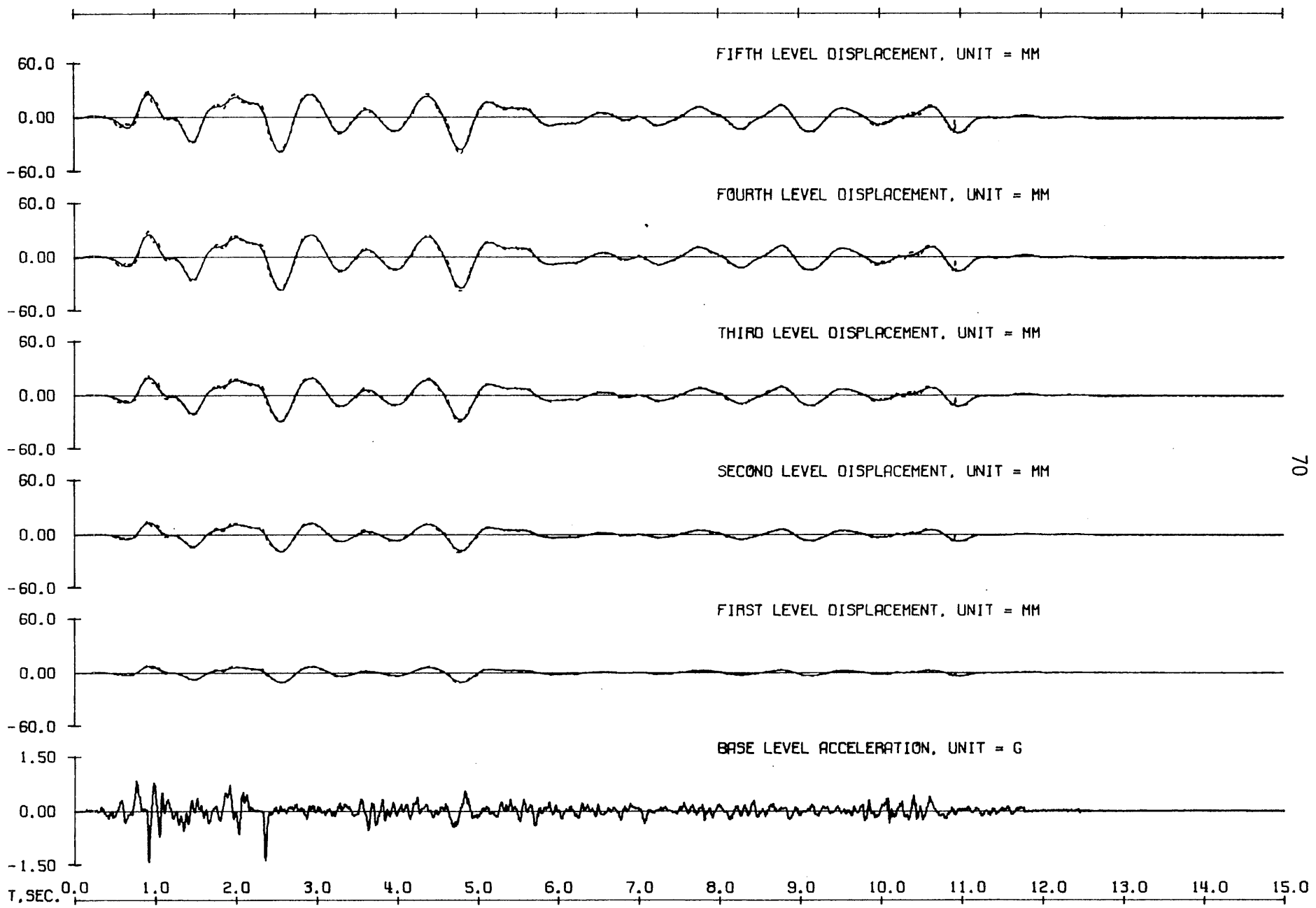
Fig. 4.18 Observed Horizontal Displacements, Run Three
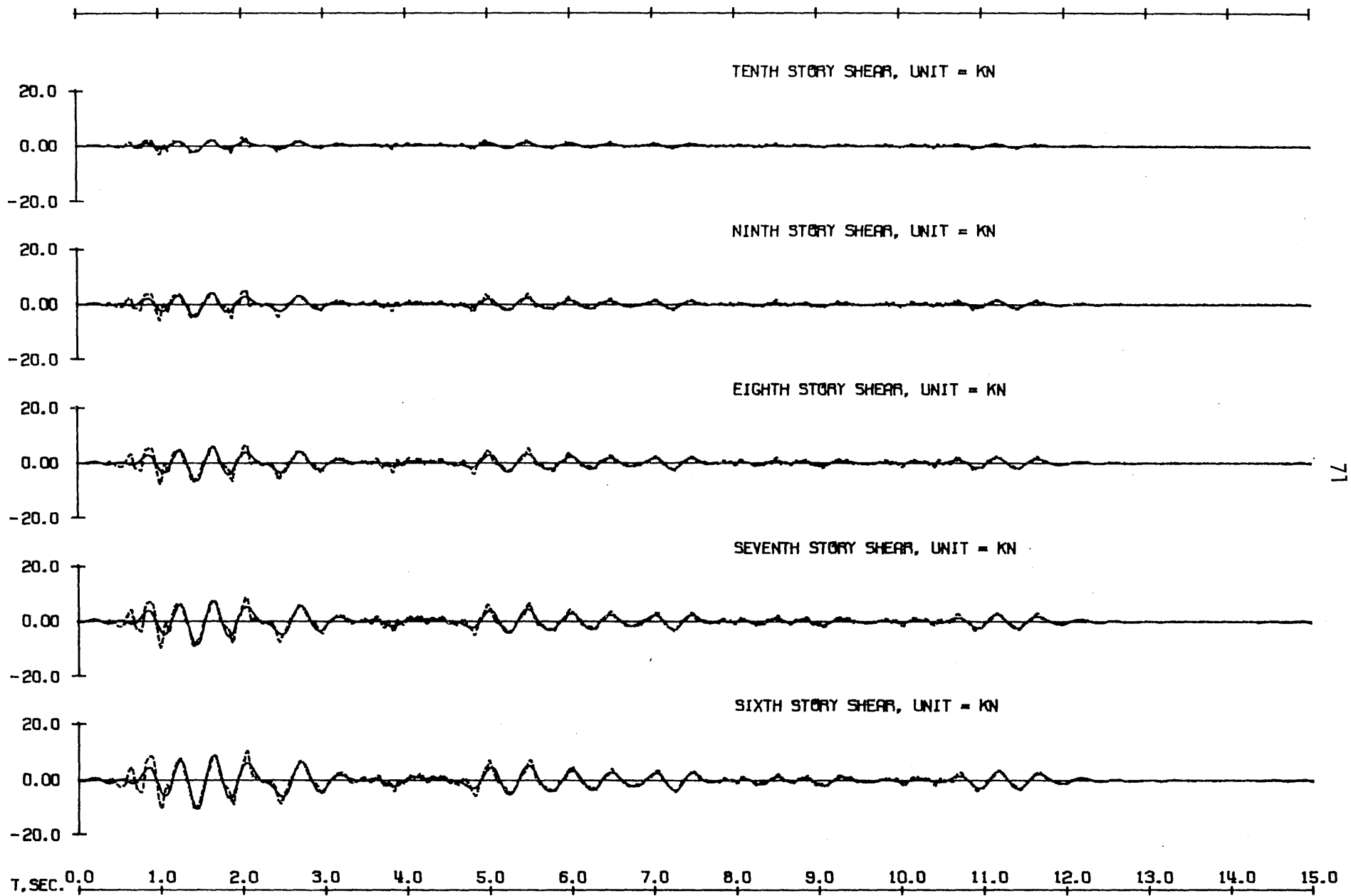
Fig. 4.19 Observed Story Shears, Run One

FIFTH STORY SHEAR, UNIT = KN

FOURTH STORY SHEAR, UNIT = KN

THIRD STORY SHEAR, UNIT = KN

SECOND STORY SHEAR, UNIT = KN

FIRST STORY SHEAR, UNIT = KN

BASE LEVEL ACCELERATION, UNIT = G
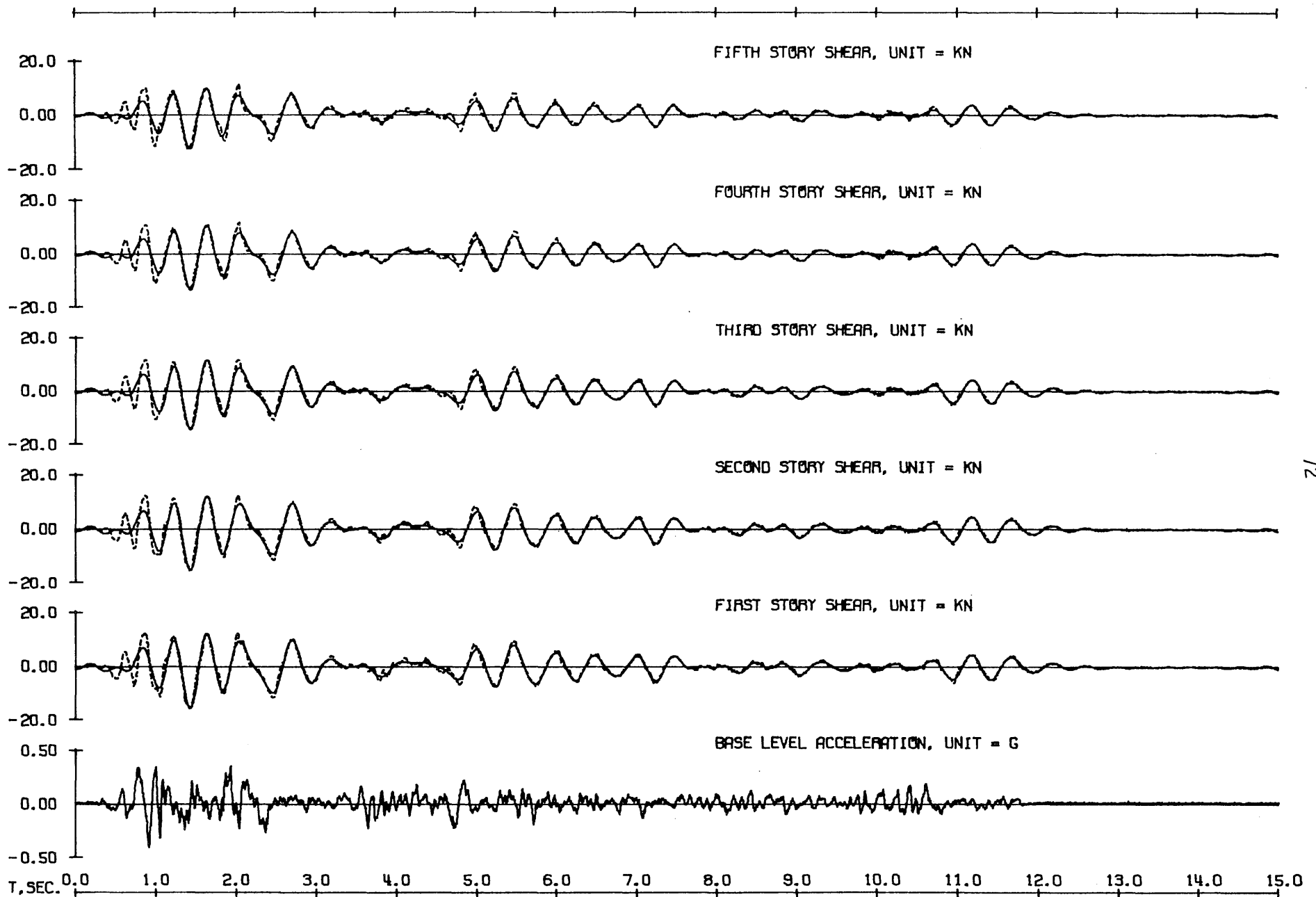
Fig. 4.20 Observed Story Shears, Run One
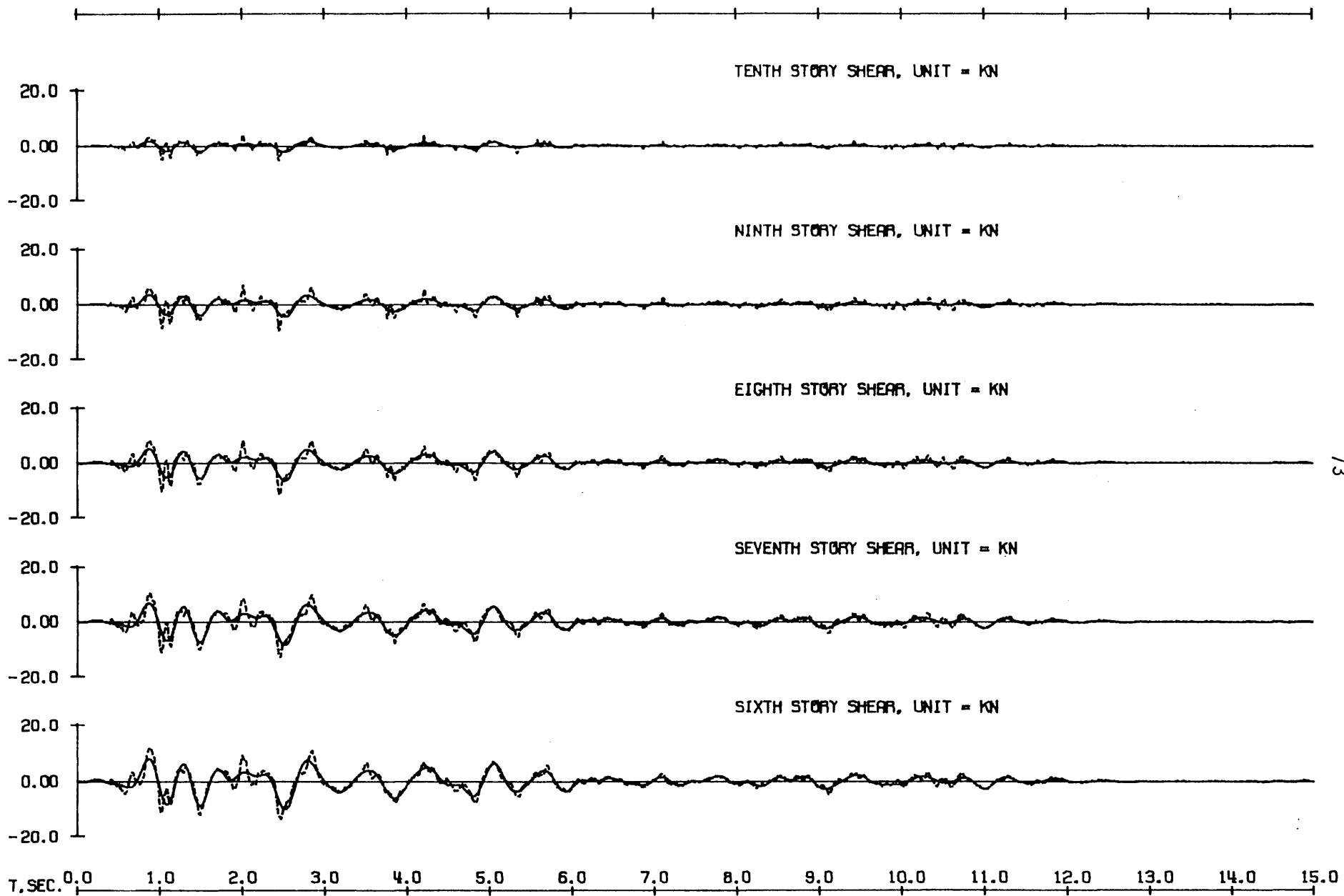
Fig. 4.21 Observed Story Shears, Run Two

FIFTH STORY SHEAR, UNIT = KN

FOURTH STORY SHEAR, UNIT = KN

THIRD STORY SHEAR, UNIT = KN

SECOND STORY SHEAR, UNIT = KN

FIRST STORY SHEAR, UNIT = KN

BASE LEVEL ACCELERATION, UNIT = G

20.0
0.00
-20.0

20.0
0.00
-20.0

20.0
0.00
-20.0

20.0
0.00
-20.0

20.0
0.00
-20.0

1.00
0.00
-1.00

T,SEC. 0.0   1.0   2.0   3.0   4.0   5.0   6.0   7.0   8.0   9.0   10.0   11.0   12.0   13.0   14.0   15.0
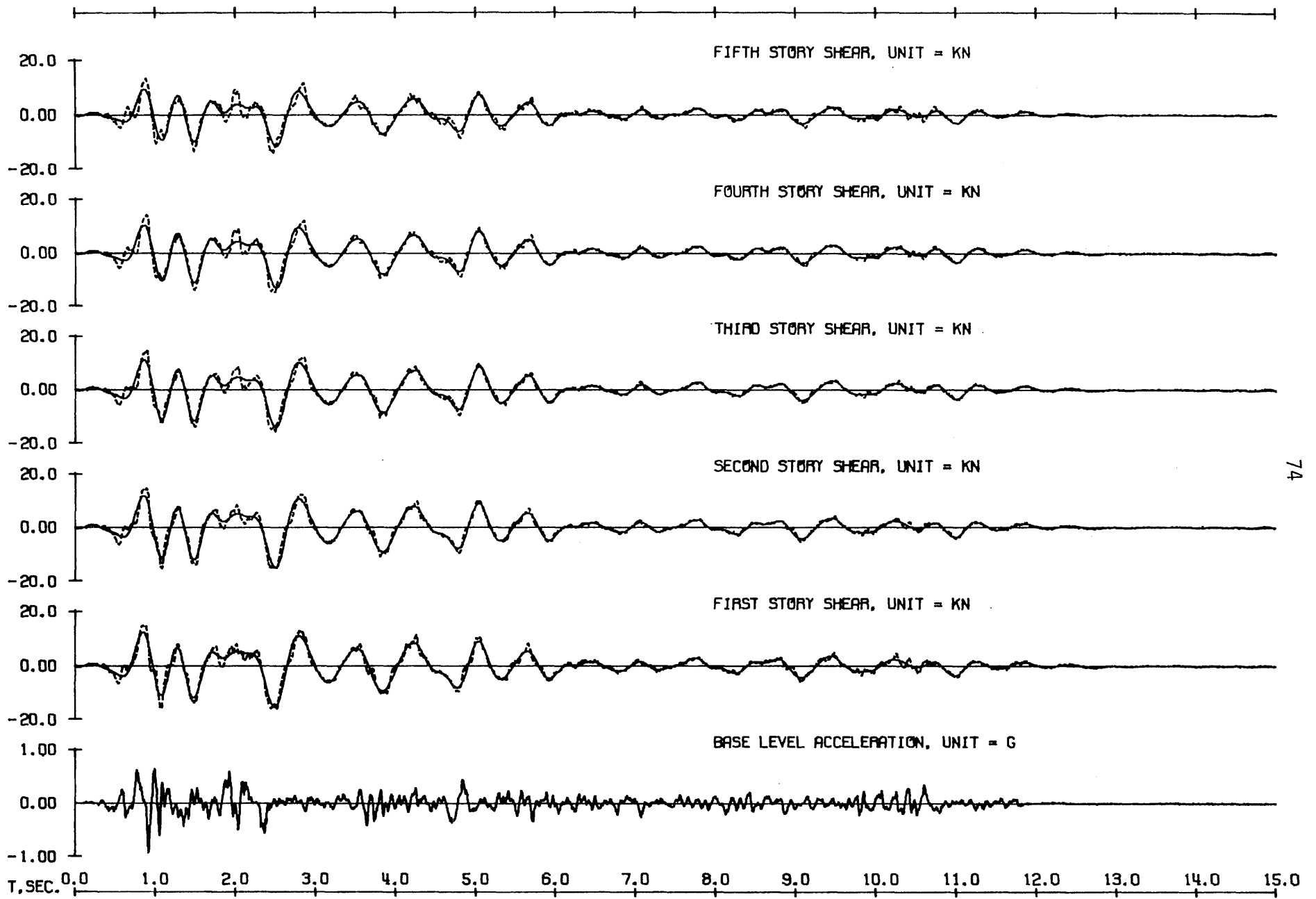
Fig. 4.22 Observed Story Shears, Run Two

74
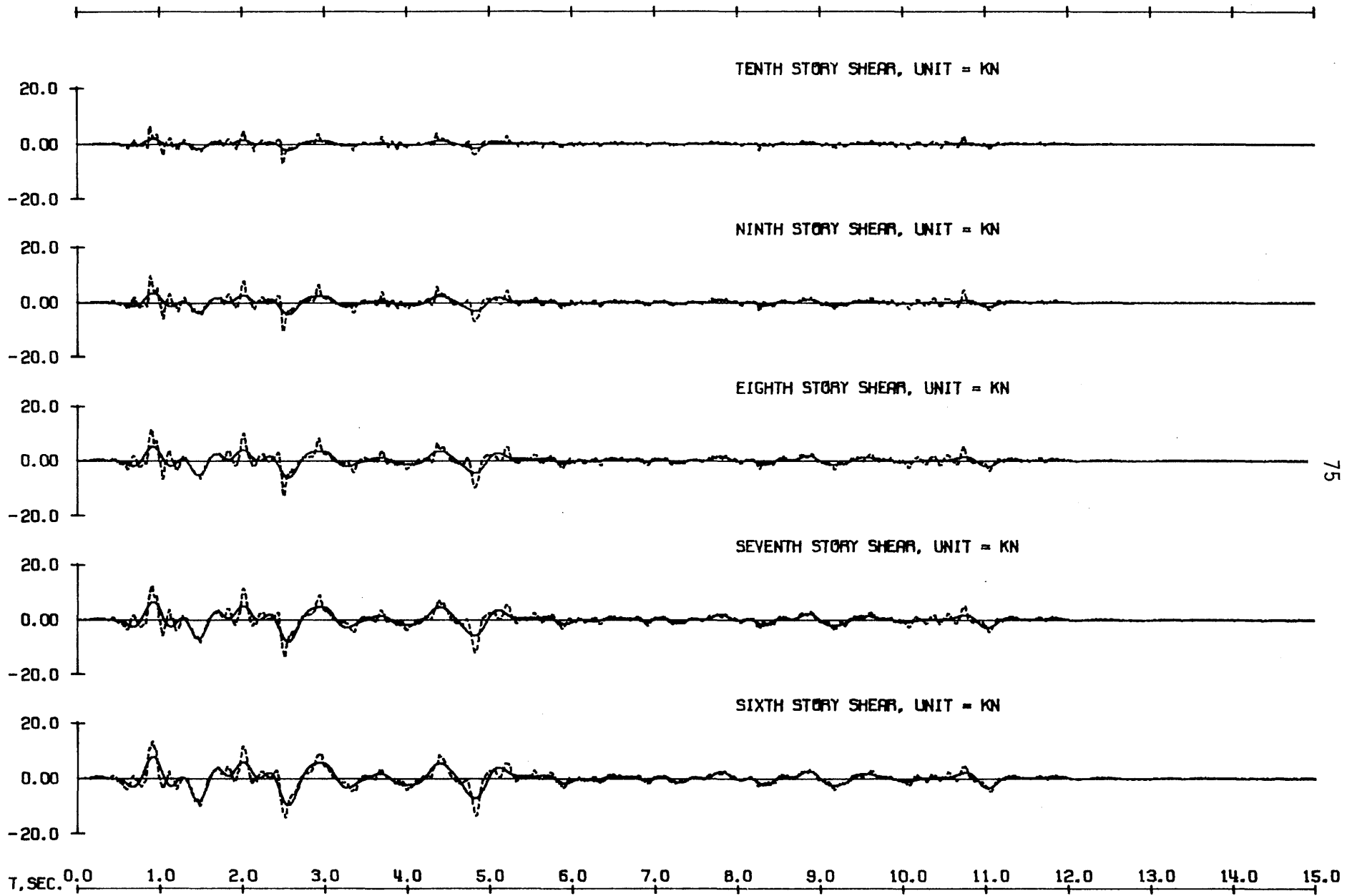
Fig. 4.23 Observed Story Shears, Run Three
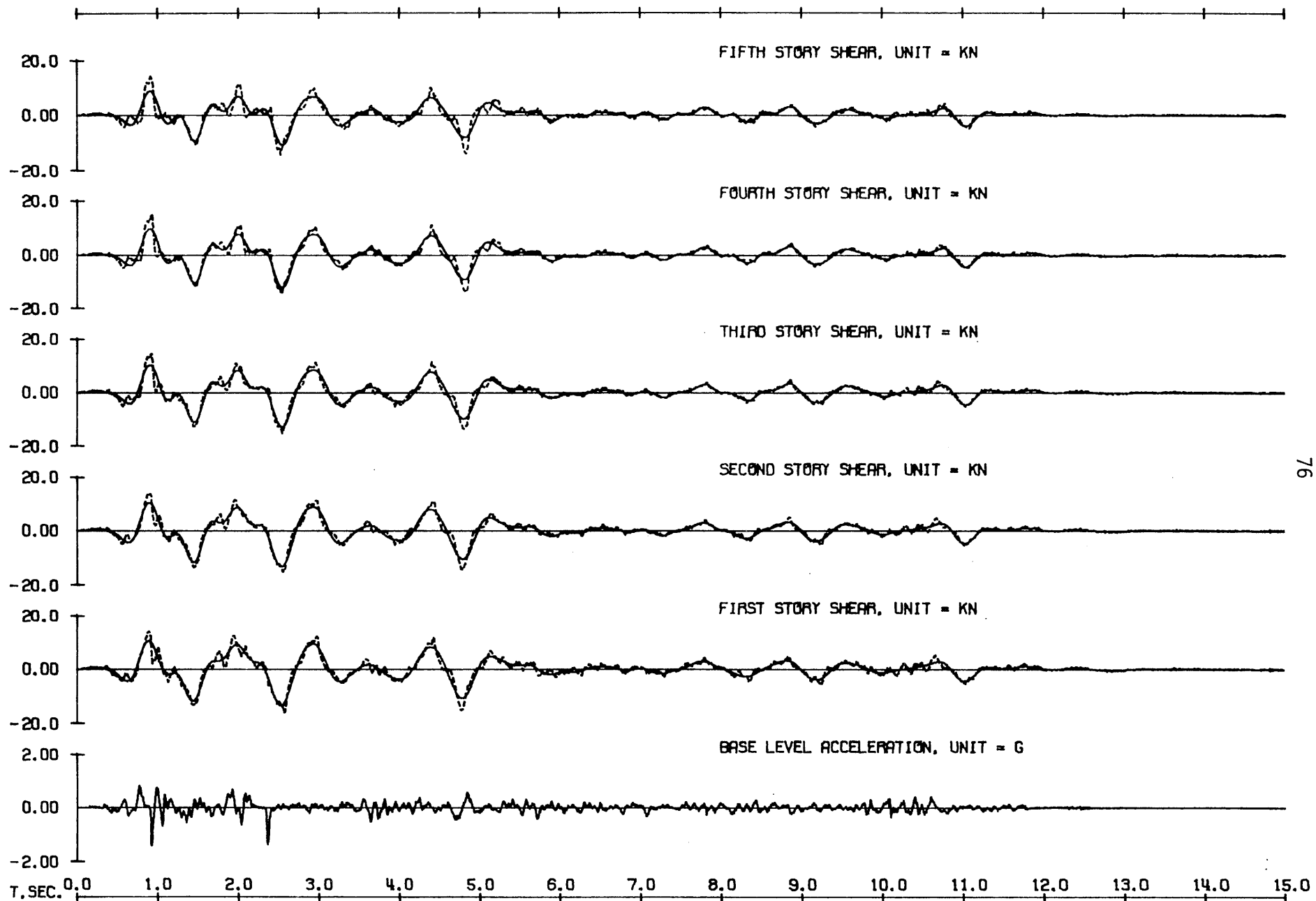
Fig. 4.24 Observed Story Shears, Run Three
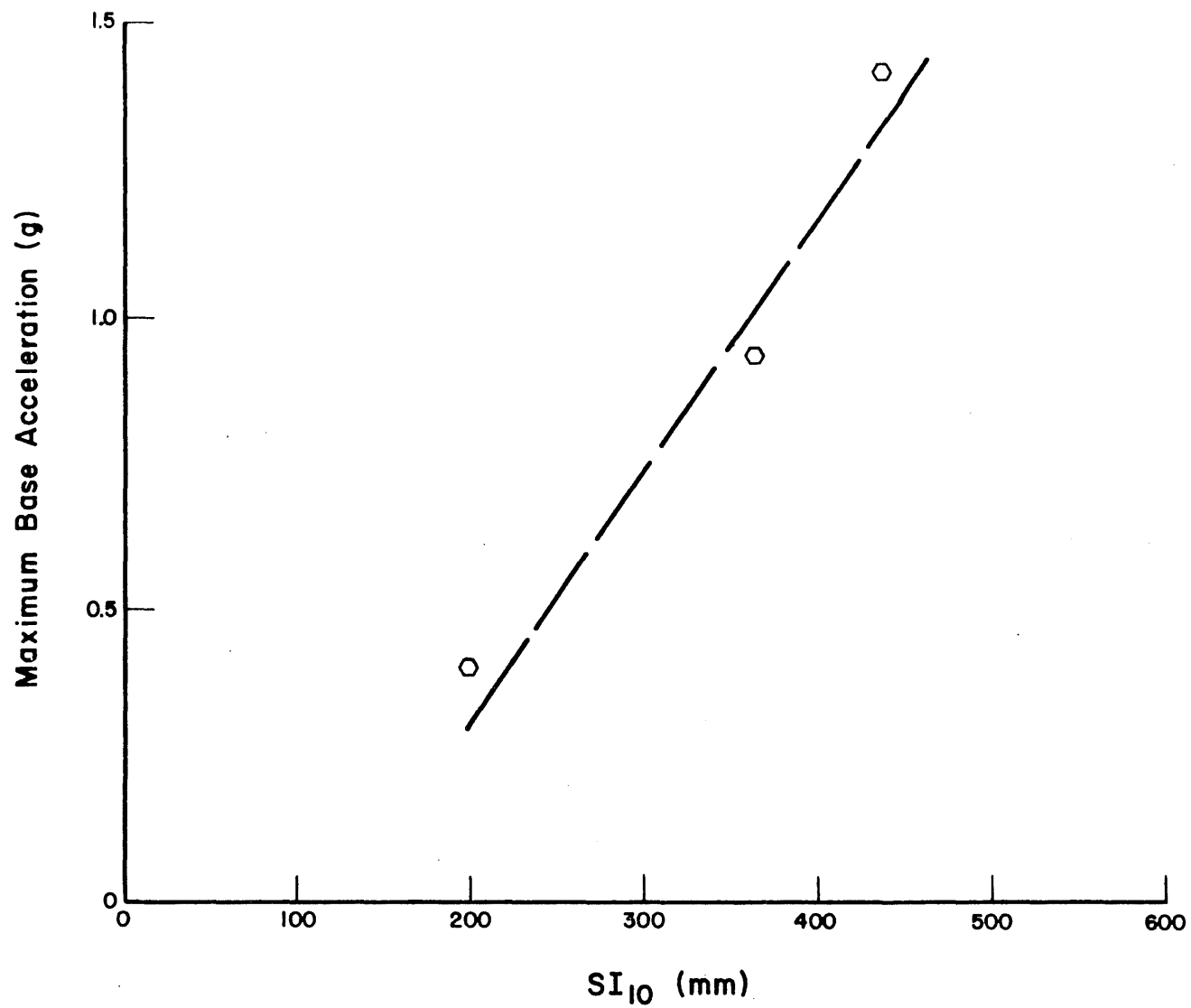
Fig. 4.25 Maximum Observed Base Acceleration Versus Spectrum Intensity, β = 20%
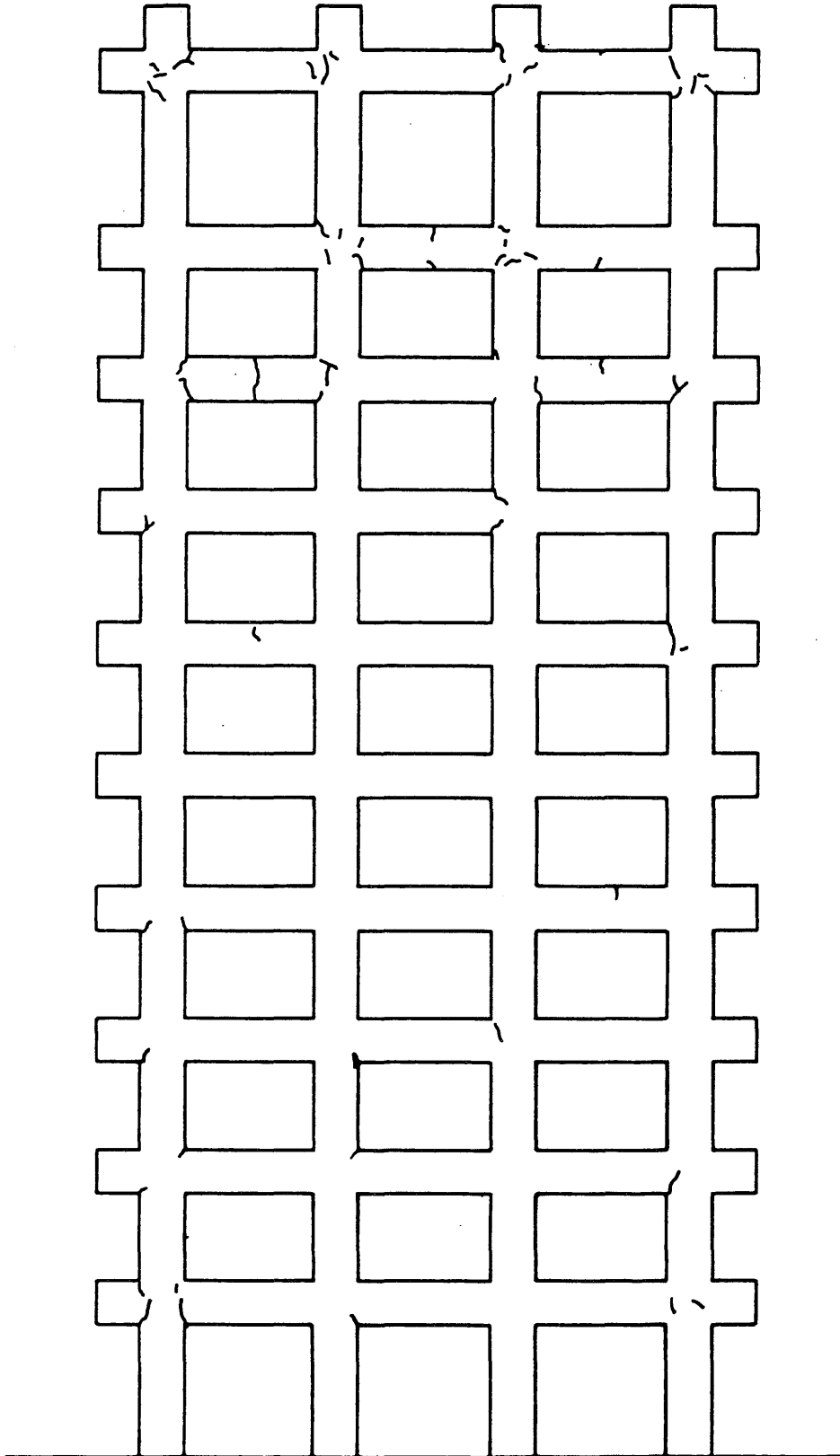
(Not to Scale)

Fig. 4.26 Crack Patterns Observed Before Testing
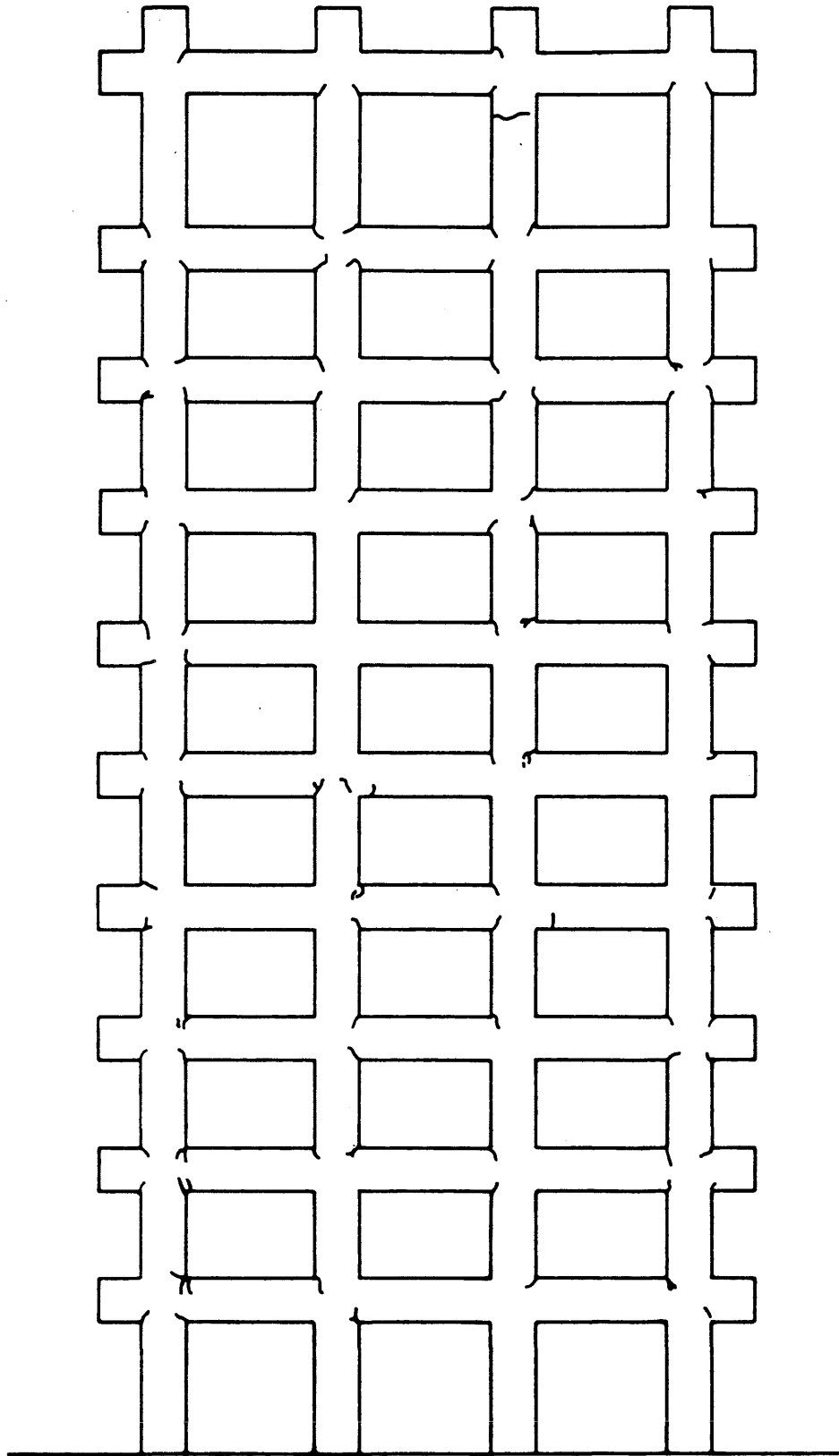
(Not to Scale)

Fig. 4.27 Crack Patterns Observed After Run One
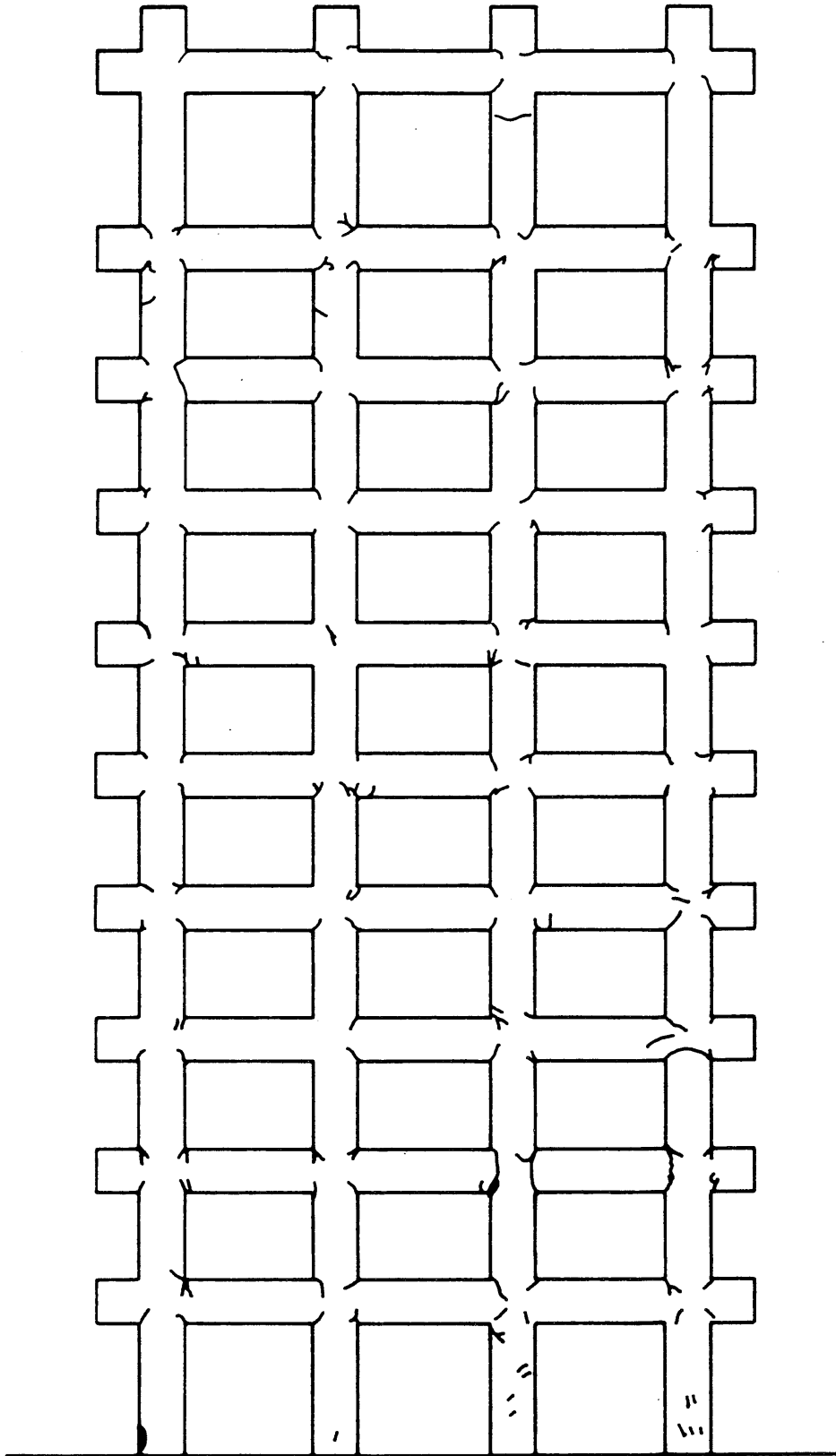
(Not to Scale)

Fig. 4.28 Crack Patterns Observed After Run Two
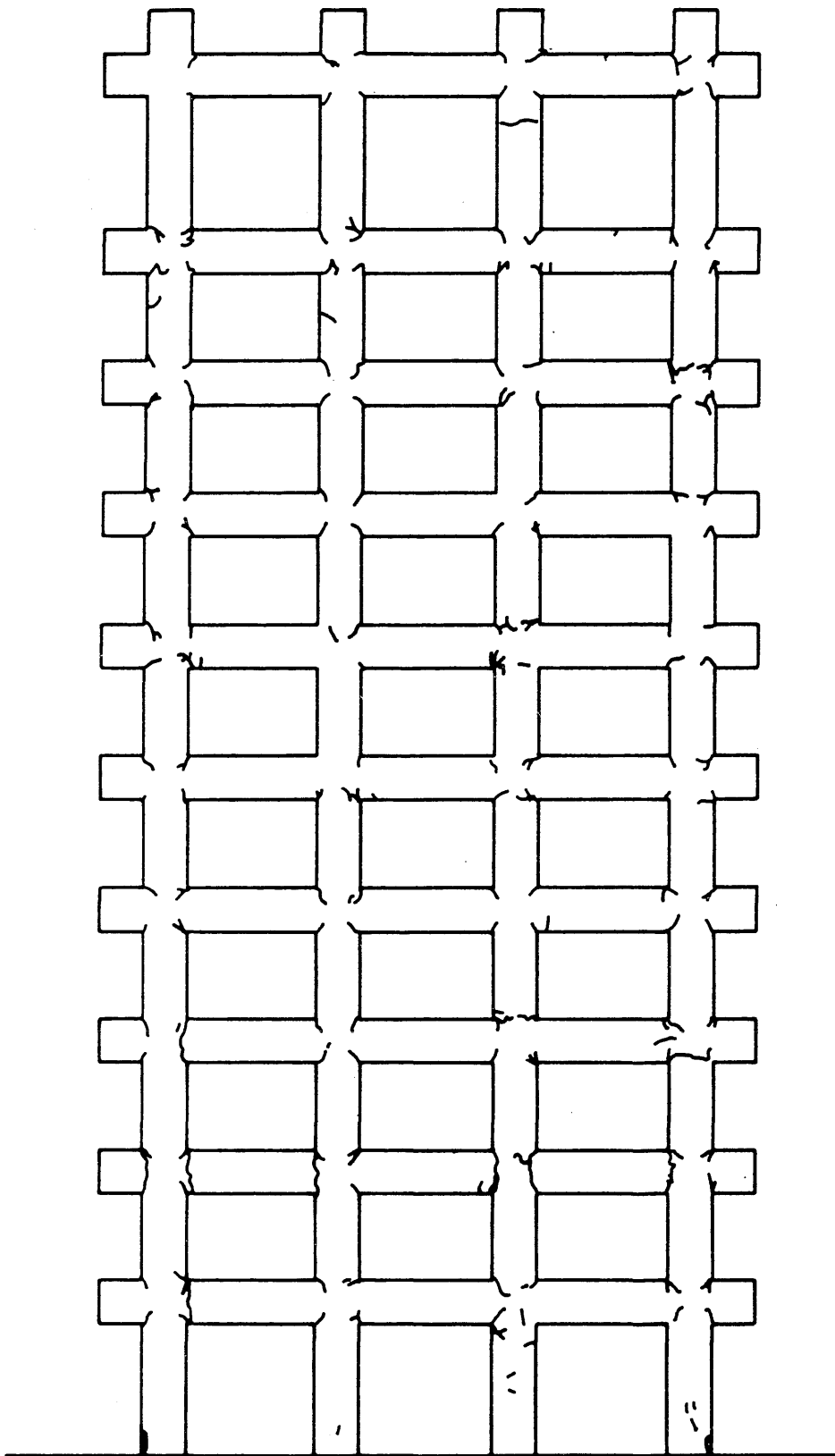
(Not to Scale)

Fig. 4.29 Crack Patterns Observed After Run Three

Fig. 4.30 Spalling at the Outside of an Exterior Column, Run Two

Fig. 4.31 Spalling at the Outside of an Exterior Column, Run Three

FIRST LEVEL DISPLACEMENT RUN 1

SECOND LEVEL DISPLACEMENT RUN 1

THIRD LEVEL DISPLACEMENT RUN 1

FOURTH LEVEL DISPLACEMENT RUN 1

FIFTH LEVEL DISPLACEMENT RUN 1

SIXTH LEVEL DISPLACEMENT RUN 1

SEVENTH LEVEL DISPLACEMENT RUN 1

EIGHTH LEVEL DISPLACEMENT RUN 1

NINTH LEVEL DISPLACEMENT RUN 1

TENTH LEVEL DISPLACEMENT RUN 1
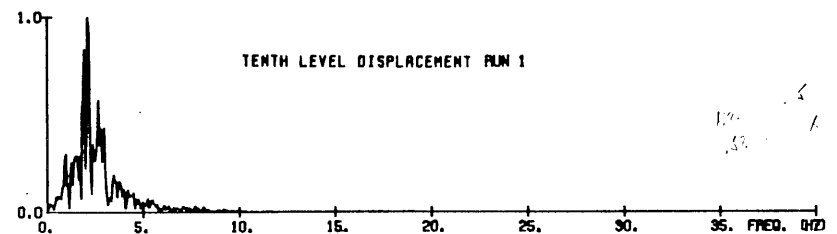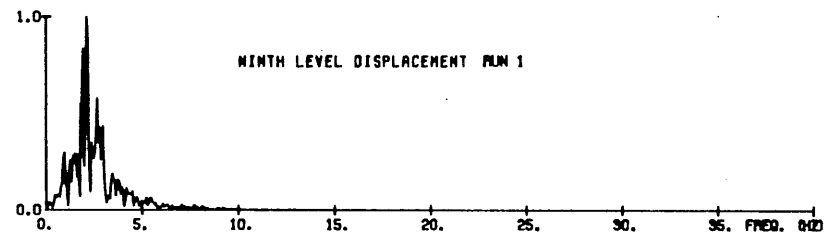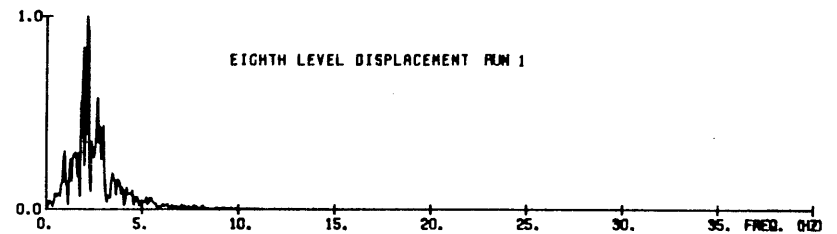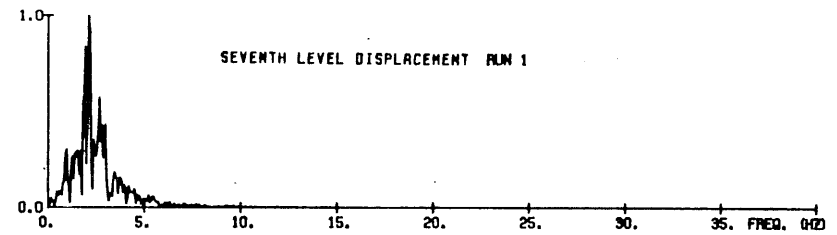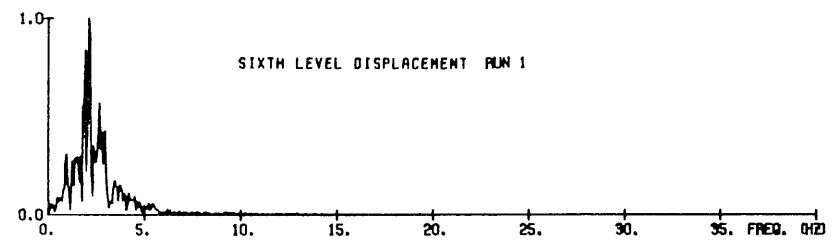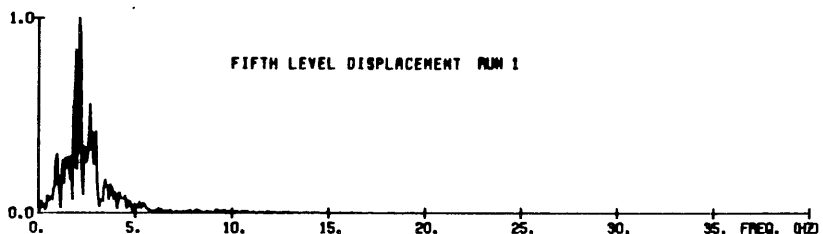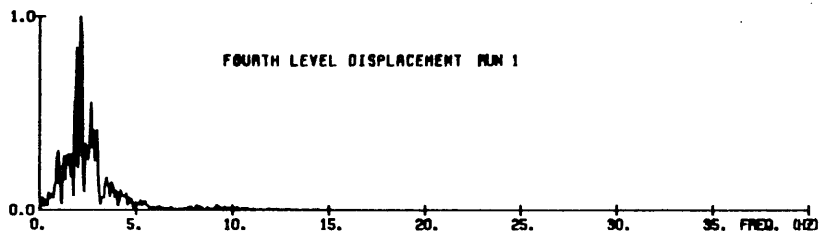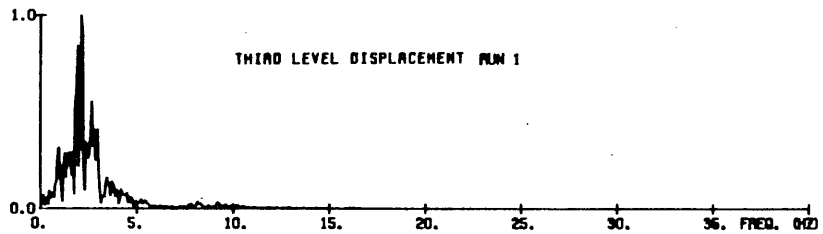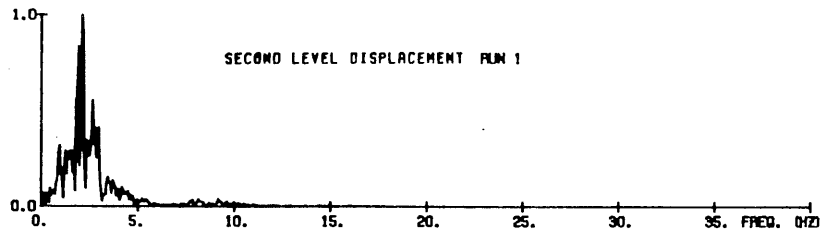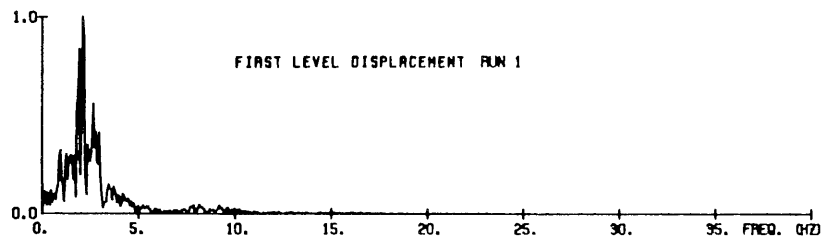
Fig. 5.1 Fourier Amplitude Spectra, Run One

84
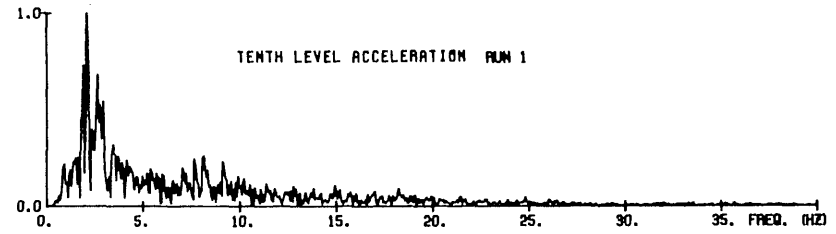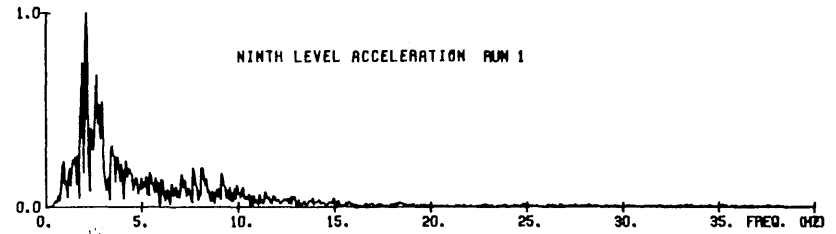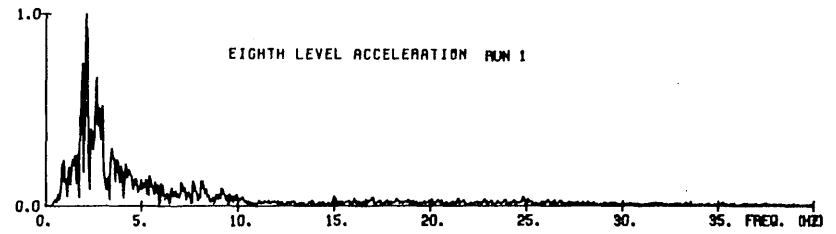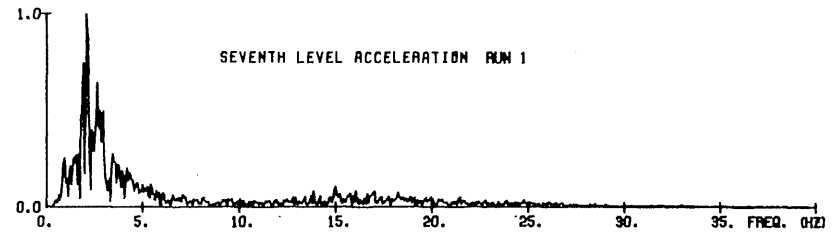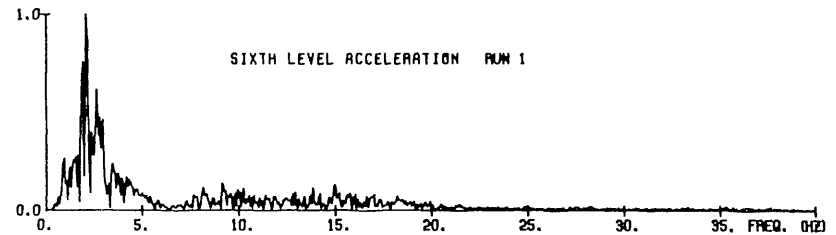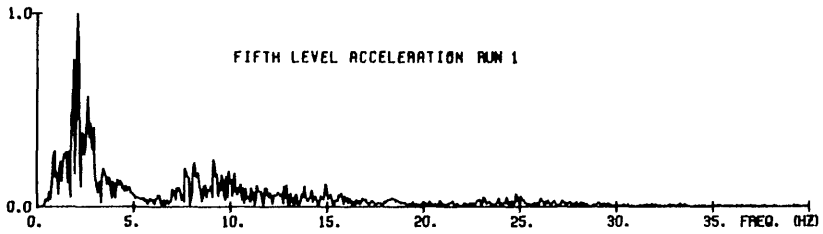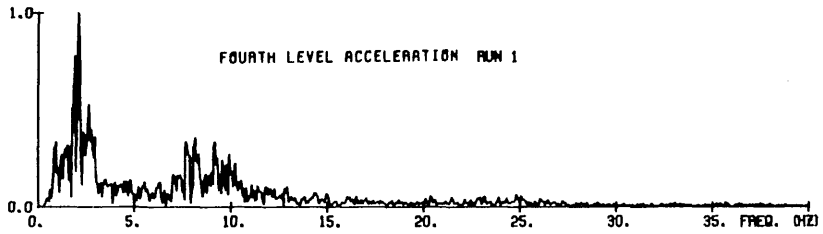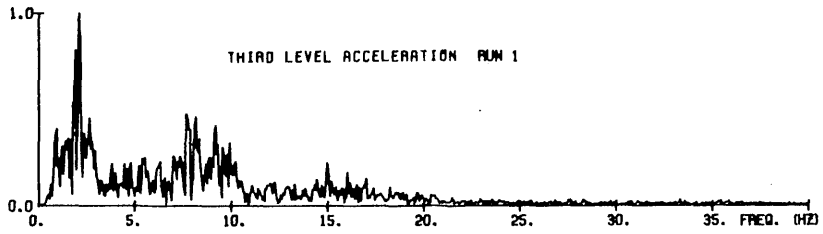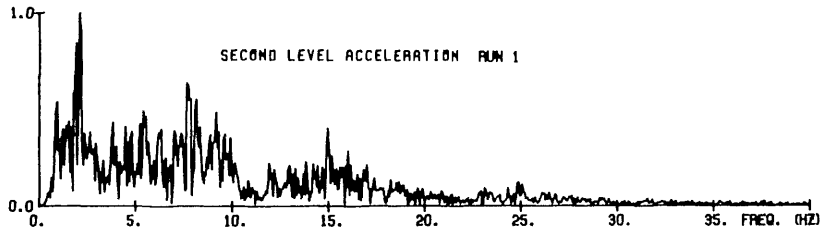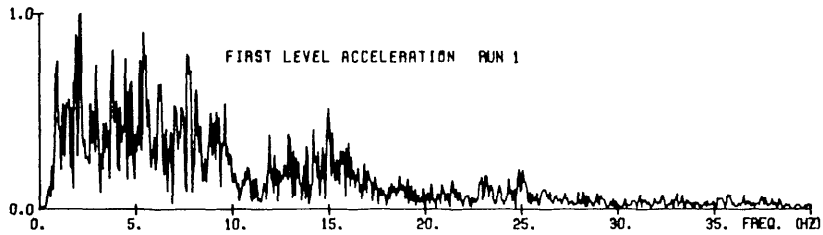
Fig. 5.2 Fourier Amplitude Spectra, Run One
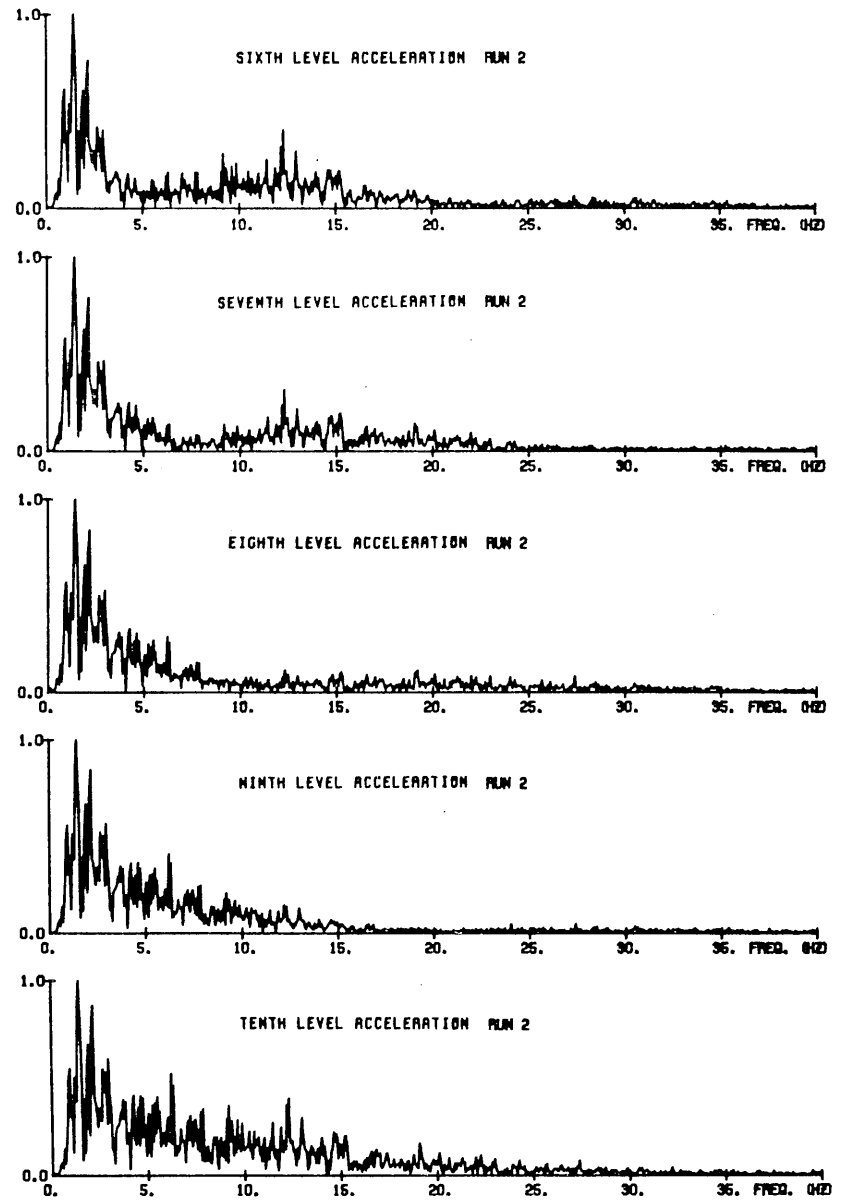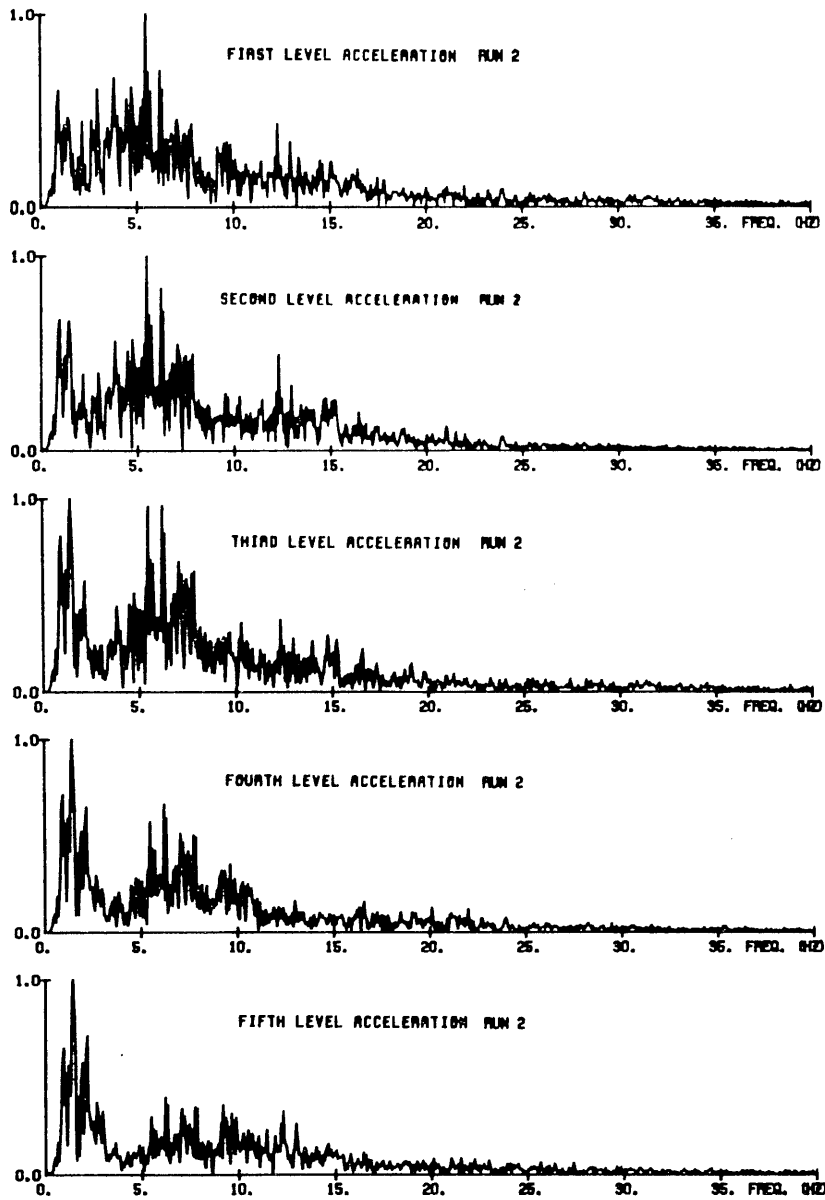
Fig. 5.4   Fourier Amplitude Spectra, Run Two

87

FIRST LEVEL DISPLACEMENT RUN 3

SECOND LEVEL DISPLACEMENT RUN 3

THIRD LEVEL DISPLACEMENT RUN 3

FOURTH LEVEL DISPLACEMHT RUN 3

FIFTH LEVEL DISPLACEMENT RUN 3

SIXTH LEVEL DISPLACEMET RUN 3

SEVENTH LEVEL DISPLACEMENT RUN 3

EIGHTH LEVEL DISPLACEMENT RUN 3

NINTH LEVEL DISPLACEMENT RUN 3

TENTH LEVEL DISPLACEMENT RUN 3
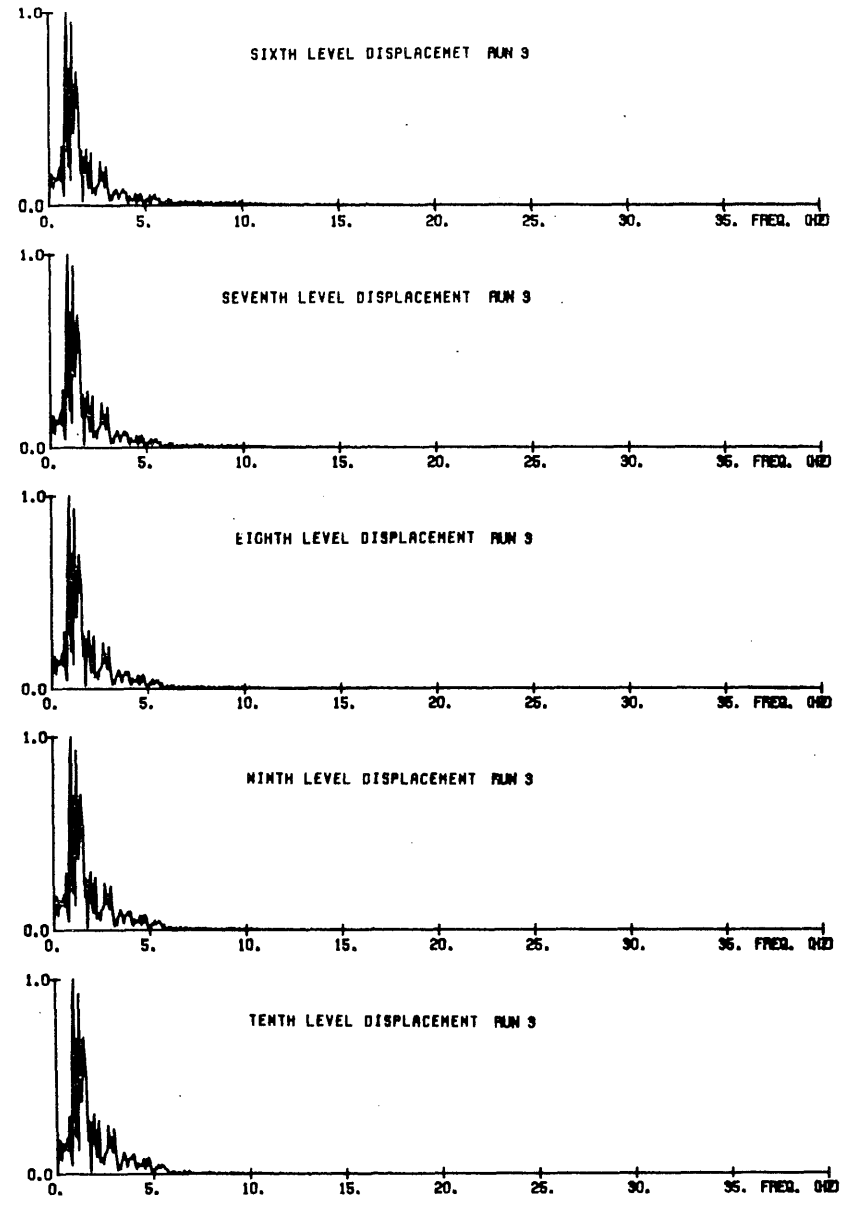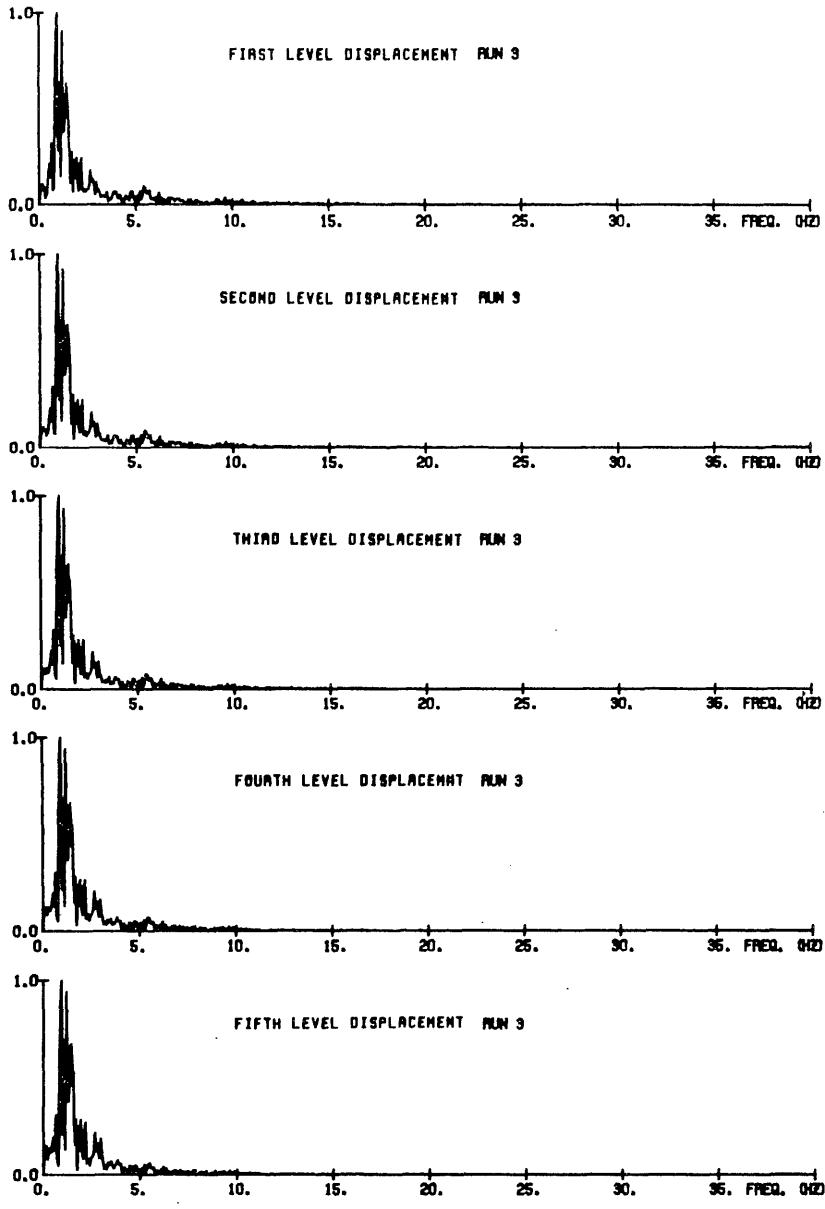
Fig. 5.5 Fourier Amplitude Spectra, Run Three
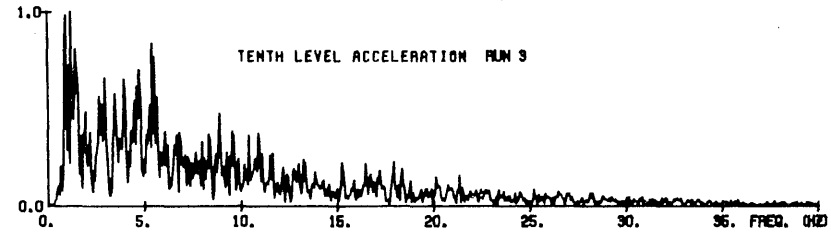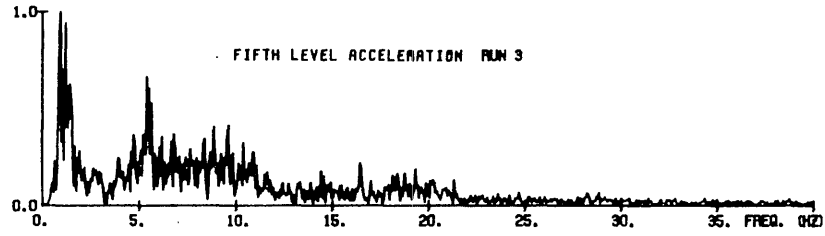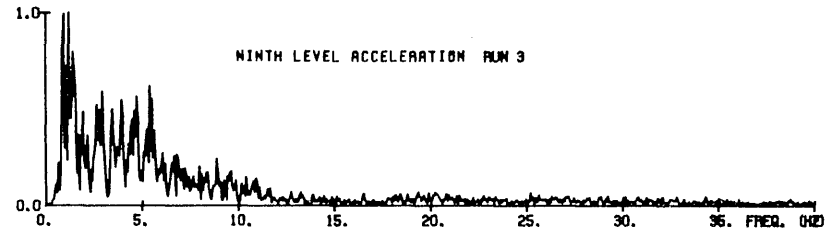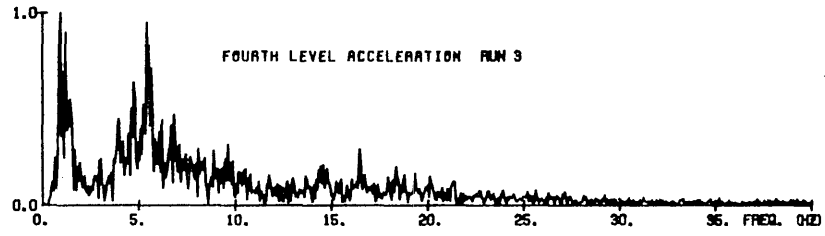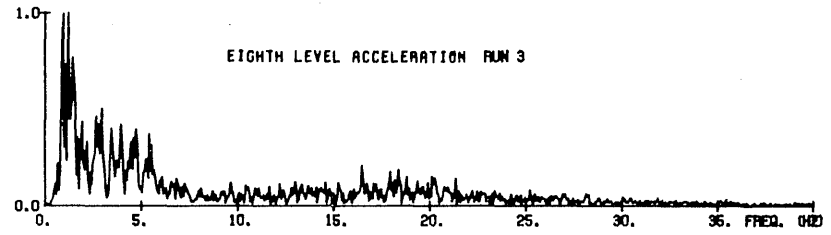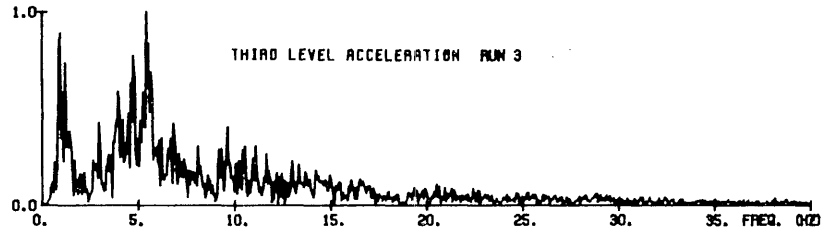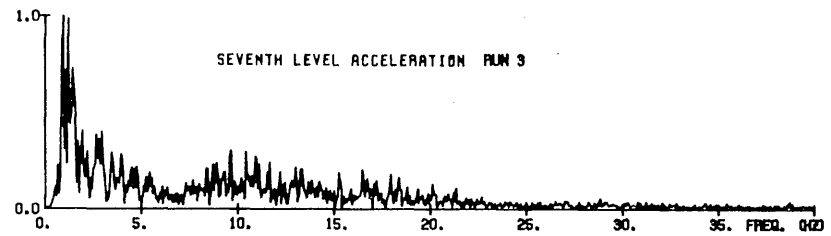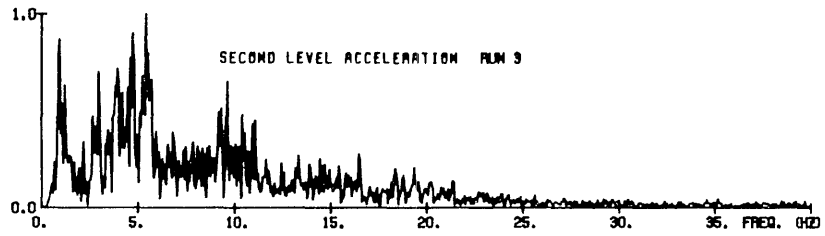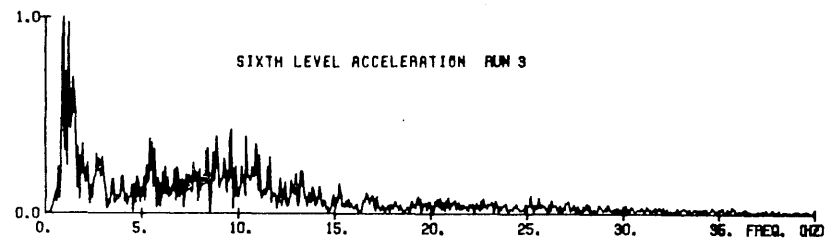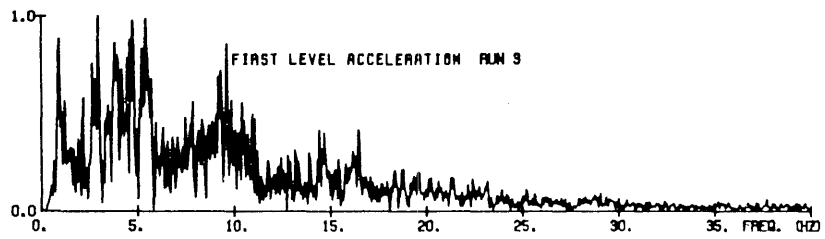
Fig. 5.6 Fourier Amplitude Spectra, Run Three

Fig. 5.7 Observed Free-Vibration Responses with Fourier Amplitude Spectra

TENTH LEVEL ACCELERATION, UNIT = G

FREE VIBR. FOLLOWING RUN 2

TENTH LEVEL ACCELERATION, UNIT = G

FREE VIBR. PRIOR TO RUN 3

TENTH LEVEL ACCELERATION, UNIT = G

FREE VIBR. FOLLOWING RUN 3

TIME, SEC.
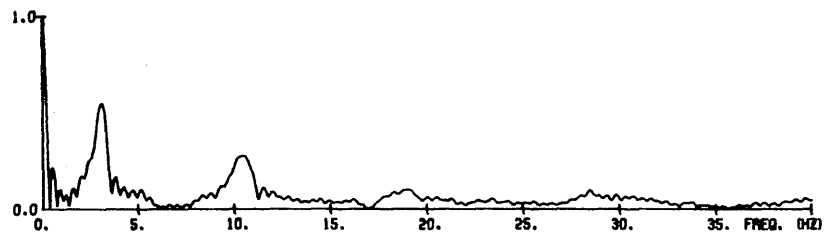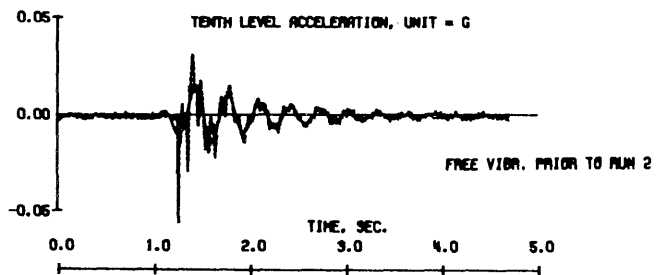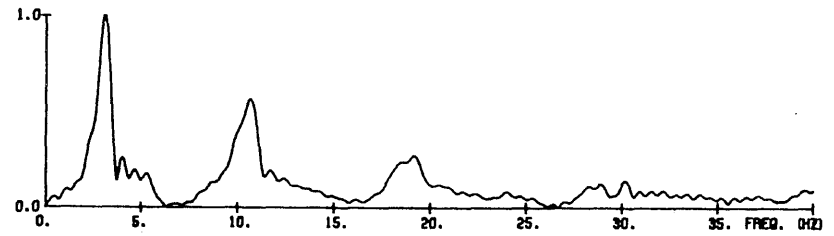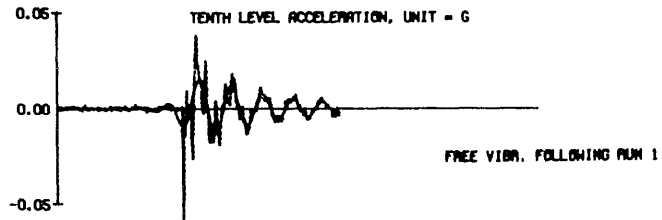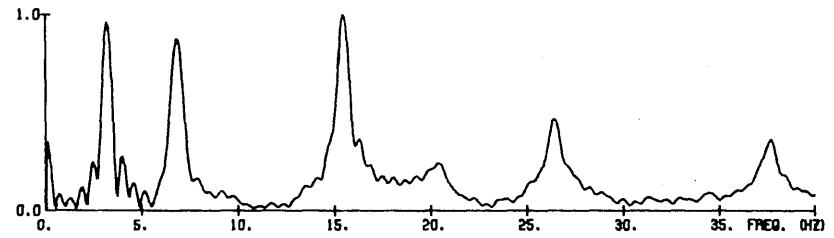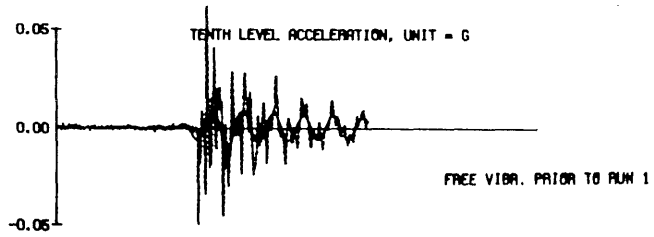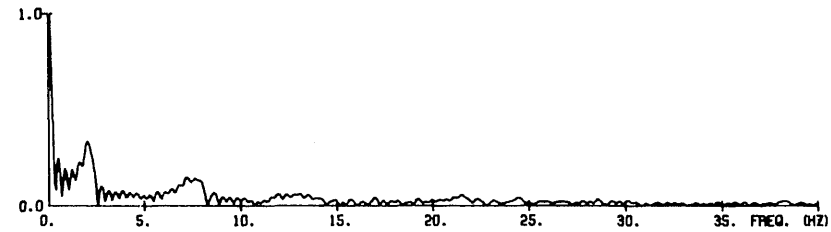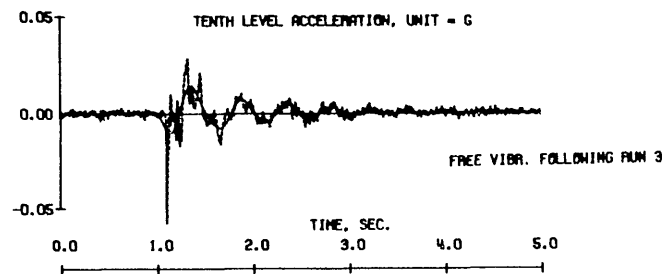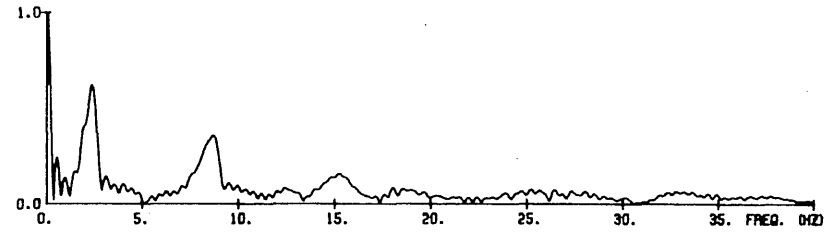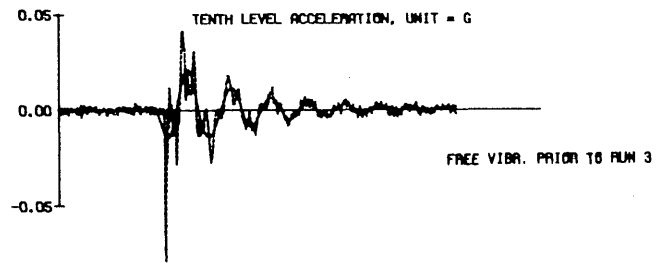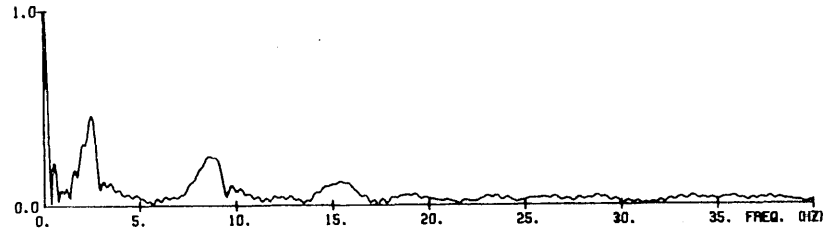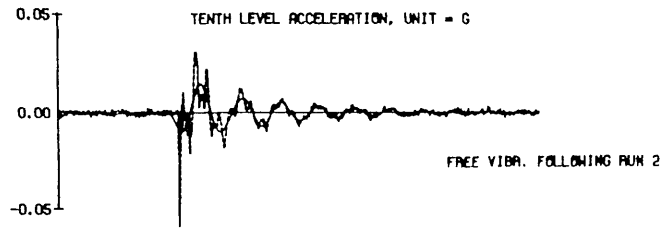
Fig. 5.8 Observed Free-Vibration Responses with Fourier Amplitude Spectra
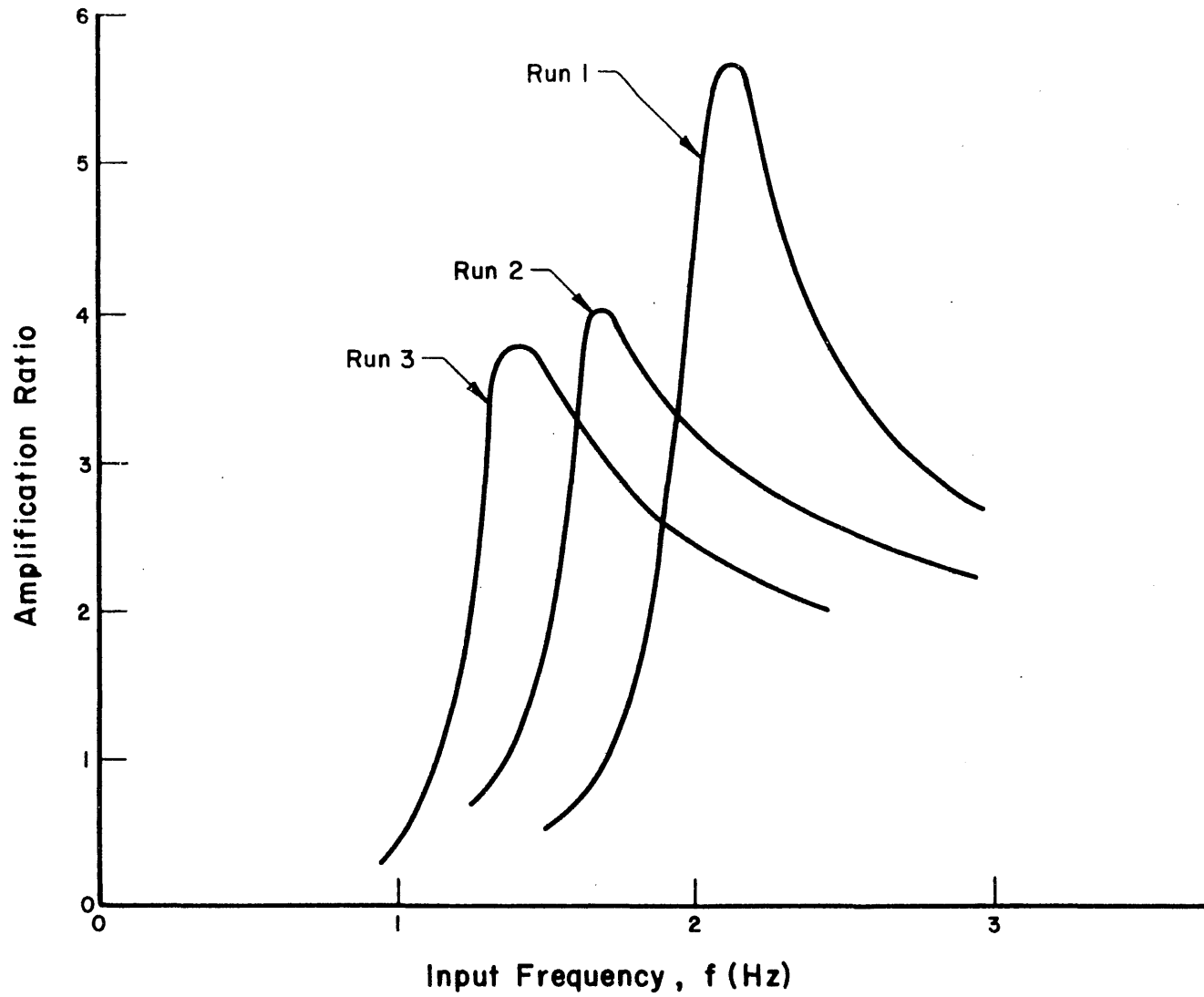
Fig. 5.9 Amplification Ratio Versus Input Frequency, Steady State Tests
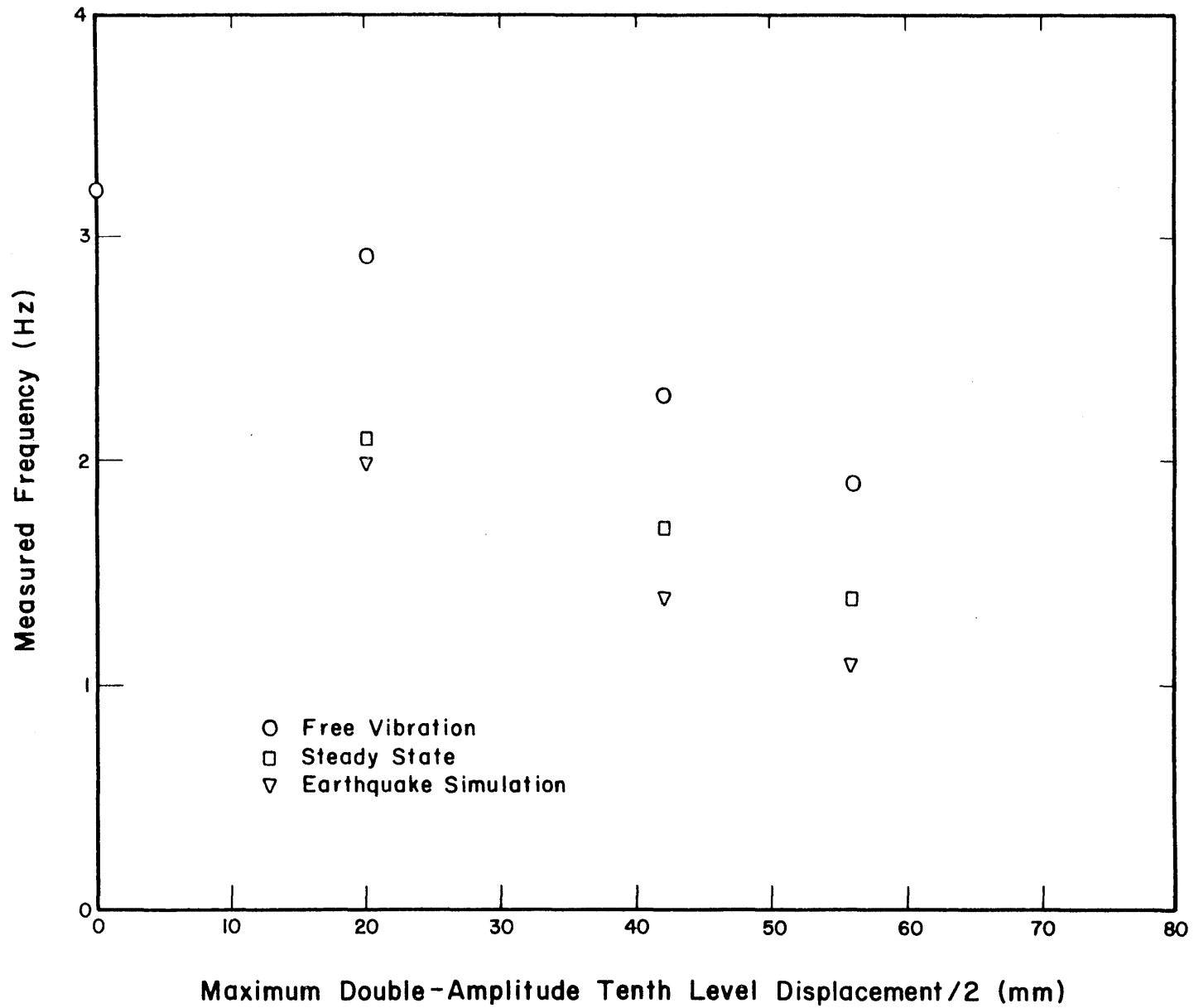
Fig. 5.10   Apparent First-Mode Frequency Versus One-Half the Maximum Observed Double Amplitude
Tenth Level Displacement
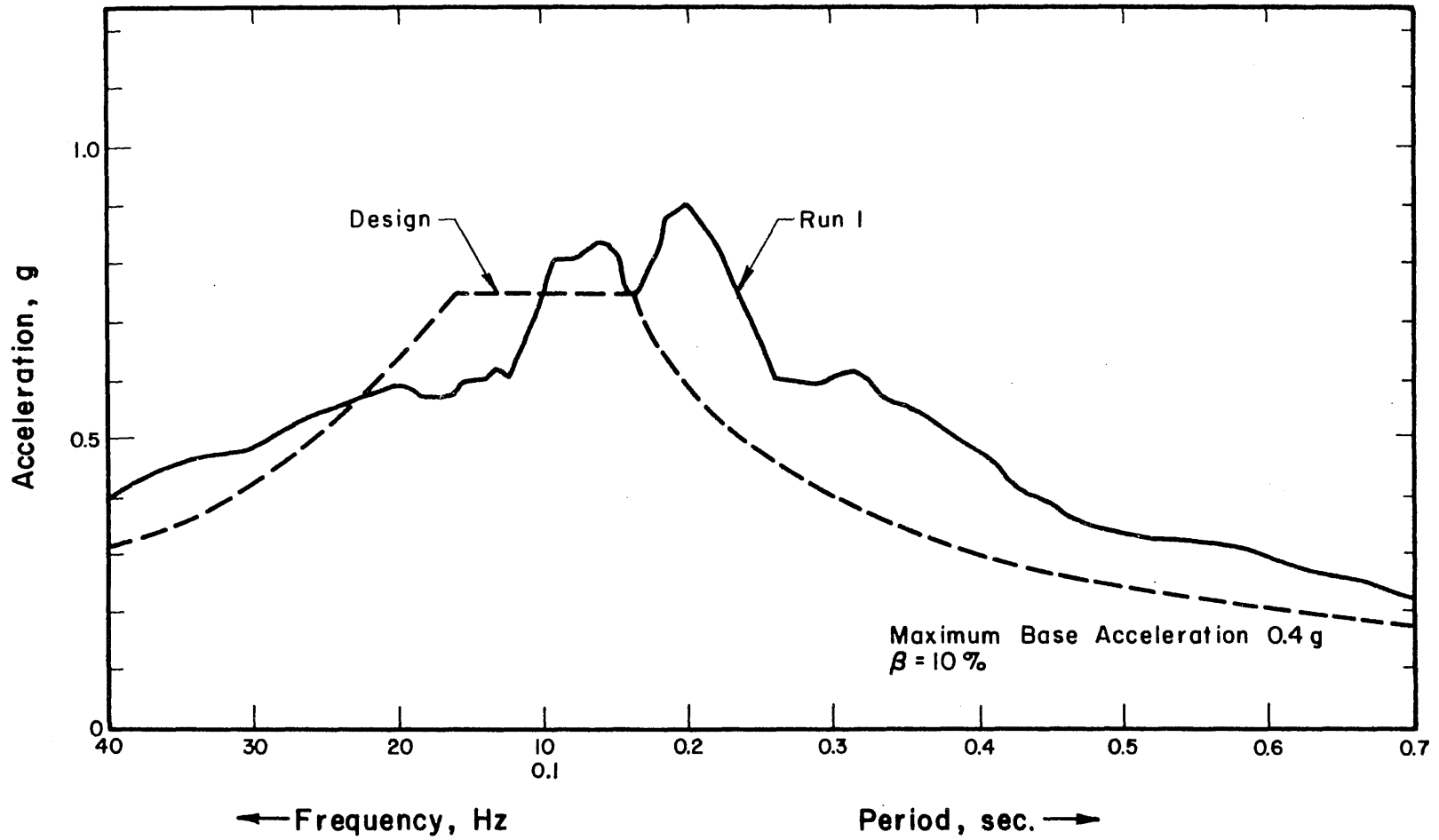
Fig. 5.11   Comparison of Design Response Spectrum with Obtained Response Spectrum, Run One
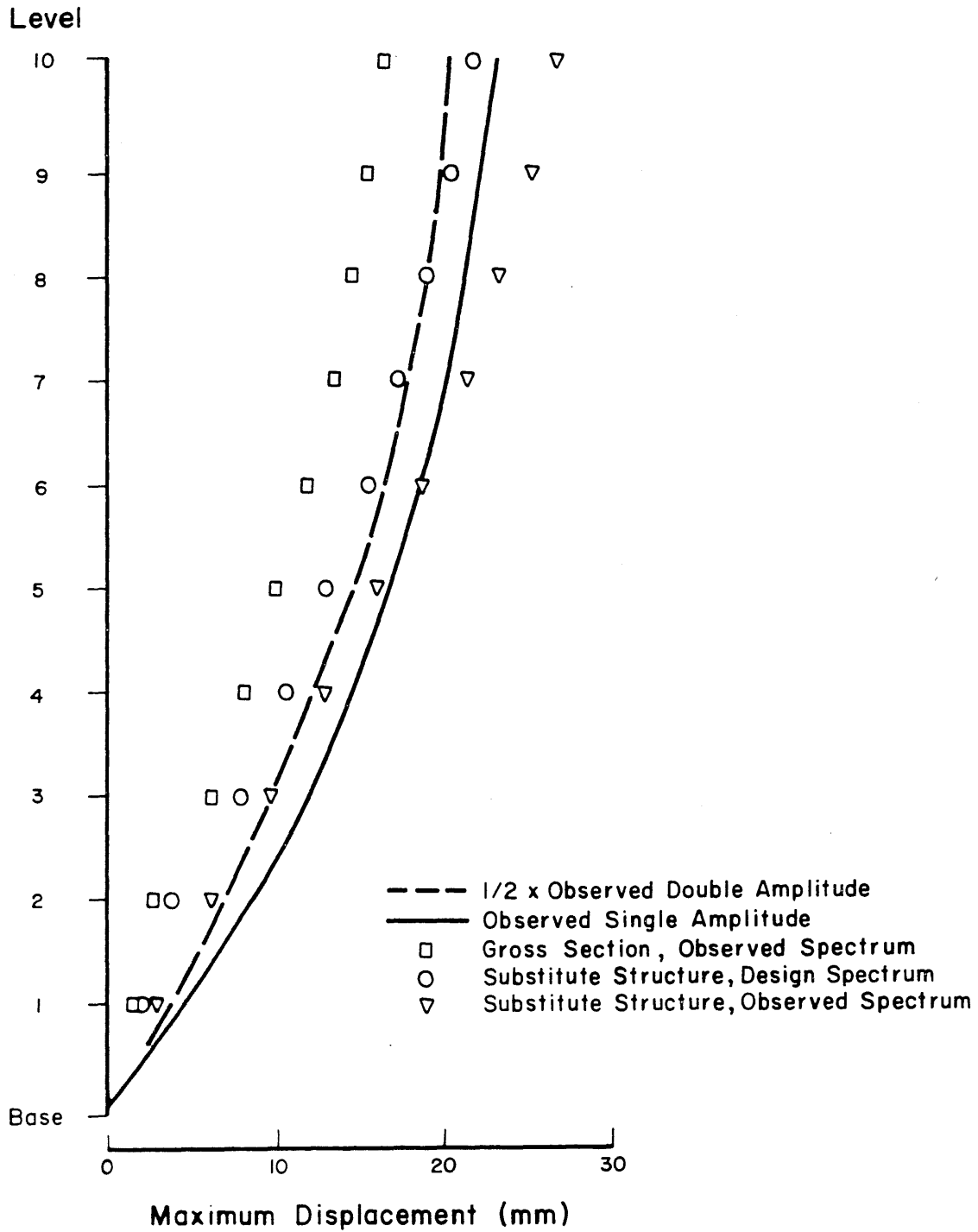
Fig. 5.12 Comparison of Maximum Observed Displacements with Calculated
Values, Run One

LEVEL

| DISPLACEMENTS (MM) | LATERAL FORCES (KN) | SHEARS (KN) | MOMENTS (KN-M) |
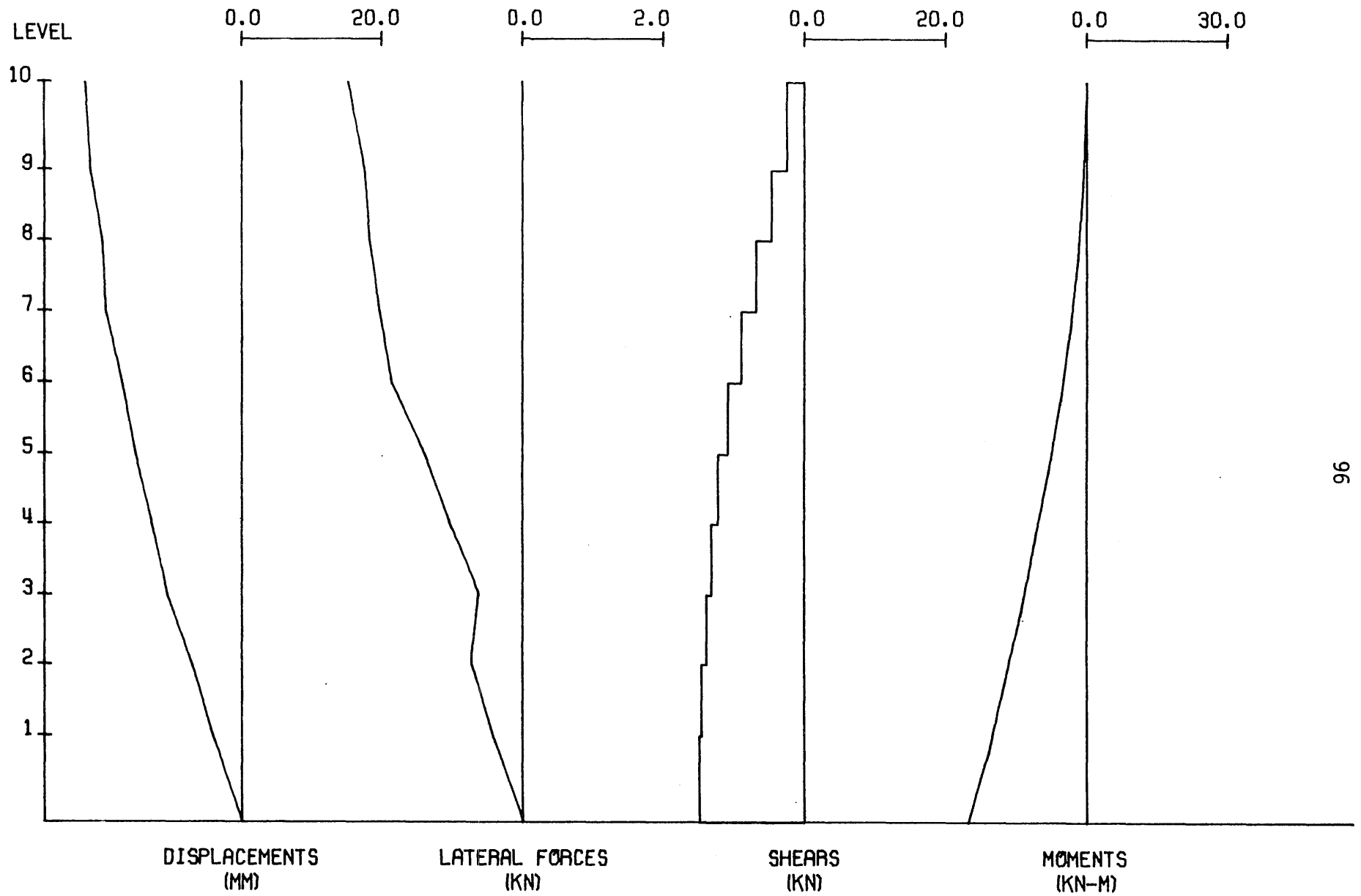
TEST STRUCTURE MF1 — TEST RUN 1 — RESPØNSE AT 1.42 SECØNDS

Fig. 5.13 Maximum Observed Displacements, Lateral Forces, Story Shears and Overturning Moments, Run One
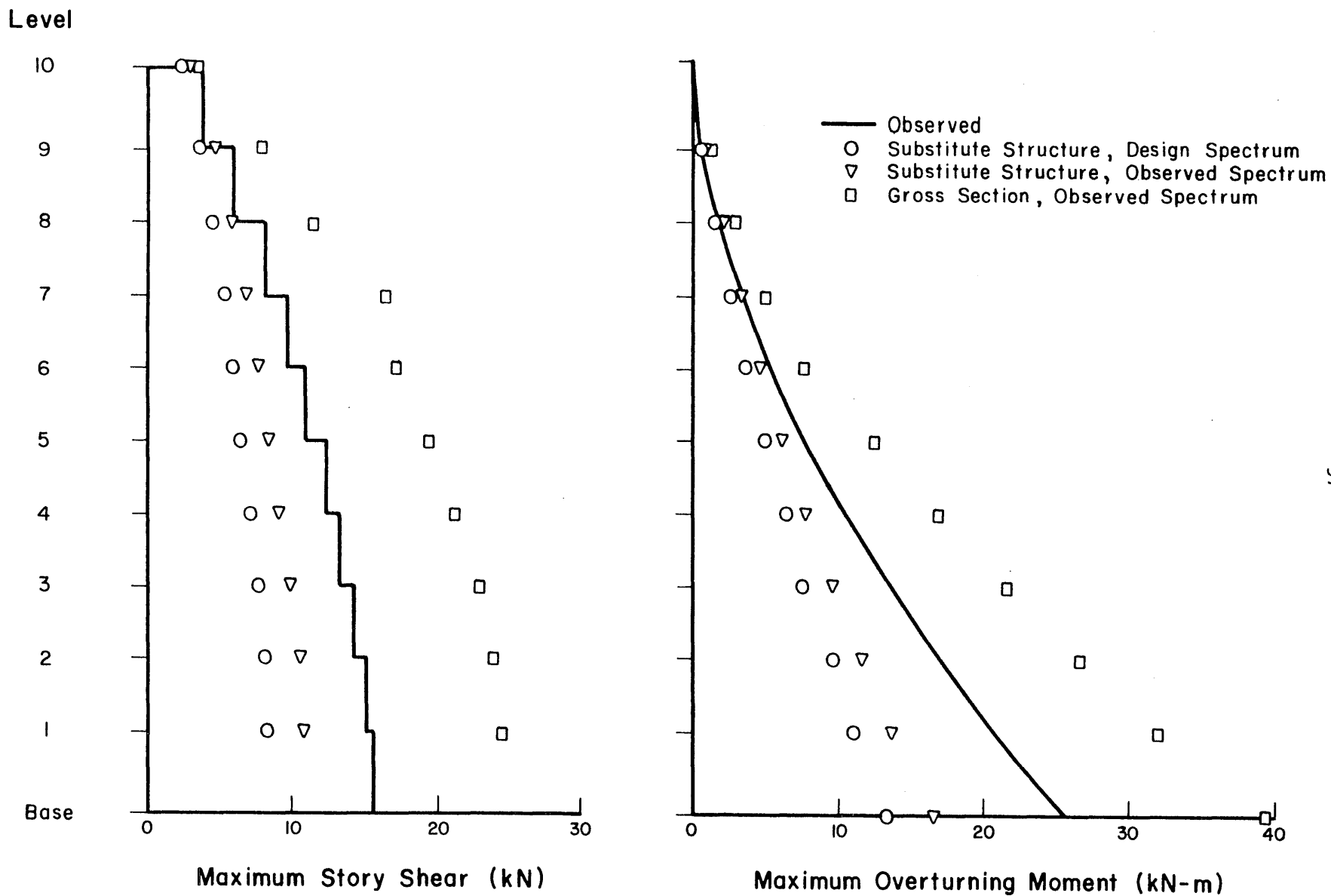
Level

Fig. 5.14 Comparison of Maximum Observed Story Shears and Overturning Moment with Calculated Values, Run One
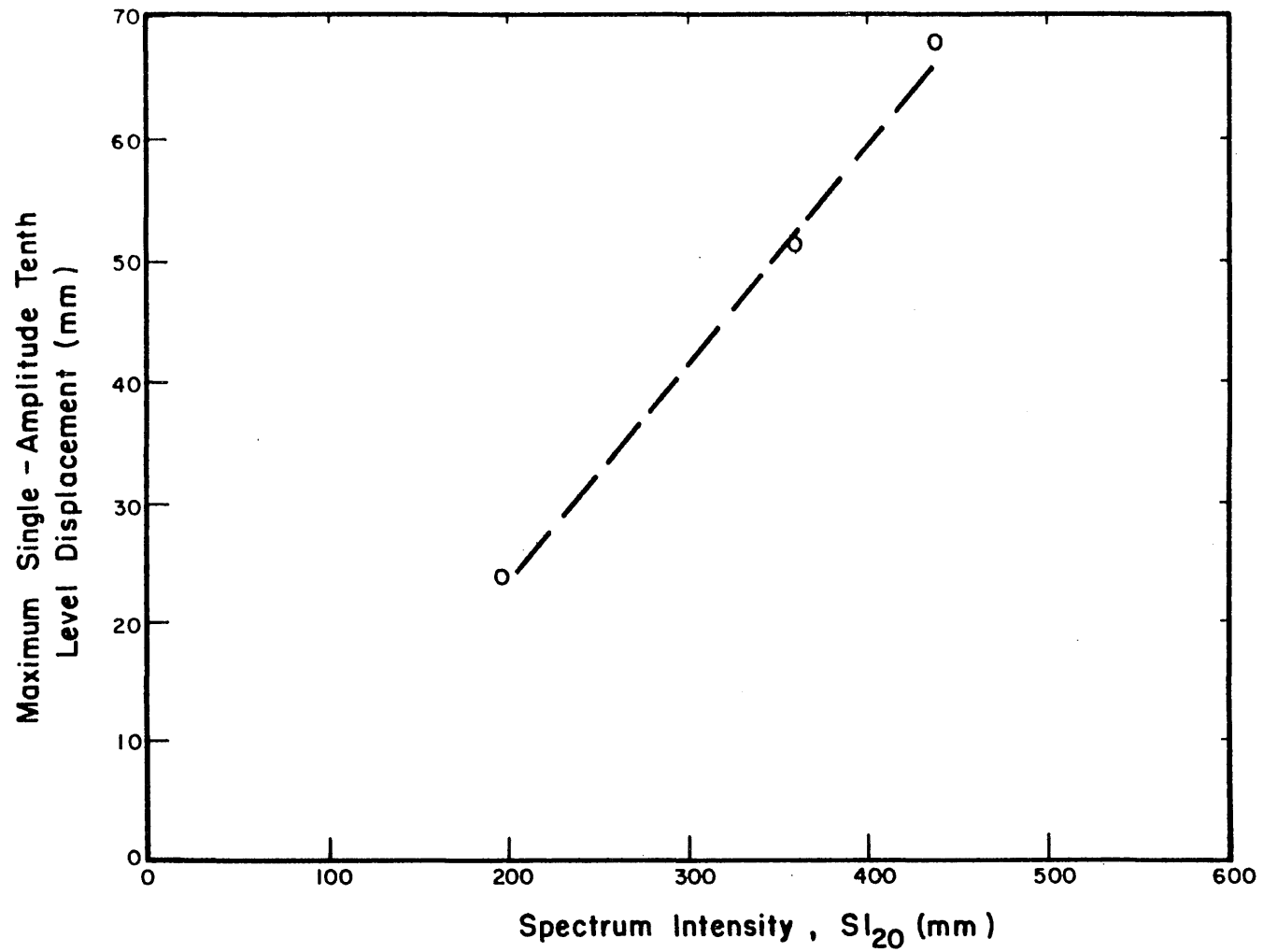
Fig. 5.15 Maximum Observed Single-Amplitude Tenth-Level Displacement Versus Spectrum Intensity, $\beta = 20\%$

LEVEL

| | 0.0   50.0 | 0.0   5.0 | 0.0   20.0 | 0.0   30.0 |

DISPLACEMENTS
(MM)

LATERAL FORCES
(KN)

SHEARS
(KN)
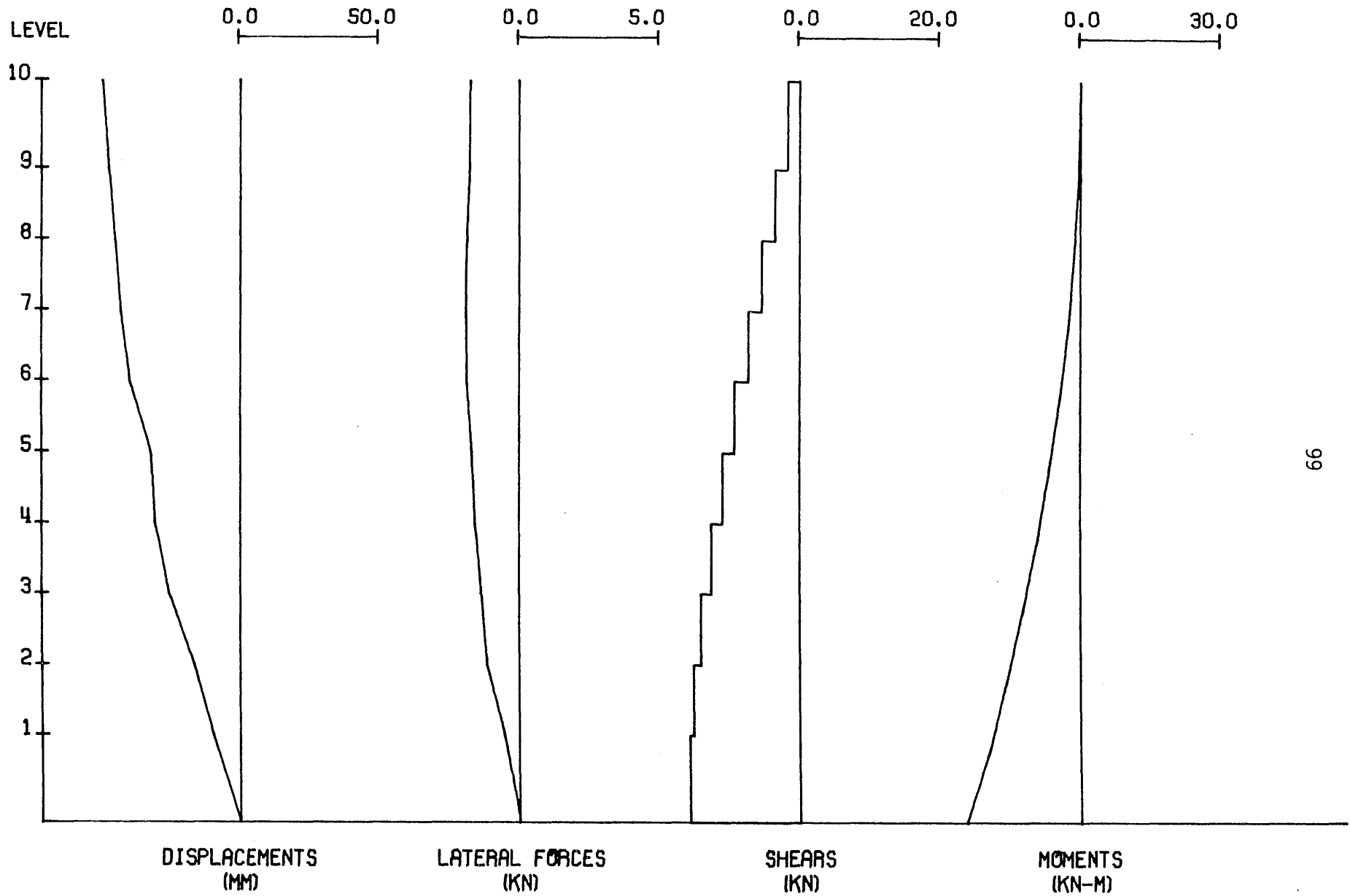
MOMENTS
(KN-M)

TEST STRUCTURE MF1 — TEST RUN 2 — RESPONSE AT 2.52 SECONDS

Fig. 5.16 Observed Displacements, Lateral Forces, Story Shears and Overturning Moments at Time
of Maximum Base Shear, Run Two

LEVEL

| 0.0 50.0 | 0.0 5.0 | 0.0 20.0 | 0.0 30.0 |

DISPLACEMENTS
(MM)

LATERAL FORCES
(KN)
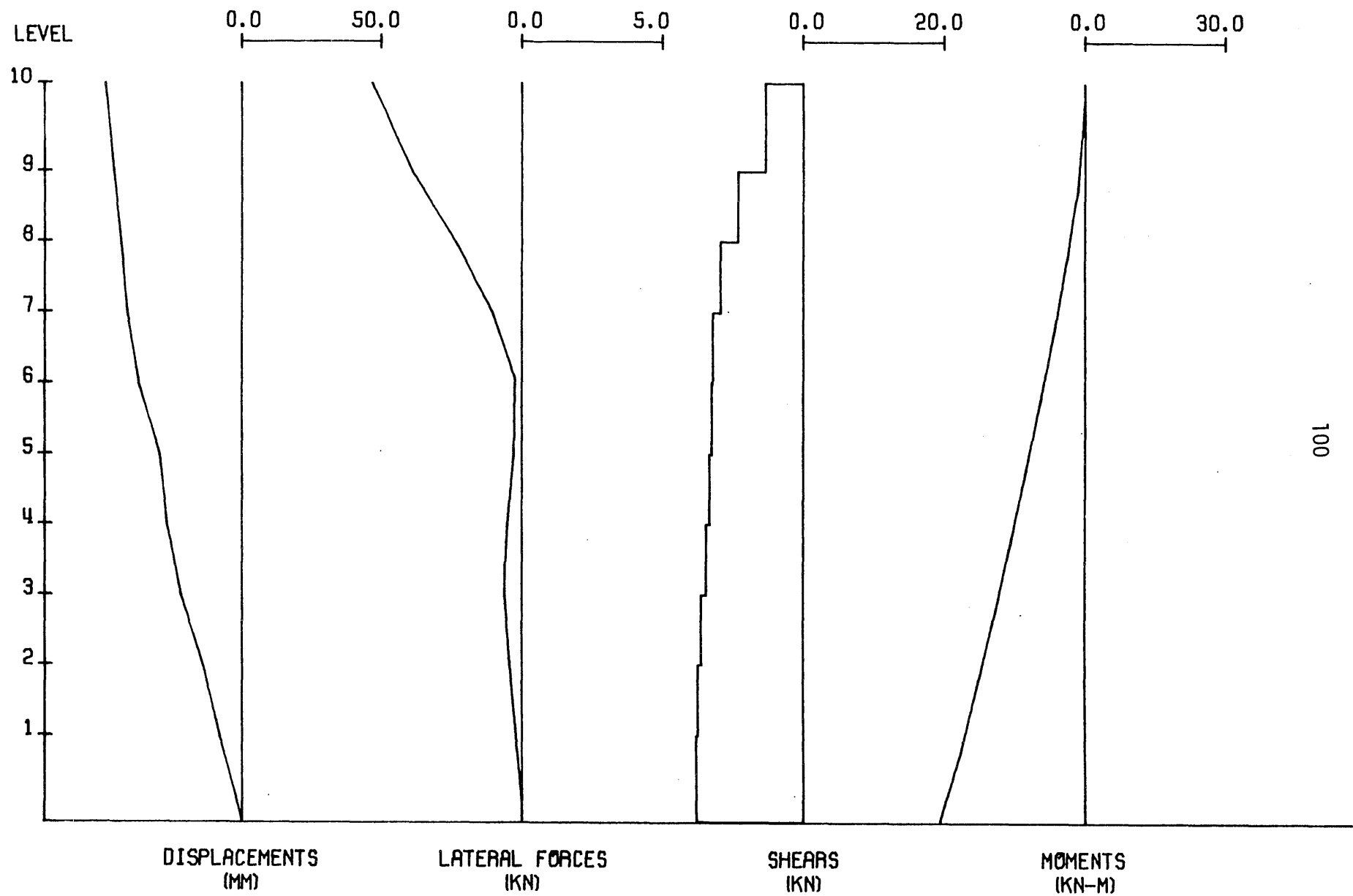
SHEARS
(KN)

MOMENTS
(KN-M)

TEST STRUCTURE MF1 — TEST RUN 2 — RESPONSE AT 2.46 SECONDS

Figs. 5.17 Observed Displacements, Lateral Forces, Story Shears and Overturning Moments at Time
of Maximum Base Overturning Moment, Run Two
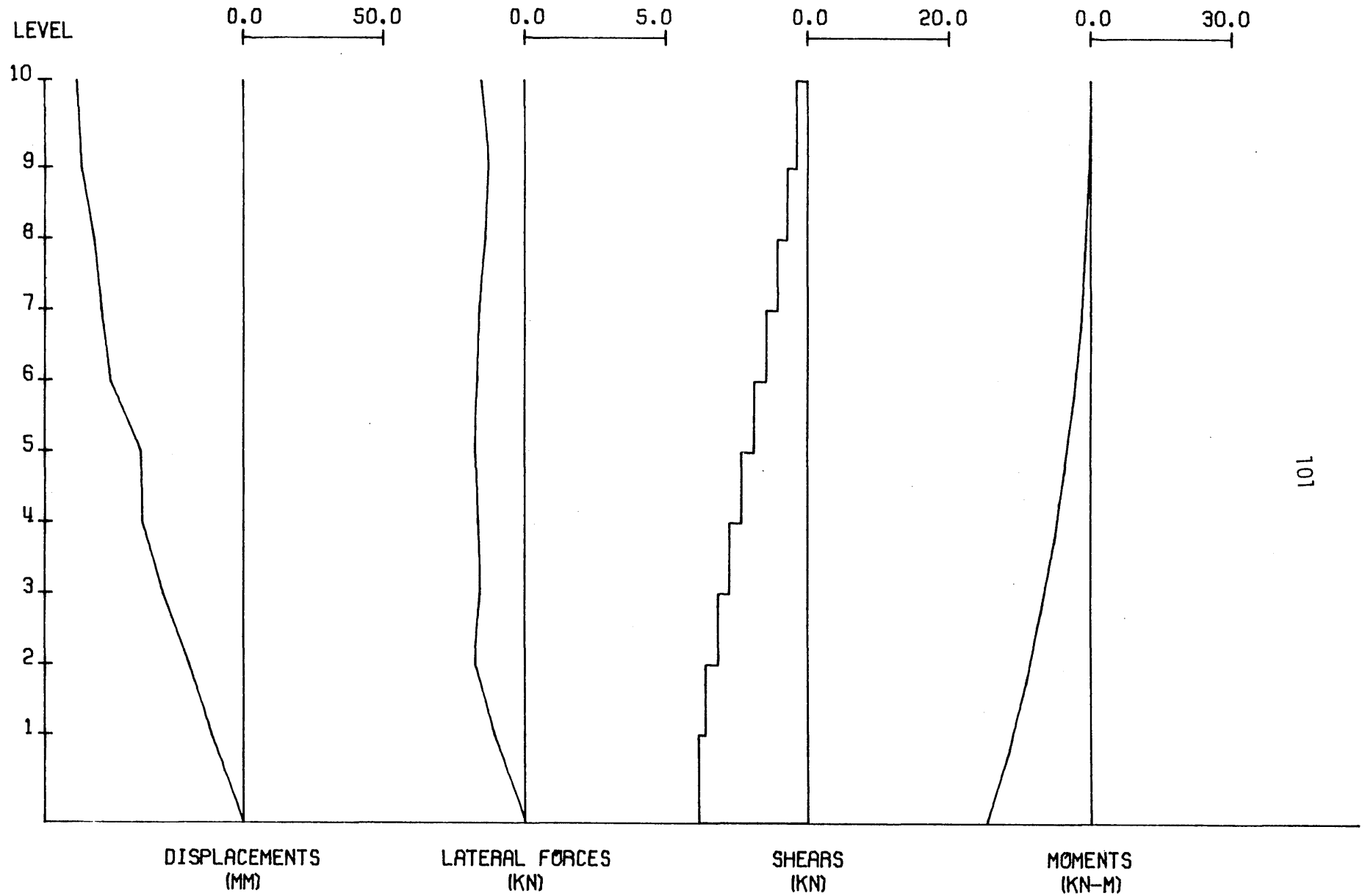
TEST STRUCTURE MF1 — TEST RUN 3 — RESPONSE AT 2.58 SECONDS

Fig. 5.18 Observed Displacements, Lateral Forces, Story Shears and Overturning Moments at Time of
Maximum Base Shear, Run Three

LEVEL — DISPLACEMENTS (MM) 0.0 50.0 — LATERAL FORCES (KN) 0.0 5.0 — SHEARS (KN) 0.0 20.0 — MOMENTS (KN-M) 0.0 30.0

102
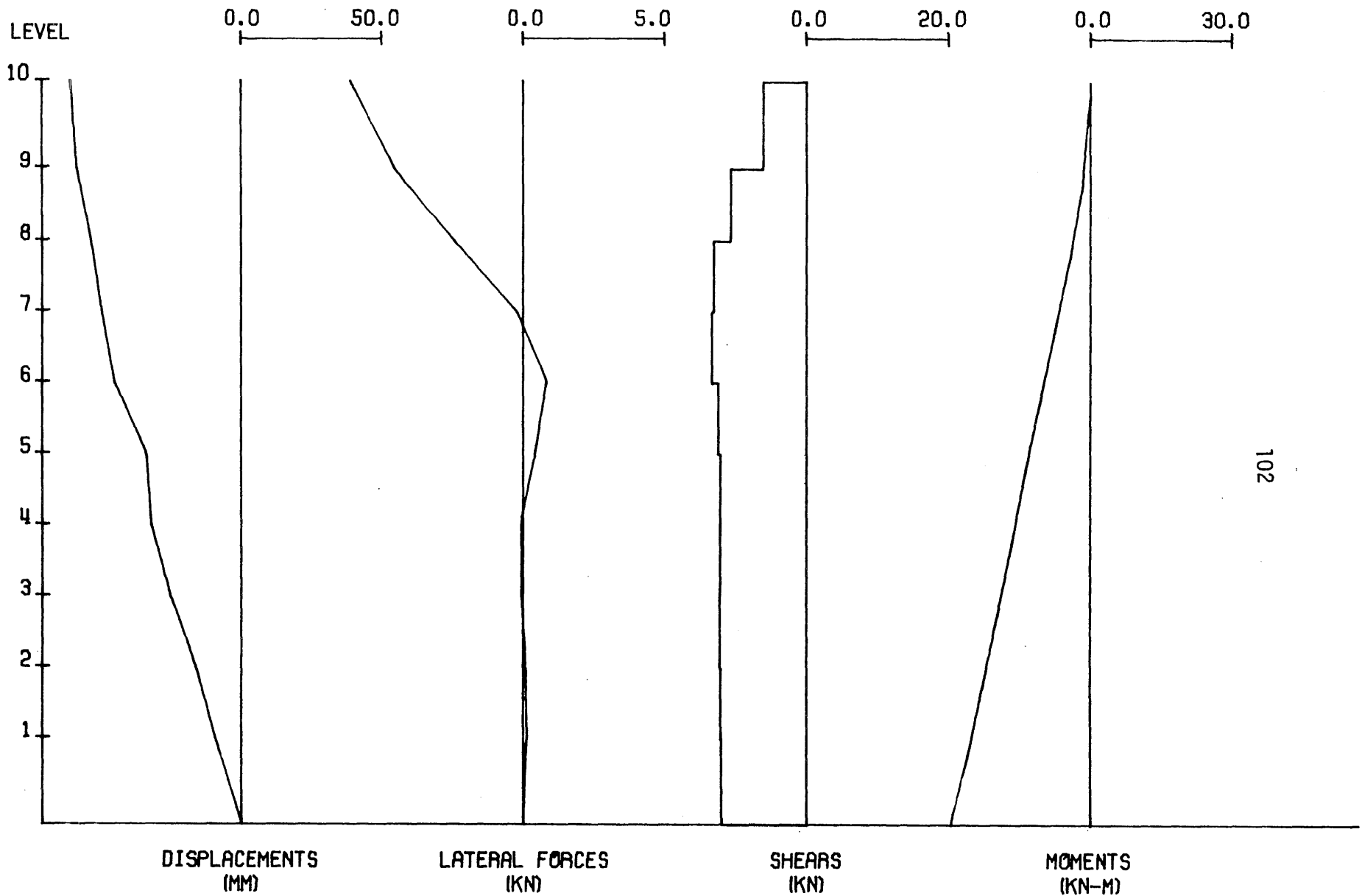
TEST STRUCTURE MF1 — TEST RUN 3 — RESPONSE AT 2.51 SECONDS

Fig. 5.19 Observed Displacements, Lateral Forces, Story Shears and Overturning Moments at Time of Maximum Base Overturning Moment, Run Three
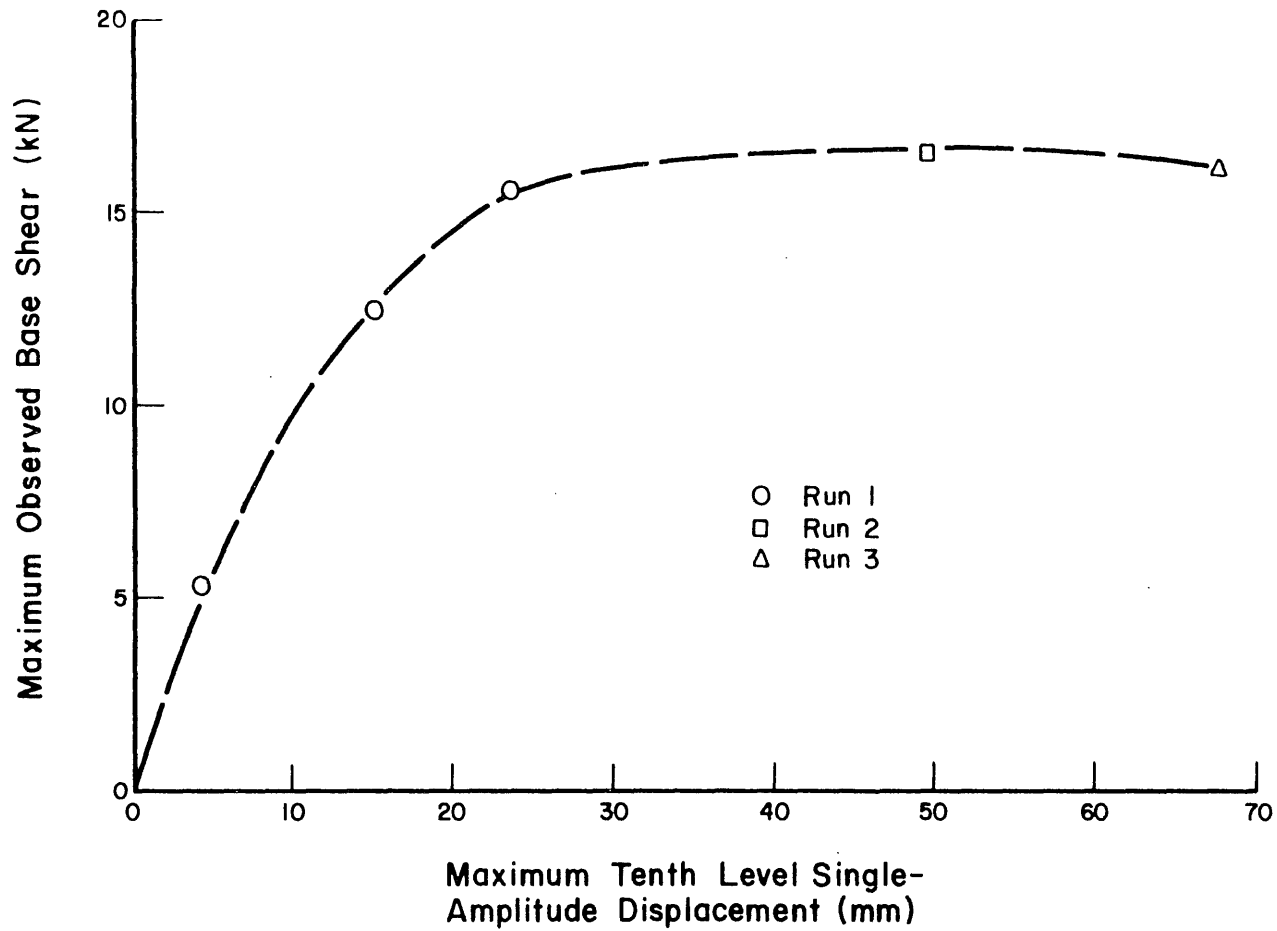
Fig. 5.20   Maximum Observed Base Shear Versus Maximum Tenth Level Displacement
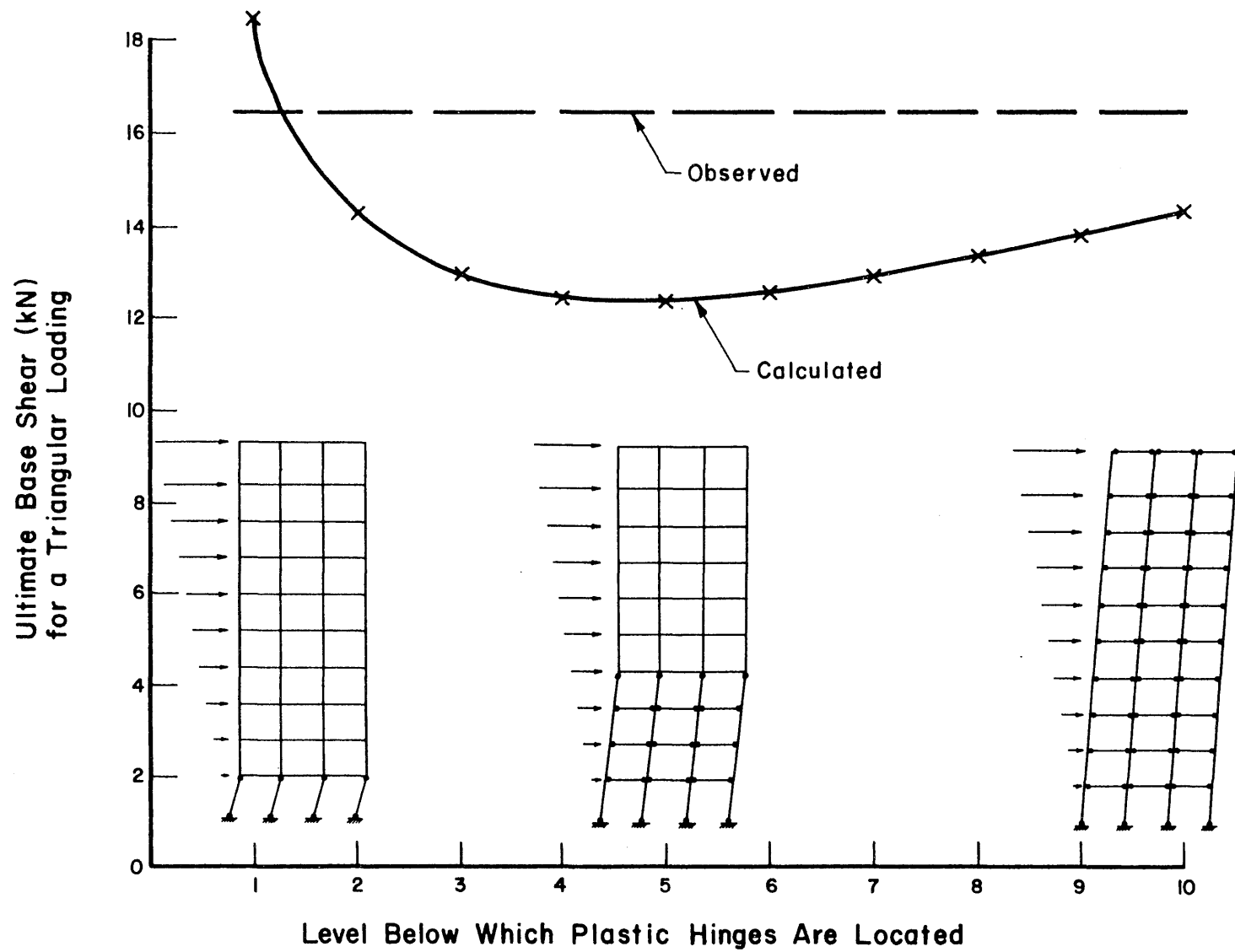
Fig. 5.21 Maximum Base Shear Versus Collapse Mechanism for a Triangular Lateral Loading Condition

APPENDIX A

DESCRIPTION OF EXPERIMENTAL WORK

A.1 Material Properties

(a) Concrete

Small-aggregate concrete was used to cast the test frame. The mix proportions by dry weight were 1:0.90:3.61 (cement:fine aggregate:course aggregate). The water-cement ratio was 0.80. The cement was high early strength (Type III), the fine aggregate was fine lake sand and the course aggregate was Wabash River sand.

Mechanical properties were determined from tests on samples which were cast simultaneously with the frame specimen. These tests were performed on the same day that the frame specimen was tested.

Compressive properties were determined by testing cylinders using a "120-kip" universal testing machine. Strains were measured using a 0.025-mm mechanical dial gage with a 127-mm gage length up to maximum stress. A representative stress-strain relation is shown in Fig. A.1. Young's modulus of the concrete was taken as the slope of the secant drawn from zero to seven MPa.

The tensile properties were determined by splitting tests on 102X204-mm cylinders. The modulus of rupture was determined by loading 51X51-mm cross sections at the center of a 152-mm span. The average strength of the concrete control specimens is summarized in Table A.1.

(b) Steel Reinforcement

(1) Flexural Reinforcement: No. 13 gage plain bright basic annealed wire was used as flexural reinforcement. The nominal cross-sectional area and diameter are 4.242 mm^2 and 2.324 mm, respectively.

Twenty random samples of no. 13 gage wire were picked from the same lot
that the flexural reinforcement was taken. The average measured diameter
was 2.326 mm with a standard deviation of .002 mm.

Tension tests were performed on twenty coupons using a "1.5-
kip" MTS testing machine. Strains were determined using an electrical-
resistance clip gage with a .5-in. gage length.

Ten of the coupons were tested at a strain rate of .001/sec., and
the other ten were tested at a strain rate of .005/sec. The results of
these tests are summarized in Table A.2. A typical stress-strain relation
is shown in Fig. A.2.

(2) Transverse Reinforcement: No. 16 gage plain wire was used
for transverse reinforcement in this experiment. The nominal cross-sectional
area and diameter are 1.981 mm^2 and 1.588 mm, respectively. Twenty random
samples of No. 16 gage wire were selected from the same lot that the trans-
verse reinforcement was taken. The average measured diameter was 1.584 mm
with a standard deviation of .006 mm.

The wire was deformed by a machine into a rectangular helix of
25 x 38 mm for columns, and a 19 x 25 mm rectangular helix for beams. The
helix had a pitch of 10 mm (Fig. 2.13). The average yield stress was found
to be 760 MPa.

(3) Joint Reinforcement: For confinement of the concrete at the
joints, 32 mm O.D. spirals made of No. 16 gage wire were used for joint
reinforcement. The spiral had a pitch of 10 mm. Metal tubing with a 13.11
mm O.D. was also provided at each joint to prevent deterioration of the
concrete at the connection of the masses to the frame (Fig. 2.13).

(4) Base Girder Reinforcement: Details of the reinforcement for
the base girder are shown in Fig. 2.2. Two #4 rebars grade 60 per face were
used for flexural reinforcement. Number 8 gage wire stirrups spaced at 51

mm were used as shear reinforcement. The reinforcement was provided so that the base girder could resist the maximum overturning forces. Steel tubing provided vertical holes in the base girder to bolt the specimen to the earthquake simulator.

A.2 Construction

(a) Fabrication of Steel Reinforcing Cages

For protection during shipping, the reinforcing steel was covered with heavy oil by the supplier. To remove the oil, the wire was soaked in a petroleum-based solvent. The wire was then cleaned with acetone to remove any residual film.

The reinforcing cages for both frames of the test specimen were fabricated by tying the flexural reinforcement to the transverse spiral reinforcement with a ductile .912-mm dia. wire. First the column reinforcement was assembled with continuous transverse spiral reinforcement. Then the beam flexural reinforcement was slipped through the column cages and tied to the transverse spiral beam reinforcement (Fig. 2.13).

The reinforcing cages were then sprinkled with a 10% solution of hydrochloric acid and placed in a fog room for 35 hours. This process induced slight rusting of the steel to improve bond with the concrete in the test specimen. Upon removal from the fog room, the cages were brushed and rinsed with water to remove excess rust.

The day before the specimen was cast, the reinforcing cages were placed in the forms. The spiral reinforcement was then placed at the joints. To provide imbedment at the base of each frame, a 102 x 51 x 3.2-mm steel plate was welded to the flexural reinforcing of each column 102 mm below the top of the base girder.

(b) Casting and Curing

The two frames and the control specimens were cast using concrete from the same batch. The frames were cast monolithically. Proper placement of the concrete was insured by use of a mechanical stud vibrator. Approximately one half hour after placement, the concrete was struck off and finished with a metal trowel. The frames were then covered with plastic sheet.

Approximately ten hours later, the side forms were carefully removed. The frames were then covered with wet burlap, and plastic sheet was placed over the burlap. The frames were left this way for two weeks and allowed to cure. The plastic and burlap were then removed, and the frames were stored in the lab. The cylinders and prisms received the same treatment. Table A.4. gives the chronology for the test frame.

(c) Measured Dimensions

Before the specimen was tested, the length, depth and width of all beams and columns in the test frame were measured. Within the accuracy of a tape measure, the length of every beam and column in the test frame was found to match the nominal length.

After the specimen was tested, the concrete cover was chipped off in 30 locations near joints in the structure. The cover thickness was measured to determine the depth to the flexural steel in the beams and columns in the test frame. All measurements taken of the test frame are summarized in Table A.3.

A.3 Instrumentation

Two types of gages were used to measure the response of the specimen. Twenty-seven accelerometers were installed to measure accelerations, and 21 linear voltage differential transformers (LVDT) were installed to measure displacements.

For each frame, one accelerometer was fastened to the longitudinal connections of the weights along the centerlines of the beams at each level and at the top of the base girder (Fig. A.3). Also an accelerometer was installed on the centerline of the tenth level mass between the two frames. These accelerometers were positioned to measure horizontal acceleration parallel to the imposed direction of motion.

One accelerometer was installed on the top of each frame and positioned to measure vertical acceleration. Two accelerometers were installed on the tenth level mass. These accelerometers were situated in such a way as to measure horizontal acceleration perpendicular to the imposed direction of motion.

Eighteen of the accelerometers were Endevco Model 2262C Accelerometers with a range of $\pm$ 50 g. The other nine accelerometers were Endevco Model AQ-116-15 Accelerometers with a range of $\pm$ 15g. Both models measure absolute acceleration.

Twenty-one LVDT's were used to measure relative displacements of the test specimen. Twenty of the gages were mounted on a steel A frame (Fig. A.3) which had a natural frequency of 48 Hz. These gages were mounted with their axis parallel to the direction of the imposed motion along the center-line of the beam of each floor level on both frames. One LVDT was also mounted on the ram of the earthquake simulator to measure the input motion during the experiment.

The LVDT's used in this experiment were Schaevitz AC-type differential transformers. The travel limit for the gages ranged from $\pm$ 3 in. at the top floor levels to $\pm$ 1 in. at the first level.

A.4 Data Reduction

The voltage output of the LVDT's and accelerometers was continuously recorded in an analog format on magnetic tape. Four tape recorders were used, each having the capability to record thirteen voltage signals and one audio signal. The input earthquake acceleration waveform was recorded on one channel of each of the four recording units. In this way the data on all four tapes could be synchronized.

In order to facilitate conversion from voltage units on the tape to physical units of the actual test specimen response, calibrations were performed on both the accelerometers and the linear voltage differential transformers prior to this experiment. The accelerometers were calibrated to the earth's gravity ($\pm$ g) by changing the direction of the axis of the gage from horizontal to vertical. The LVDT's were calibrated using metal blocks machined to specific dimensions. The voltage outputs corresponding to these known physical response levels were recorded on the analog magnetic tape.

The analog records of the tests were converted into digital records using the Spiras-65 computer of the Department of Civil Engineering. The digitization rate was 1000 points per second, and these records were also placed on magnetic tape. These tapes were then copied on the Burroughs 6700 computer of the Department of Civil Engineering to make them compatible with the reading device on the IBM 360-75 computer of the Digital Computer Laboratory at the University of Illinois.

A computer program was used to read the calibration factors and zero levels recorded on the tapes in voltage units. The approximate calibration factors could then be computed by comparing the known physical response level to the voltage output for each gage. By reading a portion of the

tape immediately prior to the onset of a test, the same computer program obtained zero levels for each gage.

Another computer program was used to process the data into its final form for permanent storage on magnetic tape. The previously obtained calibration factors and zero levels were applied to the data, and the data was processed into the form of a series of response-time relations.

Various other computer programs were used to plot the response-time relations, shear force and overturning moment records, Fourier Sepctra, and Response Spectra for the recorded base accelerations. The overturning effect of gravity load acting through the lateral displacements of the specimen was included in calculating the overturning moment relations. Also, a computer program was utilized to separate certain harmonic components of the wave forms.

Table A.1 Measured Properties of Concrete Control Specimens*

Parameter	Number of Tests	Mean	Standard Deviation
Secant [†] Modulus x 10^{-3} (Ec) (MPa)	6	22.0	2.2
Compressive Strength (f'c) (MPa)	6	40.2	2.1
Splitting Test (MPa)	6	3.3	0.6
Modulus of Rupture (MPa)	11	7.5	0.7

* Age of the specimens was 34 days

† Measured at 7 MPa in compression test of 102 x 203 - mm cylinder

Table A.2 Measured Properties of Flexural Reinforcement

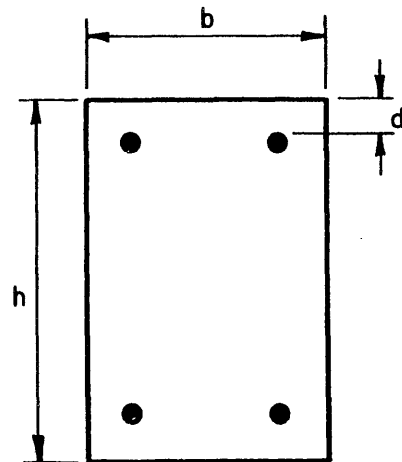| Young's Modulus x 10^{-3} (MPa)	Strain Rate (sec^{-1})	Yield Stress (fy) (MPa)	
		Mean	Standard Deviation
200.0	.001	350	9.7
	.005	360	5.2

Table A.3 Measured Dimensions of the Test Structure

Parameter		Size of Sample	Nominal (mm)	Mean (mm)	Standard Deviation (mm)
Column Width	(h)*	160	50.8	50.9	0.4
Beam Depth	(t)*	120	38.1	38.1	2.4
Frame Thickness	(b)*	280	38.1	39.0	2.2
Cover Thickness	(d')*	30	3.4	5.2	1.5

* See figures below
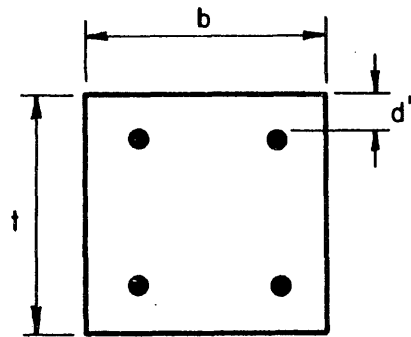
Beam Section   **Column Section**

Table A.4

Chronology For Test Structure

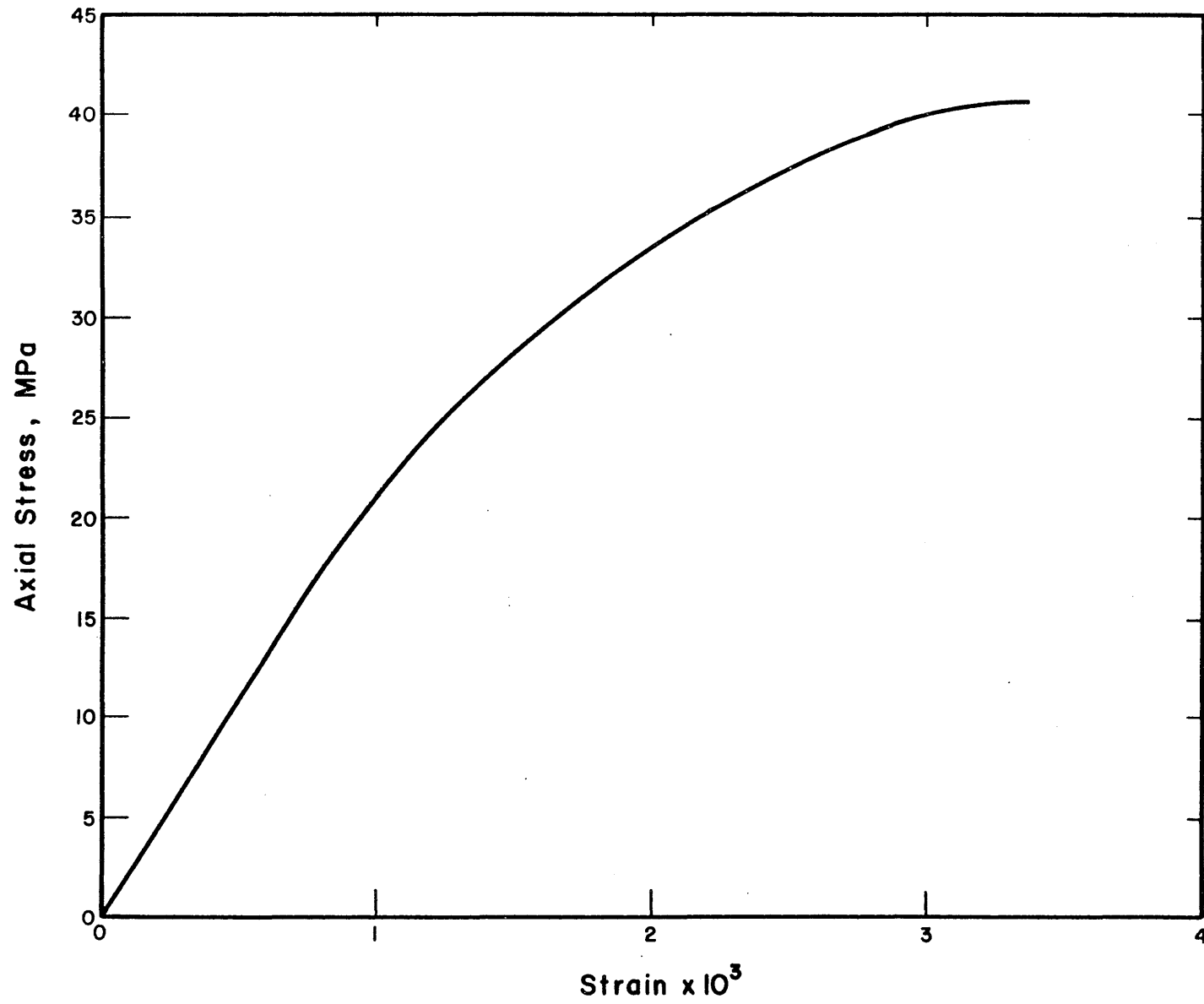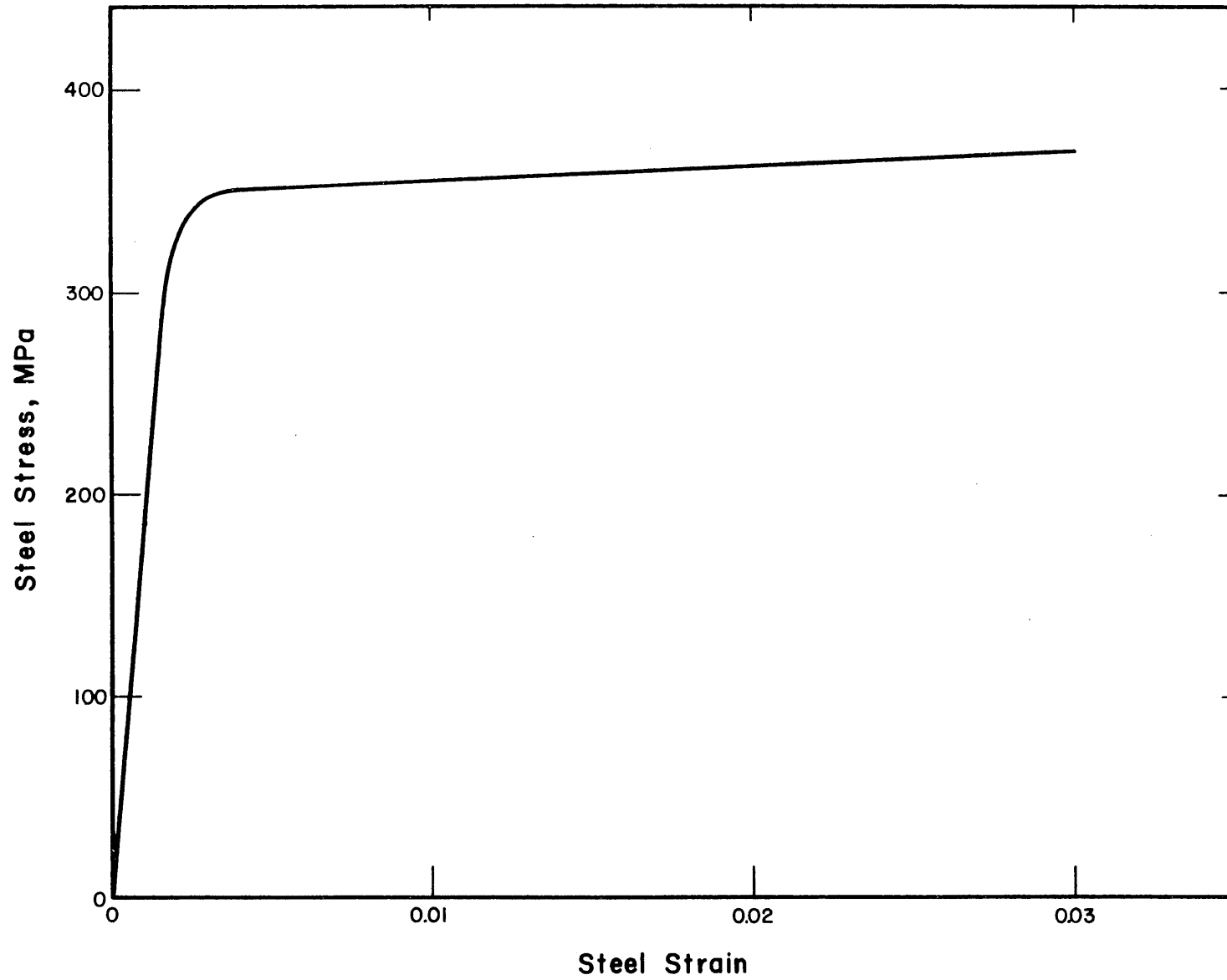|	Date
Reinforcement fabrication	23 May 1977
Casting	26 May 1977
Side forms struck	26 May 1977
Wet burlap cover removed	9 June 1977
Lifted off	9 June 1977
Mounted on the earthquake simulator	15 June 1977
Tested	29 June 1977

Fig. A.1 Measured Stress-Strain Relation for Concrete

Fig. A.2 Measured Stress-Strain Relation for Reinforcing Steel

Tenth Level Mass

Typical Accelerometer
Measures Minor Direction
Horizontal Acceleration

Typical Accelerometer
Measures Major Direction
Horizontal Acceleration

Typical LVDT
Measures Major Direction
Horizontal Displacement

Typical Accelerometer
Measures Vertical
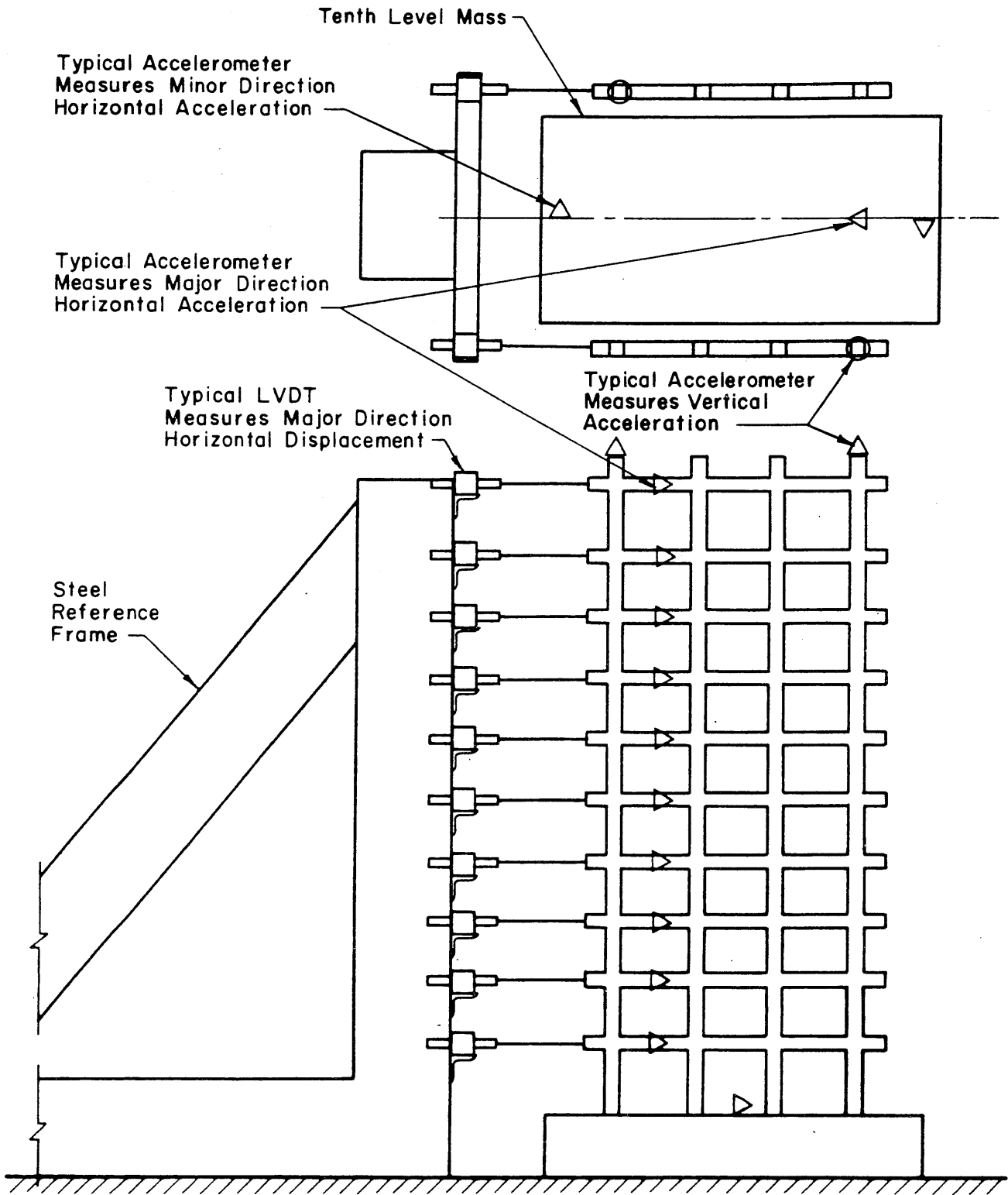Acceleration

Steel
Reference
Frame

Fig. A.3 Instrumentation Layout for the Test Structure

APPENDIX B

NOTATION

b = width of a cross section

d' = edge distance from the top of concrete to the top of steel of a cross section

E_c = initial moduls of elasticity of concrete

E_s = modulus of elasticity of steel

$(EI)_{ai}$ = actual stiffness of member i

$(EI)_{si}$ = substitute stiffness of member i

f'_c = compressive strength of concrete

f_{su} = ultimate stress of steel

f_y = yield stress of steel

g = acceleration of gravity

h = total depth of a column cross section

L = length of a structural member

M_{ai}, M_{bi} = end bending moments of member i

P_i = strain energy of member i

SI = spectrum intensity

t = time

W = weight of the test structure

X_b = base motion of the steady-state tests

X_o = amplitude of the base motion of the steady-state tests.

β = damping factor

β_n = damping factor for mode n

β_{si} = substitute damping factor for member i

μ = damage ratio

μ_i = damage ratio for member i

ω = driving frequency of the base motion of the steady-state tests